Dissertation zur Erlangung des Doktorgrades der Fakultät für Chemie
und Pharmazie der Ludwig-Maximilians-Universität München

Targeting ClpXP protease
-
Interfering with mitochondrial proteostasis as anti-cancer strategy

von

Melanie Marion Mandl

aus Altötting

2017

Erklärung

Diese Dissertation wurde im Sinne von § 7 der Promotionsordnung vom 28. November 2011 von Frau PD. Dr. Johanna Liebl betreut.

Eidesstattliche Versicherung

Diese Dissertation wurde eigenständig und ohne unerlaubte Hilfe erarbeitet.

München, den 6.3.2017
Datum, Ort Melanie M. Mandl

Dissertation eingereicht am	06.03.2017
1. Gutachterin	PD Dr. Johanna Liebl
2. Gutachterin	Prof. Dr. Angelika M. Vollmar
Mündliche Prüfung am	04.04.2017

Meinen Geschwistern Manuela und Maximilian.

Und niemand weiß, wie weit seine Kräfte gehen, bis er sie versucht hat.

Johann Wolfgang von Goethe

Contents

Summary

Targeting ClpXP protease as anti-cancer strategy

Cancer is one of the leading causes of death worldwide. The term cancer includes solid tumors as well as leukemia which affects parts of the hematopoietic system. Leukemic diseases are divided in different subtypes depending on the affected branch of the hematopoietic system and on whether the disease is in an acute or chronic phase. Despite continuous improvement of treatment and quite high survival rates, recurrence and therapy resistance are common problems. Hence, new ways of treatment are urgently needed not only for leukemia but also for cancer therapy in general.

The mitochondrion has been studied as a potential target for cancer therapy for years and revealed to be a key organelle implicated in tumorigenesis and progression. Besides interfering with mitochondrial respiration, redox balance or apoptosis signaling, targeting of mitochondrial proteases may be a novel anti-cancer approach. Recently, mitochondrial matrix proteases such as ClpXP have been reported as crucial mitoproteases (mitochondrial proteases) in various cancer types, such as acute myeloid leukemia, prostate, bladder or breast cancer. Hence, interfering with mitochondrial proteostasis (protein homeostasis) is considered as a potential cancer therapy option. ClpP, the proteolytic subunit of the ClpXP protease has been intensively studied in bacteria in terms of bacterial growth and virulence and therefore represents a target for novel antibiotics. In this regard, the group around Prof. Dr. Stephan A. Sieber identified a set of compounds by high-throughput screenings. The structures target not only the bacterial but also the human ClpXP protease, which is poorly investigated up to now. Due to the novelty of human ClpXP targeting, compounds for pharmacological inhibition of human ClpXP are still missing.

Herein, we characterized various compounds in cancer cell lines derived from acute and chronic myeloid and lymphoid leukemia. The inhibitor compounds target either the ClpP or ClpX subunit or the whole ClpXP protease and were investigated with regard to their impact on cell viability, colony formation, and cell death. Thus, we promote ClpXP as a drugable target and give first insights in mechanisms of action of novel ClpXP inhibitors as potential anti-cancer agents.

The investigations on the underlying mode of action further focused on mitochondrial integrity and energy production. ClpXP inhibition directly impaired mitochondrial function as shown by a direct decrease in ATP levels and loss of mitochondrial membrane potential. The increased mitochondrial ROS levels concomitant with enhanced carbonylation of

proteins reinforced that inhibition of the protease disturbed the mitochondrial proteostasis. Moreover, ClpXP inhibition caused cellular stress and enhanced sensitivity of various leukemia cell lines towards cytostatic drugs.

In summary, this thesis presents ClpXP as an attractive drugable target for cancer treatment. Further, novel ClpXP inhibitors were introduced and their functional characterization reinforced ClpXP inhibition as an anti-leukemic strategy (Figure 0.1). Finally, the investigations on mitochondrial integrity, energy metabolism, and stress signaling opened up new perspectives for the potential benefit of combination of ClpXP inhibitors with established cytostatic drugs.

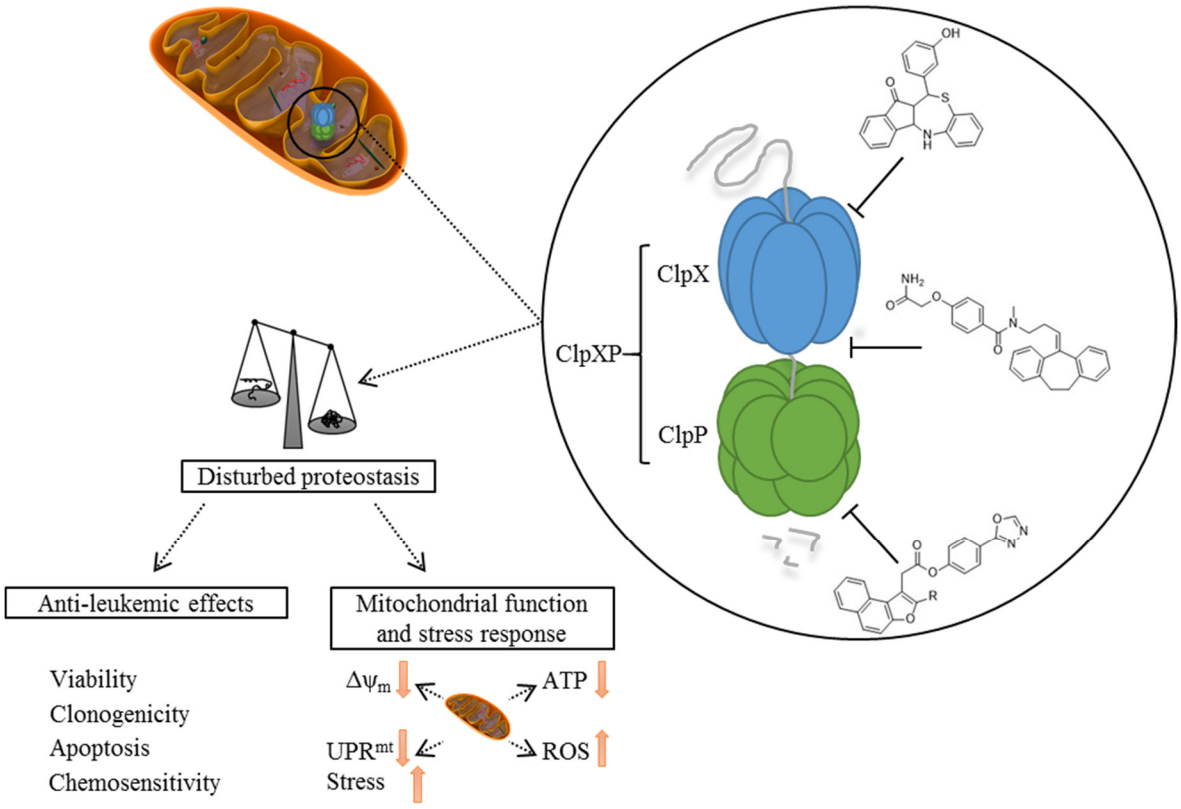

Figure 0.1: ClpXP inhibition exhibits anti-leukemic effects by triggering stress and disturbing mitochondrial integrity and function. As crucial part of the mitochondrial protein quality control network, the mitochondrial matrix protease ClpXP maintains mitochondrial function and proteostasis. Inhibition by ClpXP inhibitors leads to a misbalanced mitochondrial proteostasis which impairs energy metabolism, causes oxidative and other stress signals, and loss of membrane potential. Thus, ClpXP inhibition exhibits anti-leukemic effects.

Targeting Cdk5 to fight tumor-initiating cells

In a second project, the investigations focused on Cyclin-dependent kinase 5 (Cdk5) and its role in tumor-initiating cells (TICs). This project was successfully completed and published in the *British Journal of Cancer* in February 2017 (Appendix B, pages 66-81).

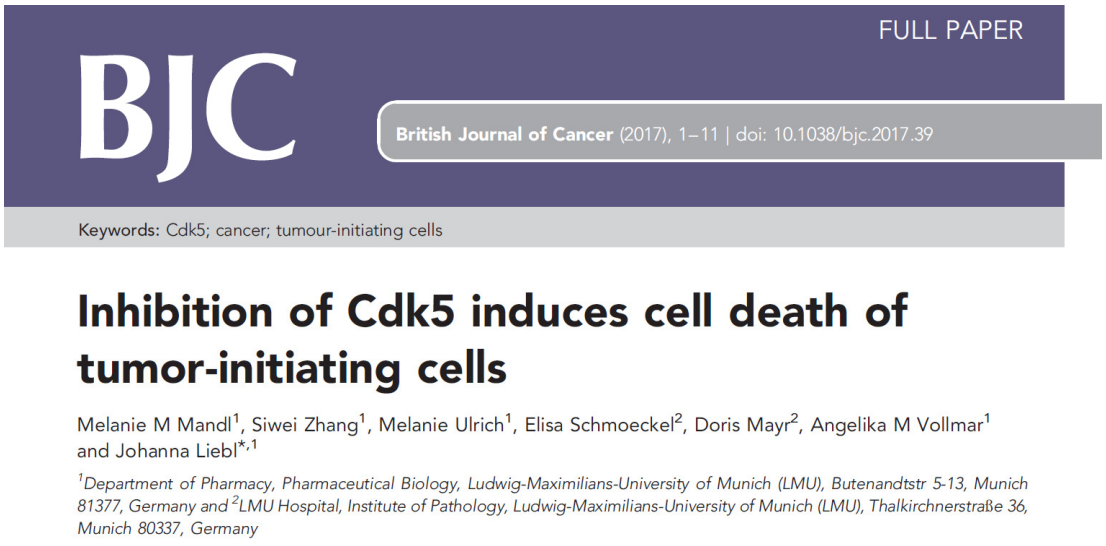

Therein, we proposed the atypical Cyclin-dependent kinase 5 as a promising target for cancer therapy by introducing a new role of the kinase in TICs. The small subset of TICs exhibits high tumorigenicity and chemoresistance and therefore mediates tumor recurrence and metastasis. Various mechanisms have been described to contribute to TIC generation such as the epithelial-mesenchymal transition (EMT). Besides, enhanced cell survival and escape from cell death of TICS are attributed to, e.g., alteration of proteins involved in intrinsic apoptosis signaling such as Bcl-2 family members. Thus, TICs represent a central field of interest for novel treatment strategies.

The serine/threonine kinase Cdk5 is crucial in neuronal development, lymphatic vessel formation, and tumor angiogenesis. More recently, increasing evidence exists for Cdk5 to have a function in cancer, e.g., in the DNA damage response of hepatocellular carcinoma or the EMT process in breast cancer. Although studies pointed to a connection between Cdk5 and TIC generation, the evidence for the kinase playing a role in TICs was missing so far. Accordingly, we focused on Cdk5 in the context of tumor initiation.

We first revealed that Cdk5 protein was increased in several cancer cell lines and in mesenchymal compared to epithelial cells. Likewise, a human tissue microarray staining underlined the enhanced expression of Cdk5 in breast cancer tissue in comparison to healthy breast tissue. Moreover, we elucidated that pharmacological inhibition and silencing of Cdk5 impaired cell viability, colony formation, and motility of various cancer cell lines, including

mesenchymal and epithelial cell lines derived from breast or bladder cancers. Furthermore, we carried out sphere formation experiments in which only TICs were allowed to grow in a detached environment. Therein, tumorsphere formation was impaired upon Cdk5 inhibition by the small molecule roscovitine. Underlining, stable Cdk5 knockdown diminished tumorsphere formation, and, vice versa, transient overexpression of the kinase in a non-cancerous cell line enhanced sphere formation *in vitro*. Likewise, Cdk5 silencing led to a delayed tumor establishment *in vivo.*

Furthermore, we revealed an enhanced detachment-induced cell death in TICs accounting for the diminished sphere formation. As a potential signaling pathway responsible for Cdk5-mediated detachment-induced cell death in TICs, we identified the Foxo1-Bim axis as one major pathway affected by Cdk5 knockdown. More precisely, we demonstrated the elevated levels of the transcription factor Foxo1. This resulted in enhanced transcription and protein expression of the pro-apoptotic BH3-only protein Bim probably accounting for the increased cell death of TICs (Figure 0.2).

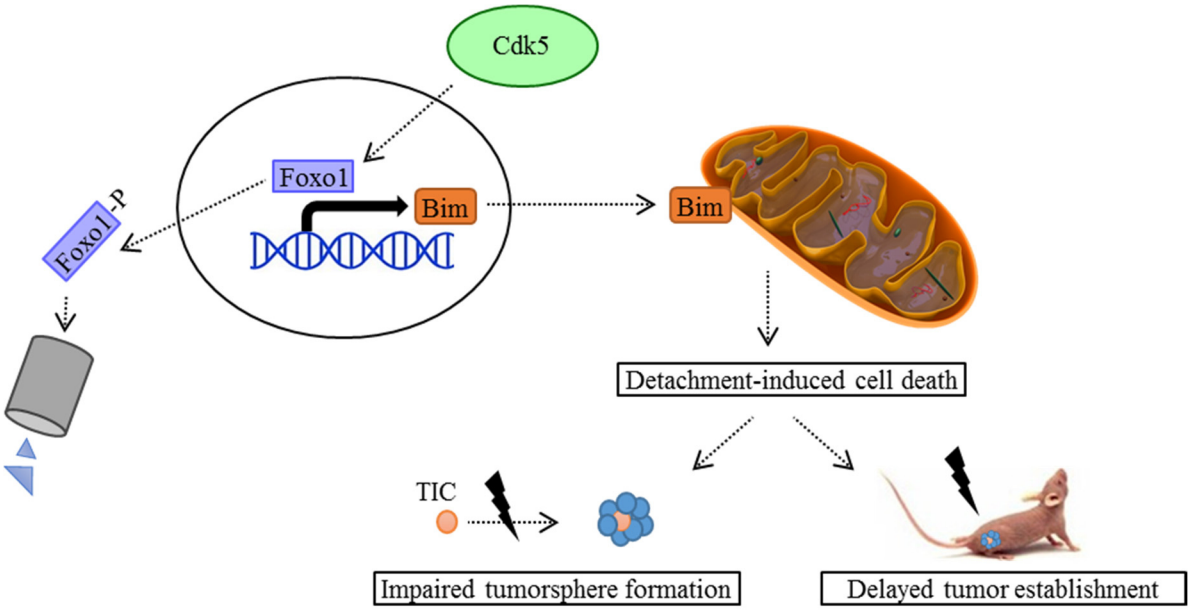

Figure 0.2: Cdk5 inhibition and knockdown induce cell death in TICs via the Foxo1-Bim axis. Cdk5 affects protein levels of Foxo1. Phosphorylated Foxo1 is degraded in the cytoplasm. Cdk5 inhibition and knockdown lead to elevated amounts of Foxo1 protein, which activates Bim transcription. Upon detachment, pro-apoptotic Bim is translocated to the mitochondrion and induces cell death in tumor-initiating cells leading to impaired tumorsphere formation *in vitro* and a delayed tumor establishment *in vivo.*

In summary, we promote Cdk5 as a potential target in cancer, especially in order to address tumor-initiating cancer cells. Besides general effects of Cdk5 inhibition and knockdown on cell viability, clonogenicity, and motility, we elucidated its impact on detachment-induced cell death. Concluding, we revealed the Cdk5-Foxo1-Bim axis as a potential target to fight TICs.

1 Introduction

1.1 Cancers of the hematopoietic system and treatment

Apart from cardiovascular diseases, cancer is among the most common causes of death nowadays. Cancers arising from the hematopoietic system include lymphoma, myeloma, and various types of leukemia which are ranked as the 11th frequent of all cancer incidences. Subdivided into acute and chronic leukemia, the disease can arise from lymphoid (chronic lymphocytic and acute lymphoblastic leukemia) or myeloid progenitors (chronic and acute myeloid leukemia) (Figure 1.1).[1] Consequently, symptoms of the disease include shortness of breath and bleedings due to low erythrocyte and platelet counts. Patients also exhibit enhanced susceptibility to infections that is caused by the lack of neutrophils and the accumulation of non-functional blasts in the bone marrow and blood.[2]

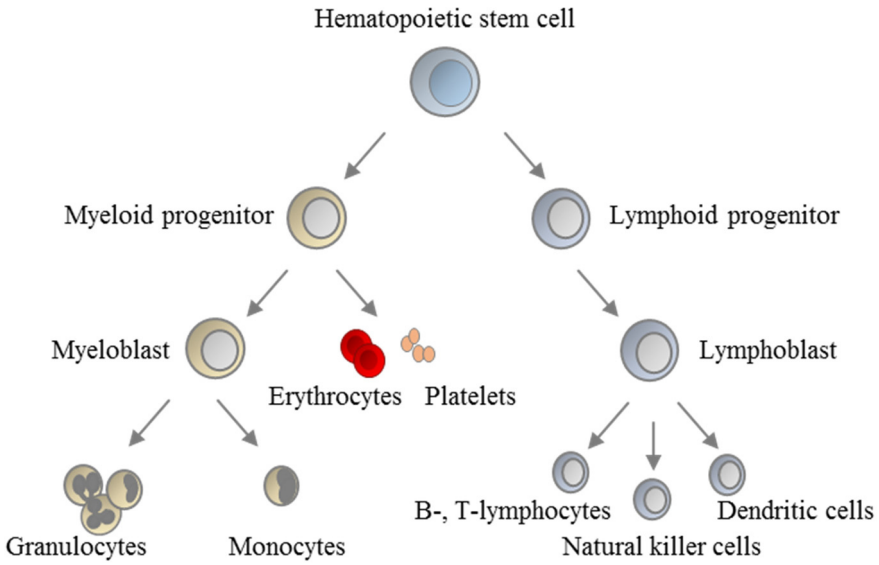

Figure 1.1: The hematopoietic tree. A simplified scheme of the hematopoietic system is shown which divides into myeloid and lymphoid branch. Cells of the immune system and blood cells arise by differentiation from hematopoietic stem cells. The different leukemia subtypes can affect the myeloid or the lymphoid branch.[3]

Chronic lymphocytic leukemia (CLL) represents the most common adult leukemia whereas young children mostly suffer from acute lymphoblastic leukemia (ALL). Despite overall five-year survival rates of about 60 % due to an improved treatment over the last decades, relapse after cytostatic therapy is a common concern.[1,4,5] Depending on disease subtype, age and health of the patient, treatment of acute forms can include high-dose induction therapy, consolidation, and maintenance therapy. Therein, combinations of cytostatic drugs are used, amongst others, cyclophosphamide, prednisone, daunorubicin, methotrexate, cytarabine,

and vincristine.[6-10] For subtypes expressing the constitutively active tyrosine kinase Bcr-Abl (Philadelphia chromosome positive leukemia), tyrosine kinase inhibitors such as imatinib can be combined with multiagent chemotherapy regimens.[11,12] Despite chemotherapy, allogenic stem cell transplantation is often the only way to cure the disease.[13-15] Therefore, the development of new treatment strategies besides the established ones is an urgent issue.

1.2 Targeting mitochondria for cancer therapy

1.2.1 Targeting cell death machinery, redox balance, and energy production

Mitochondrial dysfunction is linked to ageing as well as to neurodegenerative diseases like Parkinson's and Alzheimer's disease that are closely linked to cell death.[16-18] Hence, the idea of exploiting mitochondrial pathways or energy metabolism for cancer therapy arose over the last years (Figure 1.2).[19-21] Besides energy production and thus supporting cell viability, mitochondria are the central organelles of the intrinsic cell death. Mitochondrial apoptosis involves pro- and anti-apoptotic Bcl-2 (B cell lymphoma-2) family proteins responsible for the integrity of the mitochondrial outer membrane.[22] In general, pro-apoptotic members such as BAK and BAX are bound to anti-apoptotic proteins, e.g., Bcl-2 or Bcl-xL preventing apoptosis induction. Once activated by certain death inducing stimuli such as DNA damage BAX and BAK oligomerization renders the mitochondrial outer membrane permeable. This results in cytochrome c release from the mitochondrial intermembrane space and further activation of a cascade of caspases (cysteinyl-aspartate specific proteases) ending up in programmed cell death.[23] Loss of pro-apoptotic proteins or increase of anti-apoptotic Bcl-2 family members were predescribed to be responsible for cancer cells escaping from apoptotic cell death and their resistance to chemotherapy.[24,25] Consequently, targeting parts of the mitochondrial cell death machinery became a promising anti-cancer strategy. Moreover, apoptotic profiling which determines the tumor's reliance on anti-apoptotic Bcl-2 turned out to be predictive for the response to chemotherapy.[26-28]

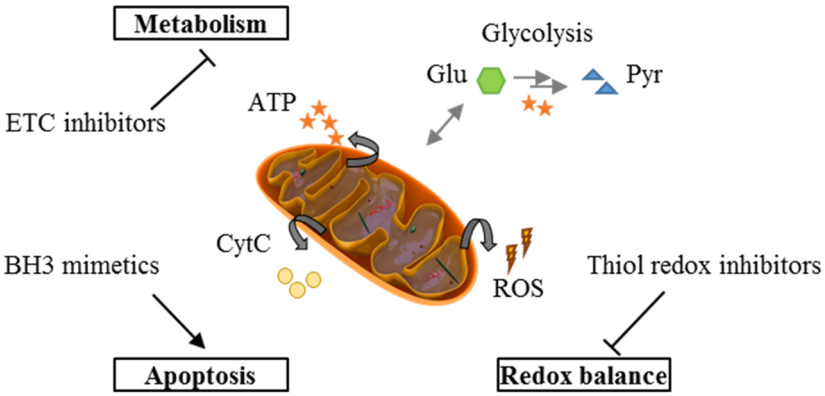

Figure 1.2: Diverse possibilities of mitochondrial targeting for cancer therapy. Mitochondria can be addressed in several ways. Mitochondrial energy metabolism or metabolic flexibility can be targeted by inhibition of parts of the electron transport chain (ETC). Redox homeostasis of the mitochondrion can be addressed by interfering with antioxidant pathways. Further, proteins of the apoptosis machinery, for example, anti-apoptotic Bcl-2 proteins which can be neutralized by pro-apoptotic BH3 mimetics, serve as target for cancer therapy. ATP, adenosine triphosphate; BH3, Bcl-2 homology domain 3; CytC, cytochrome c; ETC, electron transport chain; Glu, glucose; Pyr, pyruvate; ROS, reactive oxygen species.

Further, the electron transport chain located within the inner mitochondrial membrane is a site of reactive oxygen species (ROS) generation as a by-product of mitochondrial respiration. ROS function as signaling molecules to activate proliferation and promote cell survival at low concentrations.[29,30] Moderate amounts of increased ROS cause DNA damage and genomic instability and thus drive tumorigenesis, whereas high oxidative stress leads to cell death and senescence.[31,32] ROS production of fast proliferating cancer cells is often elevated compared to non-cancer cells.[33] This in turn forces cancer cells to increase antioxidant pathways in order to prevent cell death by high amounts of ROS. Therefore, interfering with mitochondrial redox regulation and antioxidant pathways is another interesting approach.[33,34] *In vitro* and *in vivo* studies revealed promising results with combined inhibition of glutathione and thioredoxin antioxidant pathways in breast cancer models.[35]

Furthermore, metabolic flexibility is essential for tumorigenesis and progression. Fast proliferating tumor cells mostly depend on aerobic glycolysis, known as the Warburg effect. This was formerly but erroneously thought to be an exclusive effect of mitochondrial defects.[36-39] Conversely, distinct tumor subpopulations do not show the glycolytic phenotype. A switch from glycolysis to oxidative phosphorylation reliance was observed in terms of chemoresistance. Moreover, cancer stem cells of many cancers were found to rely on oxidative phosphorylation rather than glycolysis.[40-45] Thus, targeting mitochondrial metabolism represents an additional strategy to fight resistant subpopulations of cancer cells.

1.2.2 Targeting mitochondrial proteostasis

The mitochondrial DNA (mtDNA) encodes for 13 proteins, such as parts of the ETC, 22 tRNAs, and two rRNAs. However, the mitochondrial proteome mainly consists of nuclear encoded proteins.[46,47] Moreover, ROS produced by the ETC located in the inner mitochondrial membrane cause mtDNA and protein damage.[48] Consequently, a strictly regulated protein import, folding, and quality control of newly synthesized proteins, as well as degradation of damaged proteins is crucial for proper mitochondrial function.[49-52] This network includes chaperones and proteases which in turn are divided into several groups depending on function and location within the organelle (Figure 1.3). One subgroup, the AAA proteases (ATPase associated with diverse cellular activities), is essential for mitochondrial protein quality control. The intermembrane AAA protease (iAAA) and the matrix AAA protease (mAAA) are both located within the inner mitochondrial membrane, whereas the serine proteases Lon and ClpXP are located in the mitochondrial matrix and degrade damaged proteins. In addition, mitochondrial proteases were described to participate in regulation of signal transduction by processing of regulatory proteins, mitochondrial biogenesis, dynamics, stress response, mitophagy, and apoptosis signaling.[50]

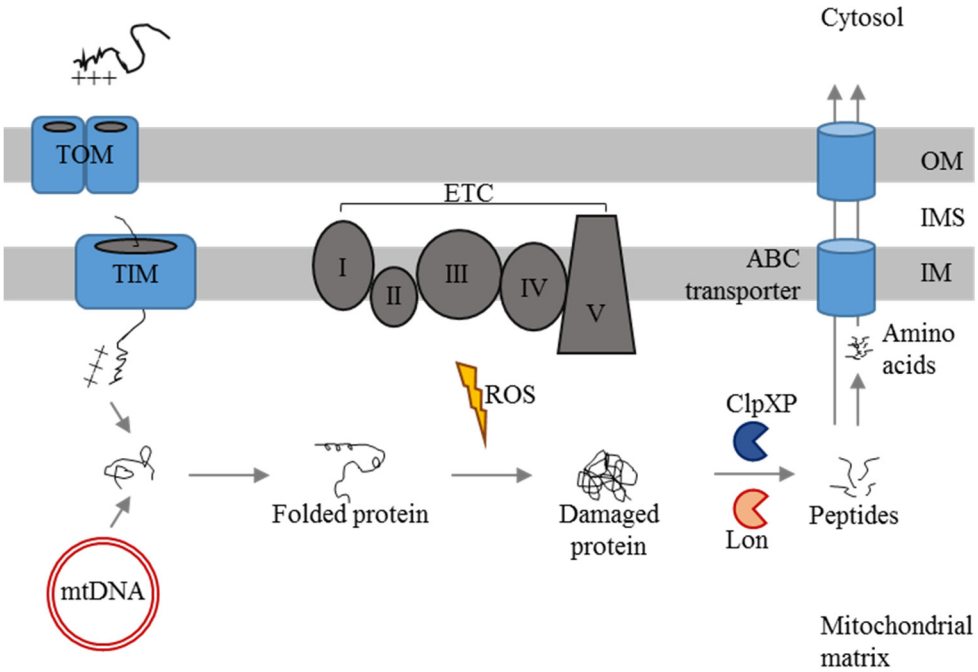

Figure 1.3: The mitochondrial proteostasis is maintained by an import, processing, and quality control network. Import of nuclear encoded proteins is conducted by translocase outer membrane (TOM) complex and translocase inner membrane (TIM) complex. Imported or mitochondrial encoded proteins are processed and folded by proteases and chaperones such as heat shock protein 60 (Hsp60). Misfolded, aggregated or oxidized proteins caused by ROS^{mt} can be cleaved by proteases, e.g., the matrix serine proteases Lon or ClpXP. Peptides can be further cleaved to amino acids or exported directly by ABC transporters and act as signaling molecules. ABC transporter, ATP-binding cassette transporter; ETC I-V, electron transport chain complex I-V; IM, inner membrane; IMS, intermembrane space; mtDNA, mitochondrial DNA; OM, outer membrane; ROS, reactive oxygen species; TIM, translocase inner membrane; TOM, translocase outer membrane.[50]

The crucial role of some mitoproteases such as Lon and ClpXP has been described recently in the cancer context.[53-59] Consequently, targeting parts of the mitochondrial proteases network and thereby interfering with mitochondrial proteostasis represents a new approach in terms of cancer therapy.[60]

1.2.2.1 The ClpXP protease

The caseinolytic peptidase proteolytic subunit (ClpP) has been studied for years in pathogenic bacteria such as *Staphylococcus aureus* or *Mycobacterium tuberculosis* because it is crucial for their growth and virulence.[61-64] Since then, targeting of ClpP has been examined using inhibitors as well as acyldepsipeptides (ADEPs) that activate ClpP as an antibiotic strategy.[65-67] However, human ClpP, the peptidase subunit of the ClpXP protease complex (Figure 1.4), is less studied than bacterial ClpP. Mutations in the ClpP gene are associated with the Perrault syndrome which is characterized by symptoms like hearing loss, ovarian insufficiency in women, and several neurological deficiencies.[68,69]

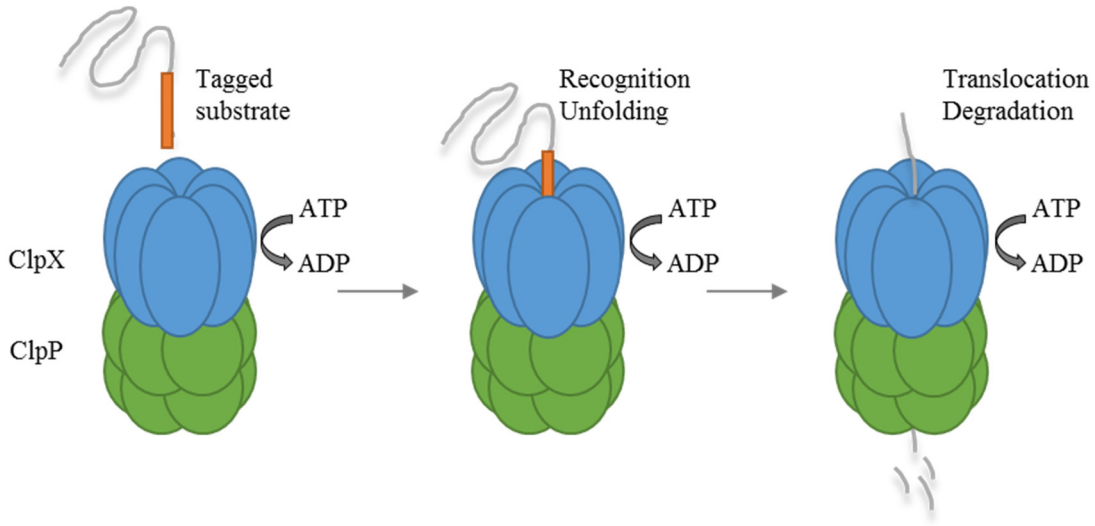

Figure 1.4: Structure of ClpXP protease. The nuclear encoded serine protease ClpXP consists of a hexameric ClpX chaperone part and a tetradecameric ClpP peptidase subunit and is located in the mitochondrial matrix. ClpX recognizes, unfolds, and translocates substrates into the proteolytic compartment in ClpP driven by ATP hydrolysis. ClpP cleaves the polypeptide into small peptides.[70]

An accumulation of misfolded or damaged proteins in mitochondria has been described to trigger an organelle-specific signaling, the mitochondrial unfolded protein response (UPR^{mt}).[71] This retrograde signaling aims to restore the mitochondrial proteostasis and function, inter alia, by enhanced transcription of nuclear encoded mitochondrial chaperones and proteases. Amongst them, heat shock protein 60 (Hsp60) and the ClpP itself were described to be upregulated to restore mitochondrial proteostasis and thus have a cell survival function.[71]

While the UPR^{mt} has been intensively studied in *Caenorhabditis elegans* during the last years, the mammalian UPR^{mt} signaling is less understood (Figure 1.5).[72] Former studies suggest that ClpXP regulates the UPR^{mt} and therefore acts as a critical protease in human disease pathogenesis.[73,74]

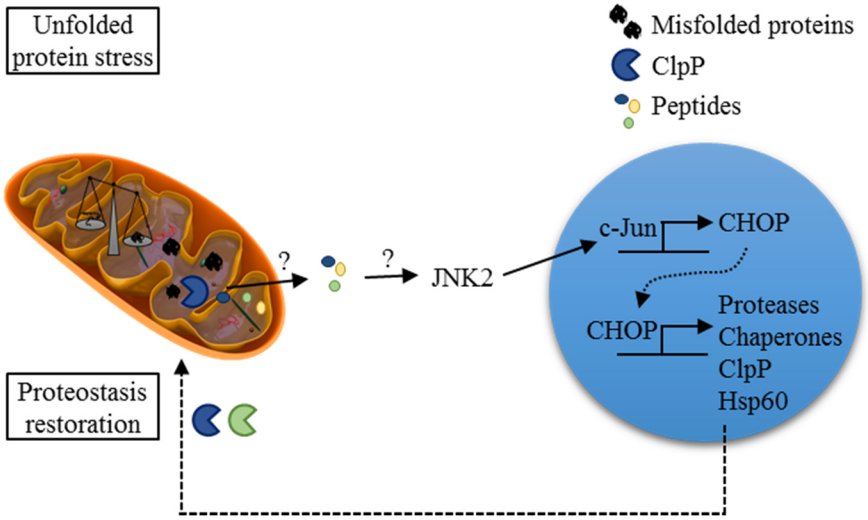

Figure 1.5: The mammalian mitochondrial unfolded protein response. A disturbed mitochondrial proteostasis can trigger the UPR^{mt}. ClpP cleaves accumulating misfolded proteins into peptides that are released into the cytosol. An activated JNK2 in turn activates c-Jun which drives CHOP transcription. CHOP promotes transcription of mitochondrial chaperones and proteases such as Hsp60 and ClpP.[71,75,76] CHOP, C/EBP homologous protein; JNK2, c-Jun N-terminal kinase 2.

1.2.2.2 ClpXP inhibitors

With regard to the increasing evidence of ClpXP's key role in human cancer, the group of Prof. Dr. Stephan A. Sieber (Department of Chemistry, Technical University of Munich, Garching) develops and investigates new compounds targeting ClpXP complex. Different structures were identified in *Staphylococcus aureus* ClpXP (*Sa*ClpXP) or *Sa*ClpP high-throughput screenings (*Sa*ClpP-HTS). Interestingly, some of the identified structures also inhibited the human ClpXP complex. The first group represents phenyl ester compounds that inhibit ClpP subunit (Figure 1.6).[77]

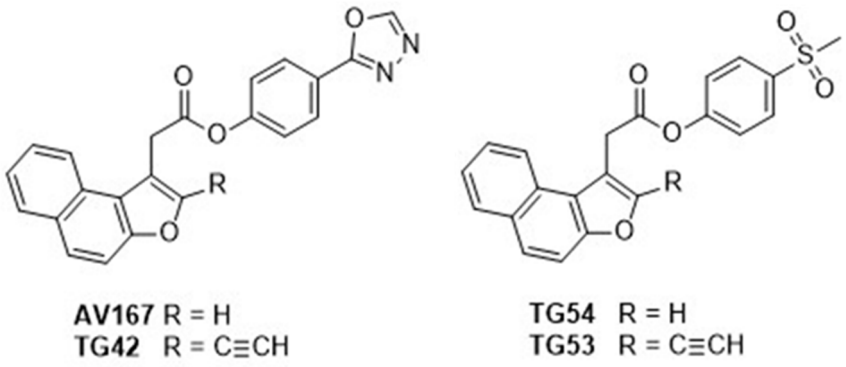

Figure 1.6: Phenyl ester ClpP subunit inhibitors and their corresponding probes. Structures with activity against ClpP peptidase subunit are shown. TG42 and TG53 represent corresponding inhibitor probes of AV167 and TG54 and possess an additional alkyne function.

The second group consists of compounds with different activity profiles towards the ClpXP subunits or the whole protease (Figure 1.7). While 334 targets the ClpX subunit, 319 and 339 revealed no inhibitory effect on either ClpX or ClpP subunit but activity on ClpXP complex. 335 exhibited no activity on human but in fact on the bacterial ClpXP.

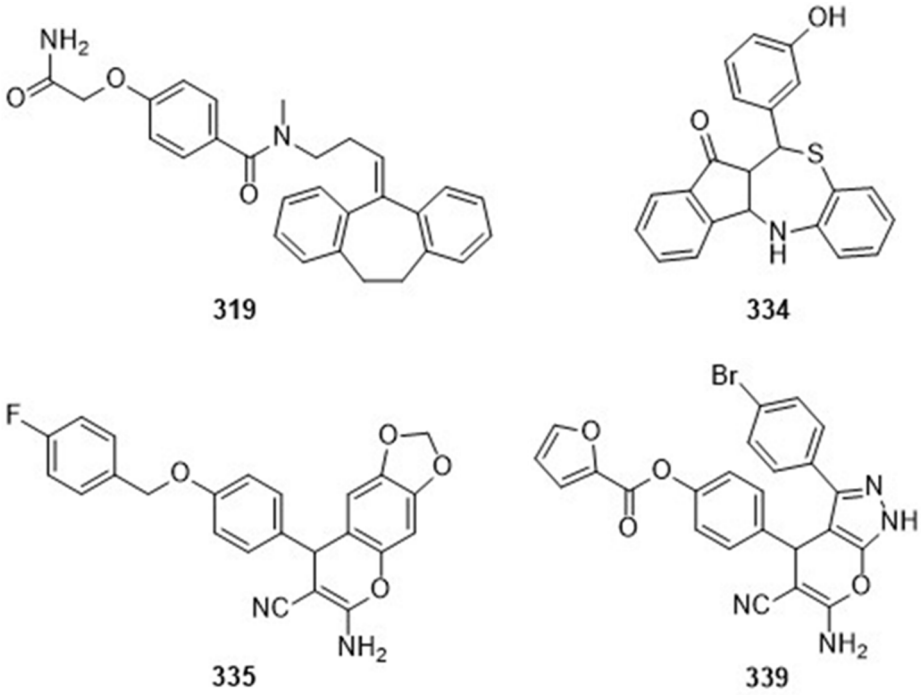

Figure 1.7: Compounds with different activity on ClpXP identified in *Sa*ClpXP-HTS. 334 represents an inhibitor of ClpX subunit. 319 and 339 are thought to prevent ClpXP complex formation. 335 has shown bacterial but not human ClpXP inhibition.

1.3 Aim of the thesis

With respect to former studies that promote ClpXP as promising target for cancer treatment, especially for cancers derived from the hematopoietic system, the aim of the thesis was to characterize and establish a set of novel ClpXP targeting compounds. We focused on their functional effects and the underlying mode of action in various leukemia cell lines, such as K562 (CML), Jurkat (T-ALL), CEM (T-ALL), and HL-60 (AML), and in a hepatocellular carcinoma cell line (Huh7).

Therefore, cell viability, colony formation, as well as cell death were initially analyzed. To underline the effectiveness of ClpXP inhibition in patient-derived xenograft (PDX) leukemia cells, cell death was analyzed in various AML and ALL PDX cell samples. Further, the analysis of the sensitivity of a hepatocellular carcinoma cell line should reinforce the relevance of ClpXP as an addressable target also for other cancer types.

In terms of elucidation of a general mode of action of ClpXP inhibition in cancer cells, we further used the most potent compound, an inhibitor of the ClpX subunit (334), and the Jurkat as well as the K562 cell line representatively for lymphoid and myeloid leukemia cells.

Hence, substrates and signaling pathways affected by ClpXP inhibition such as the mitochondrial unfolded protein response were of particular interest. To gain insight into this field, we used a quantitative proteomic approach as well as western blotting and quantitative real-time PCR. Furthermore, key experiments for analysis of mitochondrial function were performed, such as measurement of ATP levels, mitochondrial ROS production, and analysis of mitochondrial membrane potential. Moreover, we analyzed mitochondrial morphology by confocal and electron microscopy.

Finally, we investigated the effect of ClpXP inhibition on chemosensitivity of various leukemia cell lines by combining the ClpX inhibitor 334 with different cytostatic drugs, such as imatinib, etoposide or vincristine.

2 Materials and Methods

2.1 Materials

2.1.1 Compounds

ClpP inhibitors (AV167, TG42, TG53, and TG54) and ClpXP inhibitor compounds (319, 334, 335, and 339) were friendly provided by Prof. Dr. Stephan A. Sieber (Department of Chemistry, Technical University of Munich, Garching).

2.1.2 Technical equipment and reagents

Table 2.1: Technical equipment

Name	**Producer**
Axiovert 25/200 microscope	Zeiss, Jena, Germany
Canon EOS 450D camera	Canon, Poing, Germany
ChemiDoc Touch Imaging System	Bio-Rad Laboratories GmbH, Munich, Germany
Consort Electrophoresis Power Supply E835	Sigma-Aldrich, Taufkirchen, Germany
FACS CantoII	BD Biosciences, Heidelberg, Germany
Leica-SP8 confocal microscope	Leica Microsystems, Wetzlar, Germany
Megafuge 1.0s centrifuge	Heraeus, Hanau, Germany
Mikro 22R table centrifuge	Hettich, Tuttlingen, Germany
NanoDrop® ND-1000 Spectrophotometer	Peqlab Biotechnology GmbH, Erlangen, Germany
Okolab incubation chamber	Okolab S.r.l., Pozzuoli, Italy
OrionII microplate luminometer	Titertek Berthold, Pforzheim, Germany
PowerPac 200 powersupply	Bio-Rad Laboratories GmbH, Munich, Germany
Primus 25 advanced thermocycler	Peqlab Biotechnology GmbH, Erlangen, Germany
QuantStudio 3 Real-Time PCR System	Thermo Fisher Scientific, Waltham, MA, USA
SpectraFluor Plus^{TM}	Tecan, Crailsheim, Germany

TB1 Thermoblock	Biometra, Göttingen, Germany
Vi-Cell™ XR	Beckman Coulter, Krefeld, Germany

Table 2.2: Biochemicals, compounds, dyes, and reagents for cell culture and assay performance

Reagent	**Producer**
Antimycin A	Sigma-Aldrich, Taufkirchen, Germany
Bradford Reagent™	Bio-Rad Laboratories GmbH, Munich, Germany
BSA	Sigma-Aldrich, Taufkirchen, Germany
CCCP	Sigma-Aldrich, Taufkirchen, Germany
CellTiter-Blue™, CellTiter-Glo™	Promega, Madison, WI, USA
Collagen G	Biochrom AG, Berlin, Germany
Complete® mini EDTA free	Roche Diagnostics, Penzberg, Germany
Cytarabine	Sigma-Aldrich, Taufkirchen, Germany
DMEM	PAN Biotech, Aidenbach, Germany
DMSO	Sigma-Aldrich, Taufkirchen, Germany
DTT	AppliChem, Darmstadt, Germany
EDTA	Carl Roth, Karlsruhe, Germany
Etoposide	Sigma-Aldrich, Taufkirchen, Germany
FCS	PAA Laboratories, Pasching, Austria
Ficoll-Paque PLUS	GE Healthcare Life Sciences, Freiburg, Germany
FluorSave™ Reagent	Merck, Darmstadt, Germany
Formaldehyde solution 10 %	AppliChem, Darmstadt, Germany
HBSS buffer	Sigma-Aldrich, Taufkirchen, Germany
High-Capacity cDNA Reverse Transcription Kit	Applied Biosystems, Foster City, CA, USA
H_2O_2 30 %	Merck, Darmstadt, Germany
Hoechst 33342	Sigma-Aldrich, Taufkirchen, Germany
Imatinib mesylate	Sigma-Aldrich, Taufkirchen, Germany
IMDM with L-Glutamine	Thermo Fisher Scientific, Waltham, MA, USA
JC-1	Enzo Life Sciences, Farmingdale, NY, USA

Methylcellulose	Sigma-Aldrich, Taufkirchen, Germany
Mercaptoethanol	Sigma-Aldrich, Taufkirchen, Germany
MitoSOX™ Red	Thermo Fisher Scientific, Waltham, MA, USA
MTT	Promega, Madison, WI, USA
Non-fat dry milk powder (Blotto)	Carl Roth, Karlsruhe, Germany
Oxidized Protein Western Blot Kit	Abcam, Cambridge, UK
Page-Ruler™ Prestained Protein Ladder	Fermentas, St. Leon-Rot, Germany
Penicillin/Streptomycin	PAN Biotech, Aidenbach, Germany
PI	Sigma-Aldrich, Taufkirchen, Germany
PMSF	Sigma-Aldrich, Taufkirchen, Germany
PowerUp ™ SYBR Green Master Mix	Applied Biosystems, Foster City, CA, USA
Pyronin Y	Sigma-Aldrich, Taufkirchen, Germany
Pyruvate	PAA Laboratories, Pasching, Austria
Qiagen RNeasy Mini Kit	Qiagen GmbH, Hilden, Germany
Q-VD-OPh	Merck, Darmstadt, Germany
Rotiphorese™ Gel 30	Carl Roth, Karlsruhe, Germany
RPMI 1640 with L-Glutamine	PAN Biotech, Aidenbach, Germany
SILAC RPMI 1640 w/o L-Glutamine, L-Arginine, L-Lysine	Thermo Fisher Scientific, Waltham, MA, USA
Taqman Master Mix	Life Technologies Corporation, Carlsbad, CA, USA
TCE	Sigma-Aldrich, Taufkirchen, Germany
Tris base, Tris-HCl	Sigma-Aldrich, Taufkirchen, Germany
Triton X-100	Merck, Darmstadt, Germany
Trypsin	PAN Biotech, Aidenbach, Germany
Tween 20	Bio-Rad Laboratories GmbH, Munich, Germany
Vincristine sulfate	Sigma-Aldrich, Taufkirchen, Germany

Table 2.3: Commonly used media, solutions, and buffers for cell culture

PBS (pH 7.4)	
NaCl	132.2 mM
Na_2PO_4	10.4 mM
KH_2PO_4	3.2 mM
H_2O	

PBS + Ca^{2+}/Mg^{2+} (pH 7.4)	
NaCl	137 mM
KCl	2.68 mM
Na_2PO_4	8.10 mM
KH_2PO_4	1.47 mM
$MgCl_2$	0.25 mM
$CaCl_2$	0.5 mM
H_2O	

K562, CCRF/VCR-CEM medium	
RPMI 1640	500 ml
FCS	50 ml
Pen/Strep*	5 ml

Jurkat medium	
RPMI 1640	500 ml
FCS	50 ml
Pyruvate 100 mM	5 ml
Pen/Strep*	5 ml

HL-60 medium	
IMDM	500 ml
FCS	100 ml
Pen/Strep*	5 ml

Huh7/MDA-MB-231 medium	
DMEM	500 ml
FCS	50 ml
Pen/Strep*	5 ml

Collagen coating solution	
Collagen G	0.001 %
PBS	

Trypsin/EDTA	
Trypsin	0.05 %
EDTA	0.20 %
PBS	

*Pen/Strep: Penicillin 10 000 Units/ml, Streptomycin 10 mg/ml

2.2 Methods

2.2.1 Cell culture

Different cell lines of human lymphoid and myeloid leukemia were used. The chronic myeloid leukemia (CML) cell line K562 was purchased from Leibniz Institute DSMZ (Braunschweig, Germany). The T-ALL (T-cell acute lymphoblastic leukemia) cell line S-Jurkat were provided by P. H. Krammer and H. Walczak (Heidelberg, Germany). CCRF-CEM and vincristine-resistant (VCR-) CEM (T-ALL) were obtained from M. Kavallaris (Sydney, Australia) and HL-60 (Acute promyelocytic leukemia) cells were purchased from ATCC (Manassas, VA, USA). Huh7 cells were purchased from the Japanese Collection of Research Bioresources (JCRB) (Osaka, Japan) and the human mammary carcinoma cell line MDA-MB-231 was obtained from Cell Lines Service (Eppelheim, Germany). Cells were routinely cultured under constant humidity at 37 °C and 5 % CO_2. Cell density was kept between 0.1 x 10^6 and 1 x 10^6 cells/ml (K562, Jurkat, HL-60) and 0.2 x 10^6 and 2 x 10^6 cells/l (CCRF-CEM, VCR-CEM). Cell number and viability were determined using Vi-Cell^{TM} XR cell viability analyzer (Beckman Coulter, Krefeld, Germany). Huh7 and MDA-MB-231 cells were sub-cultured every three to four days. Cells were detached using trypsin/ethylenediaminetetraacetic acid (Trypsin/EDTA). Appropriate cell numbers were reseeded in either culture flasks or multiwell-plates for further experiments. For Huh7 cells, all culture flasks and multiwell-plates were coated with Collagen coating solution prior to use.
Cells were routinely tested for contamination with mycoplasma using PCR detection kit VenorGeM (Minerva Biolabs, Berlin, Germany).

2.2.1.1 Freezing and thawing

For long-term storage in liquid nitrogen cells were washed with PBS and centrifuged (1 000 rpm, 5 min). 1 - 2 x 10^6 cells were resuspended in 1 ml freezing medium and transferred to cryovials. Cells were frozen at –20 °C and transferred to liquid nitrogen afterwards.

Table 2.4: Medium for cell freezing

Freezing medium	
Culture medium	70 %
FCS	20 %
DMSO	10 %

For thawing, the content of a cryovial was dissolved in prewarmed culture medium. Cells were centrifuged immediately, resuspended in fresh culture medium, and transferred to a culture flask. For suspension cells, cell density was adjusted to 0.2 - 0.3 x 10^6 cells/ml.

2.2.1.2 Isolation of PBMCs and cultivation of PDX cells

Peripheral blood mononuclear cells (PBMCs) were isolated from anticoagulated blood (EDTA) friendly provided by Dr. Johanna Liebl (Department of Pharmacy, Ludwig-Maximilians-University, Munich). Gradient centrifugation and Ficoll-Paque PLUS (GE Healthcare Life Sciences, Freiburg, Germany) was used for PBMC isolation according to the manufacturer's protocol. PBMCs were cultured in RPMI 1640 medium supplemented with 20 % FCS. Patient-derived xenograft (PDX) acute lymphoid (ALL) and myeloid leukemia (AML) cells as well as respective growth media were generously provided by Dr. Irmela Jeremias (Research Unit Gene Vectors, Helmholtz Center, Munich Gene Vectors, Helmholtz Center, Munich). The model for PDX cell growth has been predescribed.[78,79]

Table 2.5: Media for PBMC and PDX cell culturing

PDX ALL cell medium	
RPMI 1640	500 ml
FCS	100 ml
L-Glutamine 200 mM	5 ml
Pen/Strep	5 ml
Gentamycin 50 mg/ml	1 ml
Add to 50 ml of medium	
ITS 100x	300 µl
Pyruvate 100 mM	500 µl
α-TG	21.7 µl

PDX AML cell medium	
StemPro-34 medium	50 ml
Nutrient supplement	1.3 ml
Pen/Strep	0.5 ml
L-Glutamine 200 mM	0.5 ml
FCS	1 ml
FLT3-L	10 ng/ml
SCF	10 ng/ml
TPO	10 ng/ml
IL-3	10 ng/ml

PBMC medium	
RPMI 1640	500 ml
FCS	100 ml
Pen/Strep	1 ml

2.2.2 Cell viability assays

Cell viability was analyzed using CellTiter-Blue™ and CellTiter-Glo™ Luminescent Cell Viability Assay (Promega, Madison, WI, USA). Experiments were carried out following the manufacturer's protocol. Briefly, cells were seeded in 96-well plates and treated with the compounds or DMSO as indicated for different periods of time. Cell viability was determined by addition of CellTiter-Blue™ reagent, further two to four hours of incubation followed by a fluorescence readout using SpectraFluor Plus™ (Tecan, Crailsheim, Germany). Cellular ATP levels were measured by addition of CellTiter-Glo™ reagent and measurement of luminescence signal using OrionII microplate luminometer (Titertek Berthold, Pforzheim, Germany).

2.2.3 Colony formation assay

For assessment of the impact of the compound on colony formation, cells were treated with compound as indicated or DMSO for 24 h. Cells were reseeded in 12-well plates in colony formation medium (5 x 10^3 cells/ml) and incubated for further 7 days. Colonies were visualized by addition of MTT (3-(4,5-dimethylthiazol-2-yl)-2,5-diphenyltetrazolium bromide) reagent (Promega, Madison, WI, USA) and incubation for further 2 h. Colony count was evaluated using ImageJ software.

Table 2.6: Medium for colony formation assay

Colony formation medium	
Normal culture medium	60 ml
FCS	40 ml
Pen/Strep	1 ml
Methylcellulose	0.52 %

2.2.4 Flow cytometry

For flow cytometric measurements a FACS CantoII device (BD Biosciences, Heidelberg, Germany) was used. FlowJo 7.6 software (Tree Star Inc., Ashland, OR, USA) was used for further data analysis.

Table 2.7: Buffers and staining solutions for flow cytometry

FACS Flow™	
Na_2HPO_4	1.0 %
NaCl	0.1 %
2-Phenoxyethanol	1.0 %
NaF	1.0 %
EDTA Na_2 Dihydrate	1.0 %
H_2O	

FACS Clean™	
NaClO	1.0 %
NaOH	0.8 %
H_2O	

PI staining solution	
PI	5 µg/ml
PBS	

HFS-PI solution	
Sodium citrate	0.1 %
Triton X-100	0.1 %
PI	50 µg/ml
PBS	

2.2.4.1 Propidium iodide (PI) exclusion assay

PI exclusion assay was used to evaluate cell membrane integrity and general condition of cells upon treatment. Propidium iodide is not membrane permeable but can enter the cell and intercalate into DNA in case of cell damage and loss of membrane integrity. For PI exclusion assay cells were treated as indicated and incubated for different periods of time. Cells were collected, washed with cold PBS, pelleted (600 x g, 5 min, 4 °C), and incubated with PI staining solution for 5 min on ice. The PI positive population was gated in the histogram plot.

2.2.4.2 Assessment of apoptotic cell death

Cells were treated as indicated and incubated for 48 h. In case of co-treatment with Q-VD-OPh, the pan-caspase inhibitor was added 30 min before compound treatment. Apoptotic cell death was analyzed using two different methods.

First, cell death was measured as predescribed by Nicoletti *et al.*[80] In brief, cells were collected, washed in cold PBS, pelleted (600 x g, 5 min, 4 °C), and incubated with hypotonic fluorochrome solution containing propidium iodide (HFS-PI solution). The amount of DNA within the cell depends on the stage of cell cycle and can be measured by means of the DNA intercalating dye PI. Apoptotic cells show a broad subG1 phase peak and were gated in the histogram plot (Figure 2.1).

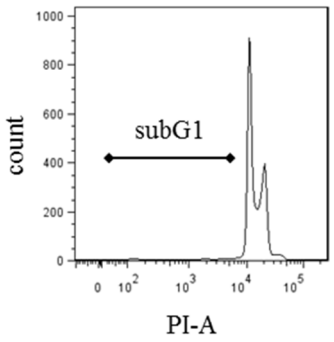

Figure 2.1: SubG1 gating in Nicoletti assay histogram plot.

Second, cell death of PDX cells and PBMCs was determined by using forward and side scatter plot signals (FSC-SSC). Depending on the FSC-SSC signal, cells can be analyzed regarding their size (FSC) and granularity (SSC). During apoptosis, cell shrinkage and a higher particle content are observed which can be measured by decreased FSC and increased SSC signals. Viable and dead cells were gated in FSC-SSC dot plots (Figure 2.2).

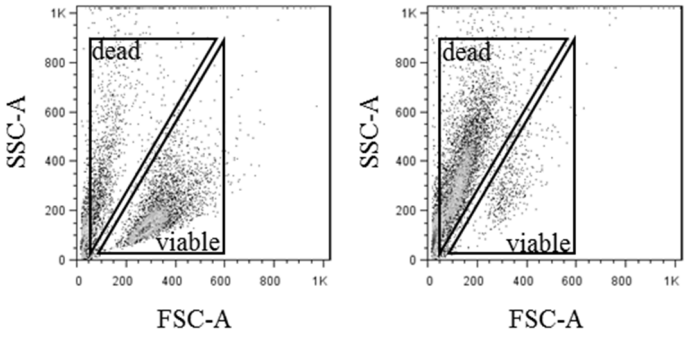

Figure 2.2: Viable and dead cell gating according to FSC-SSC signals and dot plot.

Percentage of specific cell death was calculated using the formula 100 x [experimental cell death (%) – spontaneous cell death (%)] / [100 % - spontaneous cell death (%)].[81] In order to assess chemosensitivity, Bliss values were calculated using the formula [specific cell death combined treatment / (specific cell death compound 1 + specific cell death compound 2 – specific cell death compound 1 x specific cell death compound 2)].[82] Bliss values > 1.05 indicate synergistic, 0.95 - 1.05 additive, and < 0.95 antagonistic effects.

2.2.4.3 Measurement of mitochondrial membrane potential (MMP)

Functional mitochondria are characterized by their mitochondrial membrane potential (MMP) which is disturbed for example during apoptosis. For measurement of MMP, the cationic dye JC-1 (Enzo Life Sciences, Farmingdale, NY, USA) was used. The dye exhibits green fluorescence as a monomer whereas the aggregates formed in mitochondria with an intact membrane potential show a red fluorescent signal. For assessment of MMP, cells were treated with compound or DMSO for the indicated time-points. JC-1 staining solution (10x) was prepared in prewarmed medium. As a positive control, Carbonyl cyanide 3-chlorophenylhydrazone (CCCP) (Sigma-Aldrich, Taufkirchen, Germany), an uncoupler of oxidative phosphorylation, was added during staining (50 µM). JC-1 staining solution was added directly to the intended wells for 30 min (37 °C, 5 % CO_2) to a final concentration of 2 µM. Red and green fluorescence were analyzed by flow cytometry. Compensation was performed using BD™ CompBeads Anti-Mouse Ig, κ particles and AlexaFluor488/PE mouse IgG2b, κ isotype control antibodies (BD Biosciences, Heidelberg, Germany). The compensation beads were prepared as described in the manufacturer's manual in staining buffer (2 % FCS in PBS). Cells with an intact MMP were gated in dot plots (Figure 2.3).

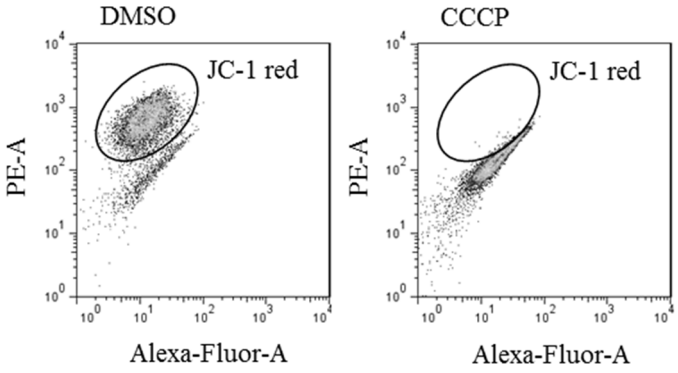

Figure 2.3: JC-1 aggregate gating in dot plot for MMP analysis.

2.2.4.4 Measurement of mitochondrial ROS generation

The electron transport chain (ETC) is a major site of reactive oxygen species (ROS) production. For assessment of mitochondrial ROS, MitoSOX™ dye (Thermo Fisher Scientific, Waltham, MA, USA) was used. The staining was conducted following the manufacturer's protocol. In brief, cells were treated with the compound in the indicated concentrations for 6 h. Antimycin A (20 µM, 45 min, 37 °C, 5 % CO_2), an inhibitor of the ETC complex III, was used as positive control (Sigma-Aldrich, Taufkirchen, Germany). The dye was diluted in DMSO to 5 mM concentration and further diluted in HBSS buffer (Sigma-Aldrich, Taufkirchen, Germany) to a 5 µM working solution. Cells were harvested, washed with PBS, and incubated with MitoSOX™ working solution for 30 min (37 °C, 5 % CO_2). Further steps were conducted at 4 °C. Cells were harvested, washed with PBS, and resuspended in an appropriate volume of PBS. Mean fluorescence intensities (MFI) and histogram plots were used for evaluation of ROS^{mt} generation.

2.2.5 Immunoblotting

2.2.5.1 Sample preparation and protein quantification

Cells were treated as indicated and lysed in Milanese lysis buffer (modified RIPA buffer). Samples were frozen at –80°C for 15 min and centrifuged (14 000 rpm, 10 min, 4 °C). Protein concentrations of the lysates (supernatants) were determined using Bradford Reagent™ (Bio-Rad Laboratories GmbH, Munich, Germany). Absorbance was measured with SpectraFluor Plus™ (Tecan, Crailsheim, Germany) and protein concentrations were determined using linear regression. 5x sample buffer was added to each sample. Protein concentrations were adjusted by addition of 1x SDS sample buffer (5x sample buffer diluted 1:5 in RIPA buffer). Protein samples were heated to 95 °C for 5 min and stored at –20 °C.

Table 2.8: Buffers for protein sample preparation

RIPA lysis buffer	
Tris-HCl (pH 7.4)	50 mM
NaCl	150 mM
Nonidet NP40	1 %
Deoxycholic acid	0.25 %
SDS	0.10 %
H_2O	

5x SDS sample buffer	
Tris-HCl, 3.125 M, pH 6.8	10 %
SDS	5 %
Glycerol	50 %
DTT	2 %
Pyronin Y	0.025 %
H_2O	

Milanese lysis buffer	
Na_2VO_3	300 µM
NaF	1 mM
β-Glycerophosphate	3 mM
Pyrophosphate	10 mM
RIPA lysis buffer	
Add before use:	
Complete®	4.0 mM
PMSF	1.0 mM
H_2O_2	0.6 mM

2.2.5.2 SDS-PAGE, tank electroblotting, and protein detection

For SDS-polyacrylamide gel electrophoresis (SDS-PAGE), discontinuous polyacrylamide gels were loaded with the protein samples. The electrophoresis was performed by means of a Consort Electrophoresis Power Supply E835 device (Sigma-Aldrich, Taufkirchen Germany) with 100 V for 21 min (protein stacking) followed by 45 min at 200 V (protein separation). The prestained protein ladder PageRuler^{TM} (Fermentas, St. Leon-Rot, Germany) was used as molecular weight marker. Protein load was measured directly after electrophoresis on the stain-free gel using ChemiDoc Touch Imaging System (Bio-Rad Laboratories GmbH, Munich, Germany).

Table 2.9: Reagents and buffers for electrophoresis

Stacking gel	
Rotiphorese™ Gel 30	17 %
Tris (pH 6.8)	125 mM
SDS	0.1 %
TEMED	0.2 %
APS	0.1 %
H_2O	

Separation gel 10 %/12 %	
Rotiphorese™ Gel 30	33 %/40 %
Tris (pH 8.8)	375 mM
SDS	0.1 %
TEMED	0.1 %
APS	0.05 %
TCE	0.05 %
H_2O	

Electrophoresis buffer	
Tris base	4.9 mM
Glycine	38 mM
SDS	0.1 %
H_2O	

After SDS-PAGE, proteins were transferred onto a nitrocellulose membrane (Hybond-ECL™, Amersham Bioscience, Freiburg, Germany) by tank blotting. Protein transfer was carried out at 4 °C, 100 V for 90 min in 1x tank buffer.

Table 2.10: Buffers for tank electroblotting

5x Tank buffer	
Tris base	240 mM
Glycine	195 mM
H_2O	

1x Tank buffer	
5x Tank buffer	20 %
Methanol	20 %
H_2O	

Membranes were blocked with 5 % non-fat dry milk powder (Blotto) (Carl Roth, Karlsruhe, Germany) and incubated with the respective primary antibody at 4 °C overnight or at RT for 2 h followed by incubation with the corresponding horseradish peroxidase (HRP)-conjugated secondary antibody (1 h, RT). Protein bands were visualized using enhanced chemiluminescence solution (ECL) and ChemiDoc Touch Imaging System. For quantification of band intensity, Image Lab™ Software was used (Bio-Rad Laboratories GmbH, Munich, Germany).

Table 2.11: Substrate solution for enhanced chemiluminescence detection

ECL solution	
Tris (pH 8.5)	100 mM
Luminol	2.5 mM
p-Coumaric acid	1 mM
H_2O_2	17 µM
H_2O	

Table 2.12: Primary antibodies

Antigene	**Source**	**Dilution**	**Provider**
β-actin	Mouse	1:1000	Merck, Darmstadt, Germany
Caspase 3	Rabbit	1:1000	Santa Cruz Biotechnology, Dallas, TX, USA
ClpP	Mouse	1:1000	Abcam, Cambridge, UK
ClpX	Rabbit	1:500	Abcam, Cambridge, UK
Hsp60	Goat	1:1000	Santa Cruz Biotechnology, Dallas, TX, USA
PARP	Rabbit	1:1000	Cell Signaling Technology, Danvers, MA, USA

Table 2.13: Secondary antibodies

Antibody	**Dilution**	**Provider**
HRP, Donkey anti-goat IgG	1:1000	Abcam, Cambridge, UK
HRP, Goat anti-mouse IgG	1:1000	Santa Cruz Biotechnology, Dallas, TX, USA
HRP, Goat anti-rabbit IgG	1:1000	DIANOVA GmbH, Hamburg, Germany

2.2.6 Carbonylation assay

For analysis of protein carbonylation the Oxidized Protein Western Blot Kit (Abcam, Cambridge, UK) was used according to the manufacturer's protocol. In brief, cells were treated with compound or DMSO for 6 h. H_2O_2 treatment (1 mM, 1 h) served as positive control. Cells were lysed and carbonyl groups in the protein side chains were derivatized to 2,4-dinitrophenylhydrazone (DNP-hydrazone) by treatment with 2,4-dinitrophenyl-hydrazine (DNPH). Polyacrylamide gel electrophoresis and western blot were performed (see 2.2.5.2). Membranes were incubated with a primary antibody against DNP followed by a secondary HRP-conjugated antibody and chemiluminescence detection.

2.2.7 Quantitative real-time PCR (q rtPCR)

Cells were treated as indicated and total RNA was isolated using RNeasy mini Kit (Qiagen GmbH, Hilden, Germany) according to the manufacturer's protocol. The concentration of the purified RNA was determined by means of a NanoDrop® ND-1000 spectrophotometer (Peqlab Biotechnology GmbH, Erlangen, Germany). The obtained RNA was re-transcribed into complementary DNA (cDNA) using the High Capacity cDNA Reverse Transcription Kit (Applied Biosystems, Foster City, CA, USA). CDNA samples were stored at 4 °C until use for quantitative real-time PCR (q rtPCR). A QuantStudio 3 Real-Time PCR System device (Thermo Fisher Scientific, Waltham, MA, USA) was used. Either TaqMan Gene Expression Master Mix (Life Technologies Corporation, Carlsbad, CA, USA) or SYBR Green Master Mix (Thermo Fisher Scientific, Waltham, MA, USA) were used depending on the utilized primer. The ClpP primer was also purchased from Thermo Fisher Scientific. GAPDH or actin were used as housekeeping genes. TaqMan primers for GAPDH were obtained from Biomers (Ulm, Germany). SYBR Green primers were purchased from metabion international AG (Planegg/Steinkirchen, Germany). Average CT values of target genes were normalized to control as ΔCT. Changes in RNA levels were shown as fold expression ($2^{-\Delta\Delta CT}$) calculated by the ΔΔCT method.

Table 2.14: Sequences of SYBR Green primers

Primer	Forward 5' – 3'	Reverse 5' – 3'
Actin	TTC ACC TAC AGC AAG GAC GA	GAA CTC GAA GAT GGG GTT GA
CHOP	TTG CCT TTC TCC TTC GGG AC	CAG TCA GCC AAG CCA GAG AA
Hsp60	GGA CAC GGG CTC ATT GCG	TTC TTC AGG GGT GGT CAC AG

2.2.8 Stable isotope labeling with amino acids in cell culture (SILAC)

For SILAC experiment, K562 cells were cultured with SILAC medium (Thermo Fisher Scientific, Waltham, MA, USA), containing different stable isotope labeled (medium, heavy) or non-labeled amino acids (light). Media and amino acids were friendly provided by Prof. Dr. Stephan A. Sieber (Department of Chemistry, Technical University of Munich, Garching). Prior to compound treatment, K562 cells were cultured for 5-6 doublings in light, medium, and heavy labeled SILAC medium (Table 2.15).

Labeled cells were treated with 10 µM compound for 24 and 48 h or with DMSO. Cell lysis, sample preparation, and quantitative mass spectrometry analysis was done by Anja Fux and Matthias Stahl (Department of Chemistry, Technical University of Munich, Garching).

Table 2.15: Medium for SILAC experiment

SILAC medium	
SILAC RPMI 1640	500 ml
FCS, dialyzed, heat inactivated	50 ml
L-Glutamine 200 mM	5 ml
L-Arginine*	375 µl
L-Lysine*	375 µl

*light, medium, and heavy isotope labeled amino acids, see Table 2.16

Table 2.16: Used amino acids with different isotope labeling

Amino acid	**Mass difference**	**Isotope label**	**Stock concentration**
L-Lys-HCl (182.65 g/mol)	-	-	101.92 mg/ml
L-Lys-2HCl (223.10 g/mol)	+4	$^{2}H_4$	106.38 mg/ml
L-Lys-HCl (190.65 g/mol)	+8	$^{13}C_6$, $^{15}N_2$	126.73 mg/ml
L-Arg-HCl (210.66 g/mol)	-	-	60.04 mg/ml
L-Arg-HCl (216.60 g/mol)	+6	$^{13}C_6$	61.73 mg/ml
L-Arg-HCl (220.60 g/mol)	+10	$^{13}C_6$, $^{15}N_4$	62.87 mg/ml

2.2.9 Assessment of mitochondrial morphology

For analysis of mitochondrial morphology, MDA-MB-231 cells were seeded in 8-well ibiTreat µ-slides (ibidi GmbH, Munich, Germany) and treated as indicated. Mitochondria were visualized using MitoTracker® Red CMXRos (Thermo Fisher Scientific, Waltham, MA, USA) according to the manufacturer´s instructions. In brief, a staining solution (1 mM in DMSO) was prepared. Growth medium was removed and the cells were incubated with staining solution (200 nM in growth medium) for 30 min (37 °C, 5 % CO_2). Afterwards, the staining solution was replaced with fresh growth medium and mitochondrial morphology was assessed by live-cell imaging by means of a Leica-SP8 confocal microscope (Leica Microsystems, Wetzlar, Germany) in an incubation chamber at 37 °C, 80 % humidity and 5 % CO_2 (okolab S.r.l., Pozzuoli, Italy).

For electron microscopy, Jurkat cells were treated as indicated, washed, pelleted, and fixed in 6.25 % glutaraldehyde. Embedding and preparation of sample sections were done by Sabine Schäfer (Institute of Pathology, Ludwig-Maximilians-University, Munich). Electron microscopy was performed in the laboratory of Prof. Dr. med. Jens Waschke (Institute of Anatomy and Cell Biology, Ludwig-Maximilians-University, Munich).

2.2.10 Statistical analysis

The experiments were performed at least three times unless otherwise indicated. Statistical evaluation was done by means of GraphPad Prism software (version 5.04; GraphPad Software, San Diego, CA, USA). Bar graphs are shown as mean ± SEM. For comparison of two groups, a t-test was performed. Three or more groups were compared by one-way analysis of variance (ANOVA) followed by Tukey’s Multiple Comparison Test unless otherwise indicated. Statistical significance was assumed if $p < 0.05$.

3 Results

3.1 Characterization of functional effects of ClpXP inhibitors

3.1.1 ClpXP expression in different leukemia cell lines

In a first western blot experiment, expression of the ClpX chaperone and the ClpP peptidase subunit in different leukemia cell lines was determined (Figure 3.1). Both were expressed most prominent in the cell lines K562 (CML) and Jurkat (T-ALL). The subunits occurred to a lower extent in CEM cells (T-ALL). HL-60 (AML) cell line showed the lowest ClpP and ClpX protein levels.

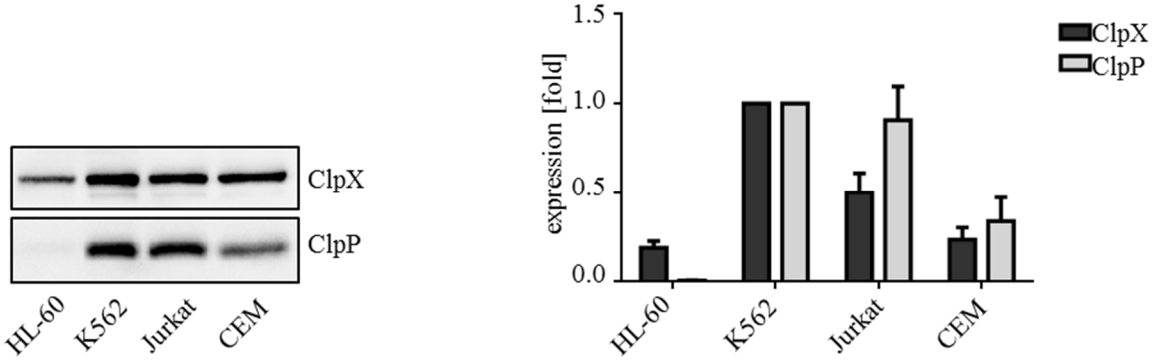

Figure 3.1: ClpX and ClpP subunits are expressed in various leukemia cell lines. Western blot for ClpX and ClpP in HL-60, K562, Jurkat, and CEM cells is shown. Bar diagram displays quantification of ClpX and ClpP protein expression normalized to K562 cell line. Whole protein bands served as loading control for quantification (n=3).

3.1.2 ClpXP inhibition affects cell viability

Several above mentioned structures with different activity against ClpXP subunits or the whole complex were tested regarding their inhibitory properties in human leukemic cancer cell lines. K562 and Jurkat cells representative for leukemia cells from myeloid and lymphoid trait were used (Figure 3.2 A, B). In the first group of structures (319, 334, 335, and 339) 334 revealed to have the strongest effect on cell viability of both cell lines. 335 showed to be least effective (Figure 3.2 A) in accordance to its activity on bacterial ClpXP complex but not human ClpXP complex. The second inhibitor group with activity towards the ClpP subunit affected cell viability of the cell lines only moderately with TG53 being the most potent ClpP inhibitor structure (Figure 3.2 B). In general, Jurkat cell viability was decreased to a greater extent than K562 cell viability. A table of IC50 values is attached (Appendix A.2, Figure A.1).

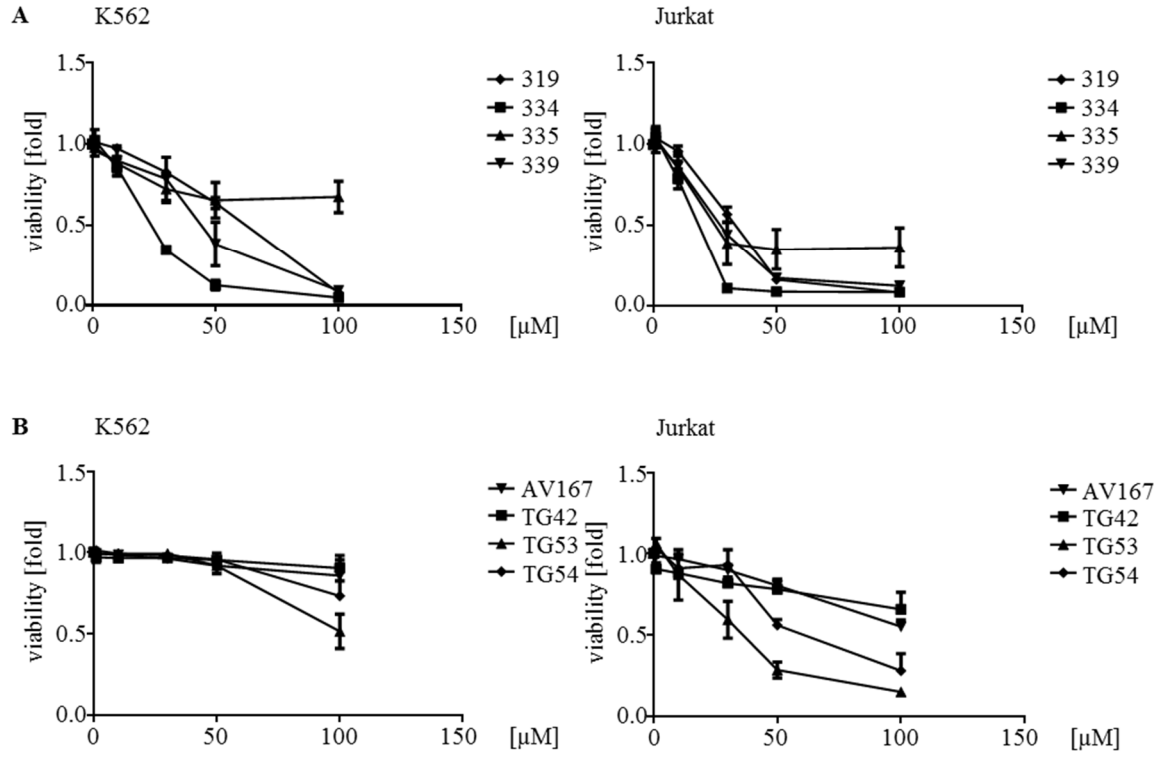

Figure 3.2: ClpXP inhibitors affect cell viability of K562 and Jurkat cells. Cell viability of K562 and Jurkat cells upon indicated ClpXP/ClpX (A) or ClpP (B) inhibitor treatment is shown (72 h). CellTiter-Blue™ reagent was used. Viability was normalized to DMSO treated control (n=3).

In order to characterize the most potent compound 334, an inhibitor of the ClpX subunit, further viability assays were performed in additional leukemia cell lines HL-60 and CEM (Figure 3.3). Cell viability was notably decreased in all four cell lines K562, Jurkat, CEM, and HL-60. HL-60 cells with the lowest ClpXP protein expression showed the lowest sensitivity towards the inhibitor 334.

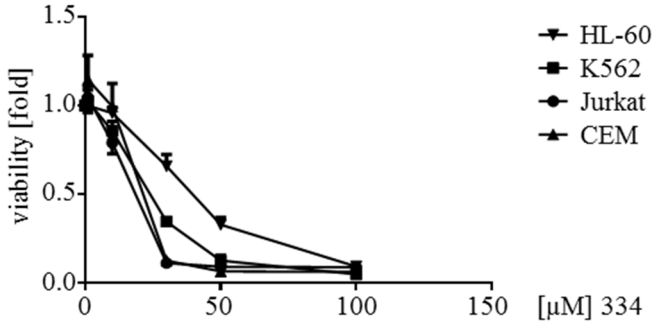

Cell line	IC50 [µM]
HL-60	37.29
K562	21.83
Jurkat	12.93
CEM	16.98

Figure 3.3: ClpX inhibition decreases cell viability of various leukemic cell lines. Cell viability of HL-60, K562, Jurkat, and CEM cells upon ClpX inhibitor treatment (72 h) is shown. CellTiter-Blue™ reagent was used. Viability was normalized to DMSO treated control. Table shows IC50 values calculated using nonlinear regression (n=3).

3.1.3 ClpX inhibition decreases colony formation

For further characterization, the effect of 334 on colony formation was investigated. Therefore, cells were pretreated with 334, reseeded, and grown for further 7 days in the absence of the inhibitor. Colony formation was concentration-dependently decreased in both cell lines K562 and Jurkat (Figure 3.4). Notably, clonogenic growth of K562 cells was affected at lower inhibitor concentrations compared to Jurkat cells.

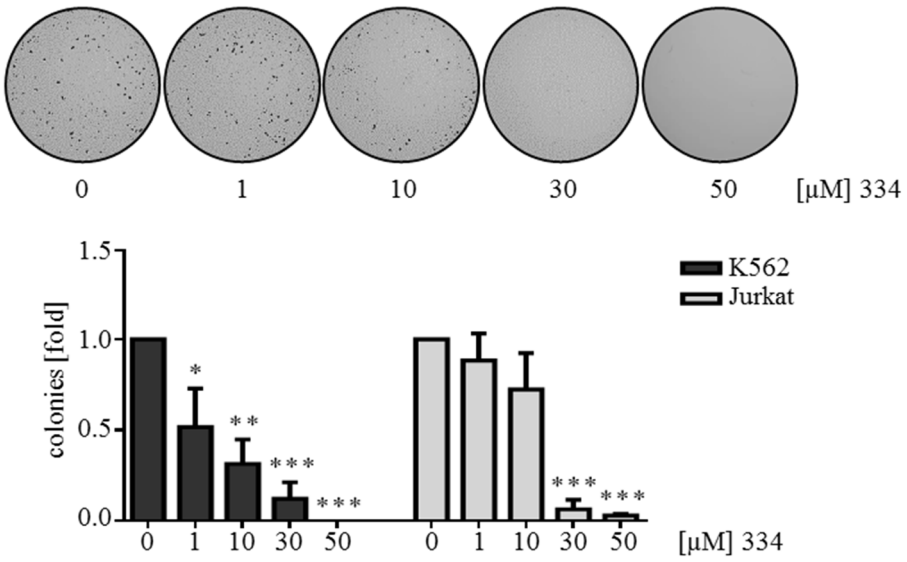

Figure 3.4: ClpX inhibitor impairs clonogenic growth of K562 and Jurkat cells. Colonies formed by Jurkat cells pretreated with 334 for 24 h and grown in the absence of 334 for further 7 days are representatively shown in the upper panel. Bar diagram represents colony count of K562 and Jurkat cells normalized to solvent treated control cells (* $p < 0.05$, ** $p < 0.01$, *** $p < 0.001$, One-way ANOVA, Tukey's Multiple Comparison Test, n=3).

3.1.4 ClpX inhibition induces apoptotic cell death

Besides the impact of ClpX inhibition on cell viability and colony formation, we further focused on apoptotic cell death using the Nicoletti assay. Apoptotic cell death was induced in both cell lines at a concentration of 30 µM of the ClpX inhibitor (Figure 3.5 A). In line, western blot analysis showed PARP cleavage concomitant with the activation of Caspase 3 (Figure 3.5 B) which represent further hallmarks of apoptotic cell death. Pretreatment with the pan-caspase inhibitor Q-VD-OPh was able to prevent K562 and Jurkat cells from cell death induced by high concentrations of 334 (50 µM) underlining the induction of caspase-dependent cell death by the ClpX inhibitor (Figure 3.5 C). In contrast, HL-60 cells with low protein levels of ClpX and ClpP subunits were less sensitive to 334 treatment and showed moderate apoptosis induction at 50 µM of the ClpX inhibitor (Figure 3.5 D).

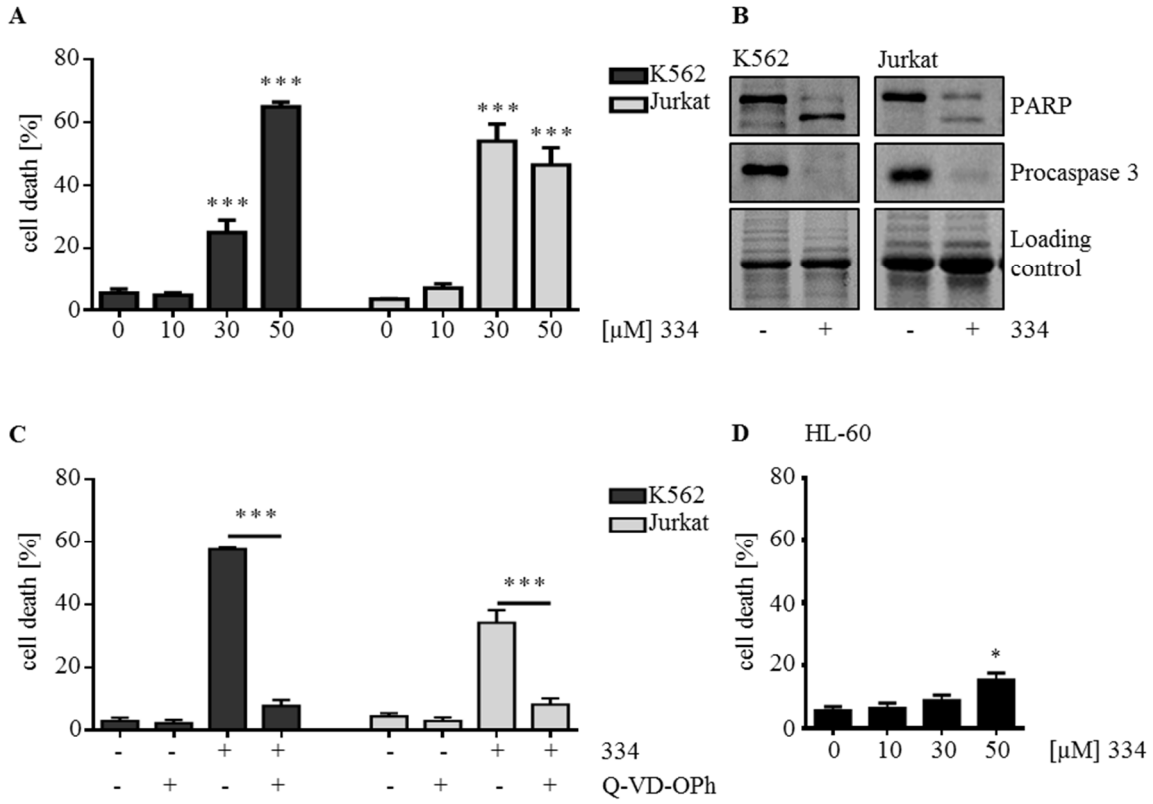

Figure 3.5: ClpX inhibitor induces apoptotic cell death in K562 and Jurkat cells. (A) Bars represent cell death induced by 334 in the indicated concentrations after 48 h of treatment. Cell death was analyzed by flow cytometry using Nicoletti assay. (B) Western blot for PARP and Procaspase 3 is shown for K562 and Jurkat cells treated with 50 µM of 334 (24 h). Stain free whole protein bands serve as loading control (n=3). (C) Bars show cell death induced in cells treated with 334 (50 µM), pretreated with Q-VD-OPh (20 µM, 30 min) alone or a combination of 334 and Q-VD-OPh (48 h). (D) Cell death of HL-60 cells treated with 334 for 48 h is shown (* $p < 0.05$, *** $p < 0.001$, One-way ANOVA, Tukey's Multiple Comparison Test, n=3).

3.1.5 ClpX inhibitor is effective in patient-derived xenograft (PDX) cells

In addition to the induction of cell death in the above mentioned cell lines, the inhibitor was tested in patient-derived xenograft (PDX) cells generously provided by Dr. Irmela Jeremias (Research Unit Gene Vectors, Helmholtz Center, Munich). In this model, primary tumor cells from ALL or AML patients are injected into immune-compromised mice. After growth and the development of the leukemia, PDX cells are re-isolated and can be used for further analysis. Inhibitor treatment induced cell death in almost all PDX cells as well as in isolated peripheral blood mononuclear cells (PBMCs) representing their healthy counterpart and control cells (Figure 3.6 A). Western blot analysis showed the expression of ClpX and ClpP subunits in the used PDX cells and PBMCs (Figure 3.6 B). No correlation between ClpXP protein expression and sensitivity towards the inhibitor could be observed.

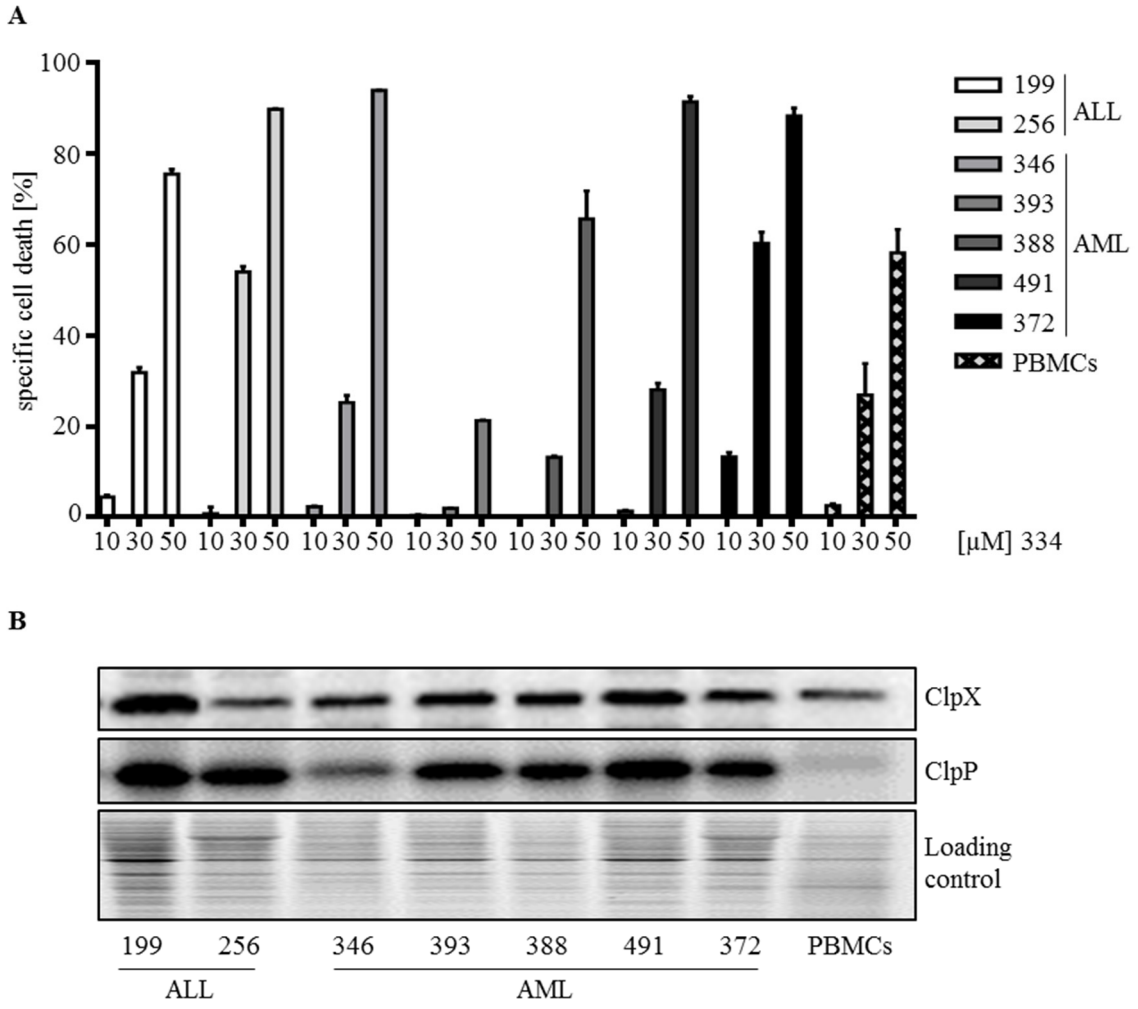

Figure 3.6: ClpX inhibitor induces cell death in PDX cells and PBMCs. (A) Bar diagram shows specific cell death of PDX cells (n=1) and isolated PBMCs (n=3) treated with 334 as indicated for 48 h. Cell death was analyzed by flow cytometry using FSC-SSC plots. (B) Western blot for ClpX and ClpP protein in different PDX cells and PBMCs is shown. Whole protein bands serve as loading control (n=1).

3.1.6 ClpP inhibitors are effective in hepatocellular carcinoma cells

Furthermore, cancer cells derived from other tissues such as liver could exhibit different sensitivity towards ClpXP inhibitors because of their distinct metabolic profile, mitochondrial mass, and reliance on mitochondrial function. In order to address this issue, cell viability and cell death of the hepatocellular carcinoma cell line Huh7 were assessed upon ClpP inhibitor treatment (Figure 3.7). Notably, viability of Huh7 cells was strongly decreased by the ClpP subunit inhibitors TG42 and TG53 which exhibited only slight effects in leukemia cell lines K562 and Jurkat. Moreover, TG42 and TG53 induced apoptotic cell death in Huh7 cells. Huh7 cells showed a medium ClpP and ClpX protein expression compared to K562 cells with high and HL-60 cells with low levels of the subunits (Figure 3.7 B).

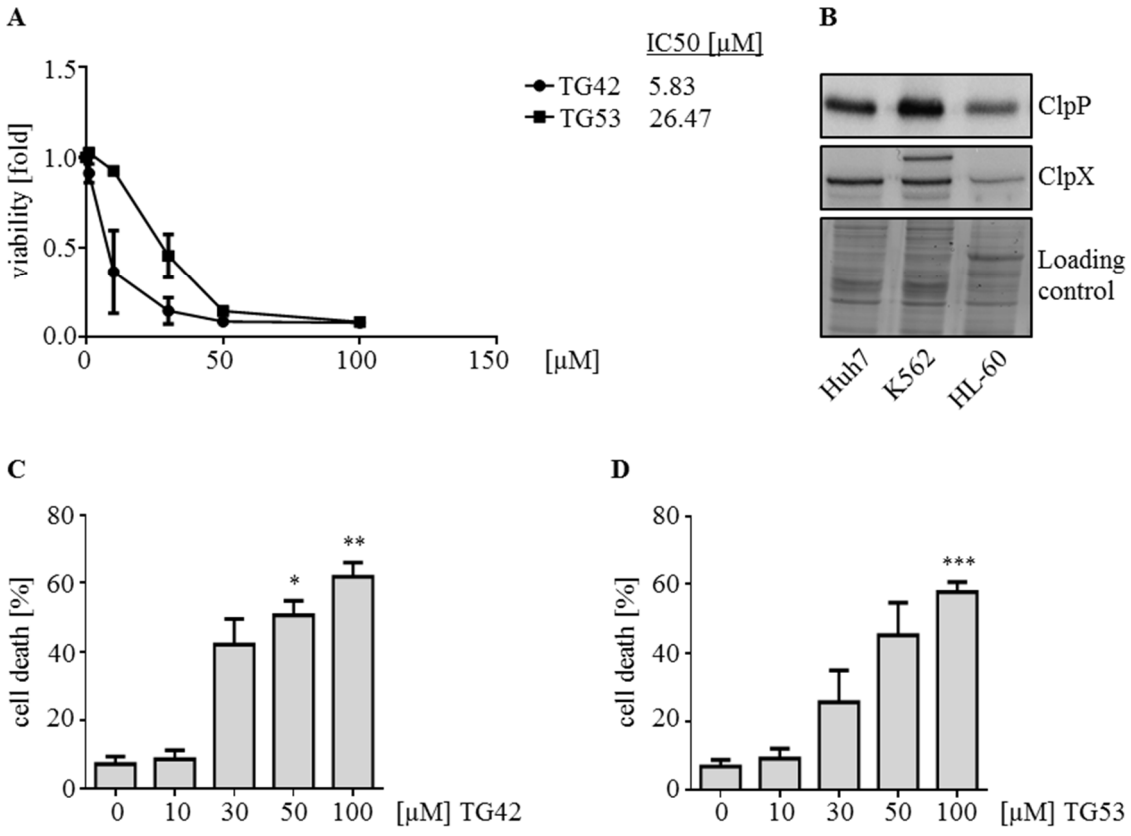

Figure 3.7: Hepatocellular carcinoma cells exhibit high sensitivity towards ClpP inhibitors in terms of cell viability and cell death. (A) Cell viability of Huh7 cells upon indicated ClpP inhibitor treatment (72 h) is shown. CellTiter-Blue™ reagent was used. Viability was normalized to DMSO treated control. IC50 values calculated using nonlinear regression are shown (n=3). (B) Western blot for ClpP and ClpX subunits expression of Huh7 compared to K562 and HL-60 cells is shown. Whole protein bands serve as loading control (n=3). (C, D) Bars represent cell death of Huh7 cells induced by TG42 (C) and TG53 (D) in the indicated concentrations after 48 h of treatment. Cell death was analyzed by flow cytometry using Nicoletti assay (* $p < 0.05$, ** $p < 0.01$, *** $p < 0.001$, One-way ANOVA, Tukey's Multiple Comparison Test, n=3).

3.2 Mechanistic studies on ClpXP inhibition

3.2.1 ClpXP inhibition leads to a fast decline in ATP

For further characterization of the inhibitors and better understanding of the underlying signaling mechanisms, additional experiments were performed with Jurkat cells. Thereby, the main focus was laid on mitochondrial function and integrity. The electron transport chain (ETC) located within the inner mitochondrial membrane is the major production site of cellular ATP. First, we analyzed cellular ATP levels after short inhibitor treatment using CellTiter-Glo™ reagent (Figure 3.8 A). Compared to cellular ATP, overall cell viability measured by CellTiter-Blue™ was decreased to about 50 % by inhibitor concentrations whereas cellular ATP was completely abolished. Accordingly, the ClpP subunit inhibitor TG53 exhibited similar effects on ATP levels (Figure 3.8 B) suggesting a specific effect on mitochondrial respiration.

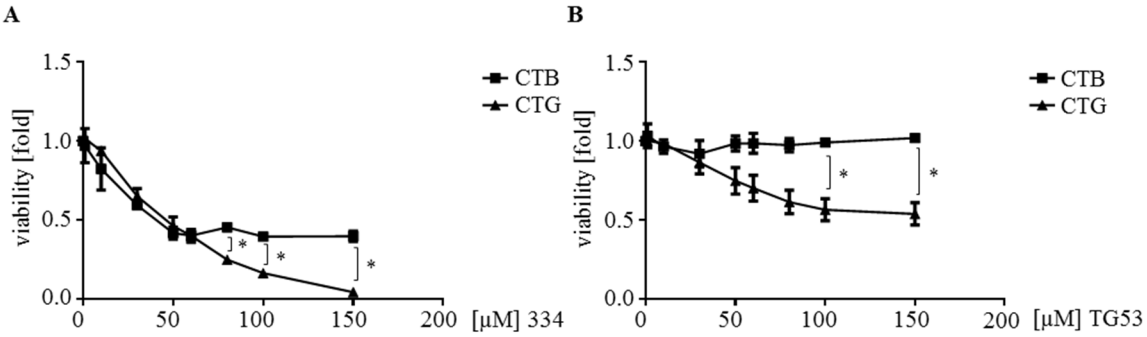

Figure 3.8: Short-term ClpXP inhibition leads to decreased ATP levels. Diagrams show cell viability of Jurkat cells assessed by CellTiter-Blue™ (CTB) and cellular ATP levels measured by CellTiter-Glo™ (CTG) reagent after 3 h of ClpX (A) or ClpP (B) inhibitor treatment in the indicated concentrations (* $p < 0.05$, t-test, Holm-Sidak method, n=3).

3.2.2 ClpX inhibition causes ROS^{mt} generation and protein carbonylation

Physiological metabolic activity of cells is accompanied with production of low concentrations of mitochondrial reactive oxygen species (ROS^{mt}) as a by-product of mitochondrial respiration. However, mitochondrial dysfunction, e.g., a defect in the ETC causes the production of high amounts of ROS^{mt} which further affect mitochondrial integrity and cell fate. As inhibitor of the ETC complex III, Antimycin A promotes the production of ROS^{mt}. Interestingly, ROS^{mt} production was increased concentration-dependently by the ClpX inhibitor 334 (Figure 3.9 A). Further, ROS are responsible for oxidation of proteins, more precisely protein carbonylation. Carbonyl proteins represent a marker for oxidative

stress. Carbonyl groups additionally serve as tag for catalytical degradation of proteins by cellular peptidases. These groups can be derivatized to 2,4-dinitrophenylhydrazone and detected by western blot using a primary antibody against the derivatized carbonyl groups. ClpX inhibitor treatment led to moderate protein carbonylation in comparison to hydrogen peroxide treated cells (Figure 3.9 B). PI exclusion assays at short time-points of treatment and the indicated concentrations of the inhibitor proof the integrity of cell membrane and exclude that effects were due to general bad condition of the cells (Figure 3.9 C).

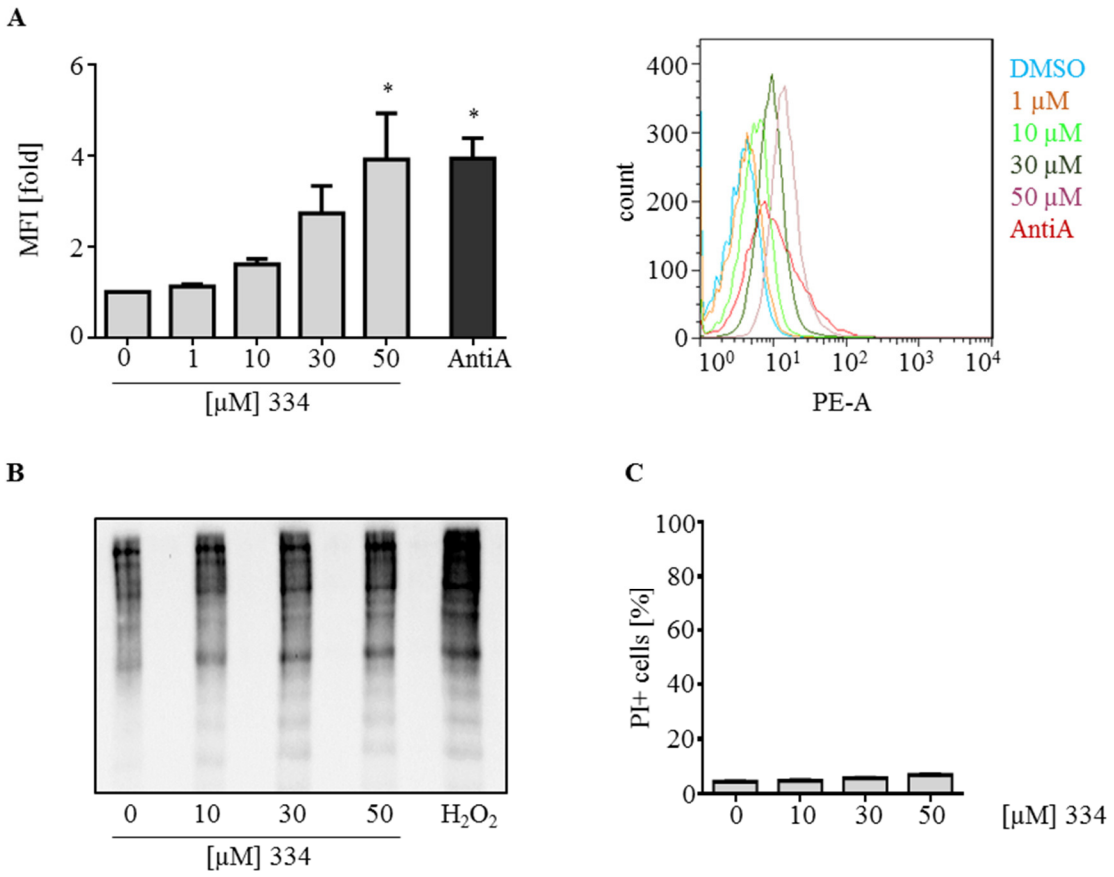

Figure 3.9: ClpX inhibition drives mitochondrial ROS production and protein carbonylation. (A) Mitochondrial ROS production assessed by flow cytometry and MitoSOX™ reagent is shown as mean fluorescence intensity (MFI) in the bar diagram (left) and histogram plot (right). Cells were treated with 334 as indicated (6 h) or Antimycin A (AntiA) as positive control (20 µM, 1 h). (B) Western blot shows bands of carbonylated proteins after treatment with indicated concentrations of 334 (6 h) or H_2O_2 serving as positive control (1 mM, 1 h). (C) Bar diagram represents PI positive (PI+) cells after 334 treatment for 6 h measured by flow cytometry (* $p < 0.05$, One-way ANOVA, Tukey's Multiple Comparison Test, n=3).

3.2.3 ClpX inhibition disrupts mitochondrial membrane potential

The mitochondrial membrane potential (MMP) presents the potential difference across the inner membrane of the mitochondrion and is essential for the maintenance of mitochondrial ATP production. Loss of MMP is observed as an initial event in intrinsic apoptosis signaling.

Former results reveal the impairment of mitochondrial function, the decrease in ATP levels, as well as the increase in ROS^{mt} production. They all point to a disturbed function of the electron transport chain. In line, mitochondrial membrane potential assessed by JC-1 dye staining and flow cytometry was disturbed already after 6 h of ClpX inhibition and complete loss of MMP was visible at later time-points (Figure 3.10 A). PI exclusion displayed that cell membrane integrity was not affected at 6 h of treatment using the same inhibitor concentration (30 µM) but started at 24 h of treatment (Figure 3.10 B).

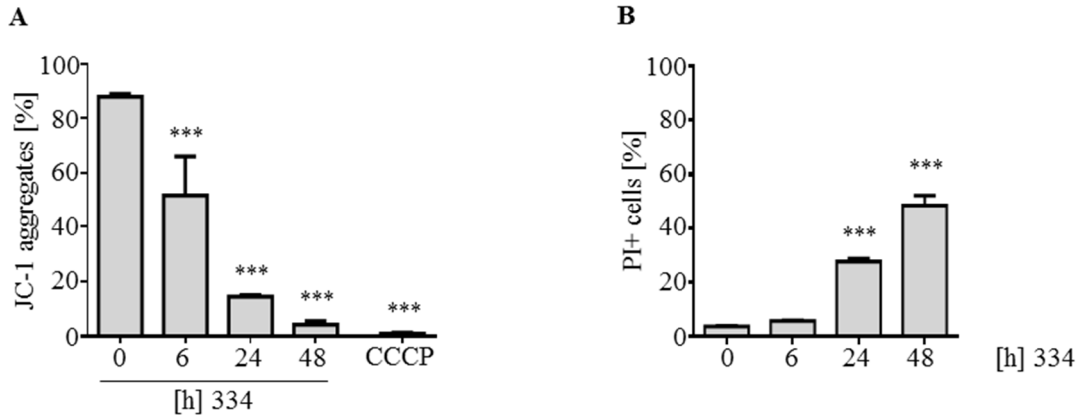

Figure 3.10: ClpX inhibition disrupts mitochondrial membrane potential. (A) Disruption of MMP by 334 (30 µM) at the indicated time-points is shown. Carbonyl cyanide 3-chlorophenylhydrazone (CCCP) served as positive control. JC-1 dye aggregates indicate mitochondria with intact MMP and were measured using flow cytometry. (B) PI exclusion assay for the indicated time-points of ClpX inhibitor treatment (30 µM) is shown (*** $p < 0.001$, One-way ANOVA, Tukey's Multiple Comparison Test, n=3).

3.2.4 ClpX inhibition influences proteins involved in the UPR^{mt}

Besides other mitochondrial proteases such as Lon protease, the role of the ClpXP protease in mitochondria includes the mitochondrial proteostasis. As already shown, inhibition of the protease promotes changes in mitochondrial energy production, mitochondrial integrity, and carbonylation of proteins. The focus was further laid on mitochondrial unfolded protein response (UPR^{mt}) stress signaling that is thought to be regulated by, inter alia, ClpXP itself. A common marker of mitochondrial stress is the heat shock protein 60 (Hsp60). Notably, Hsp60 was found to be decreased on protein (Figure 3.11 A) and transcriptional level (Figure 3.11 B). ClpP itself was decreased in cells treated with higher concentrations (30 µM) of ClpX inhibitor but only on the protein level (Figure 3.11 A). Further, quantitative real-time PCR revealed CHOP to be drastically elevated after 30 µM of ClpX inhibitor treatment. CHOP represents a common marker and transcription mediator of the mitochondrial but also the endoplasmic reticulum stress signaling response. On the one hand, this provides evidence

for general stress conditions occurring upon ClpX inhibition, but on the other hand, an impairment of the UPR^{mt} signaling displayed by a missing induction of Hsp60 and ClpP.

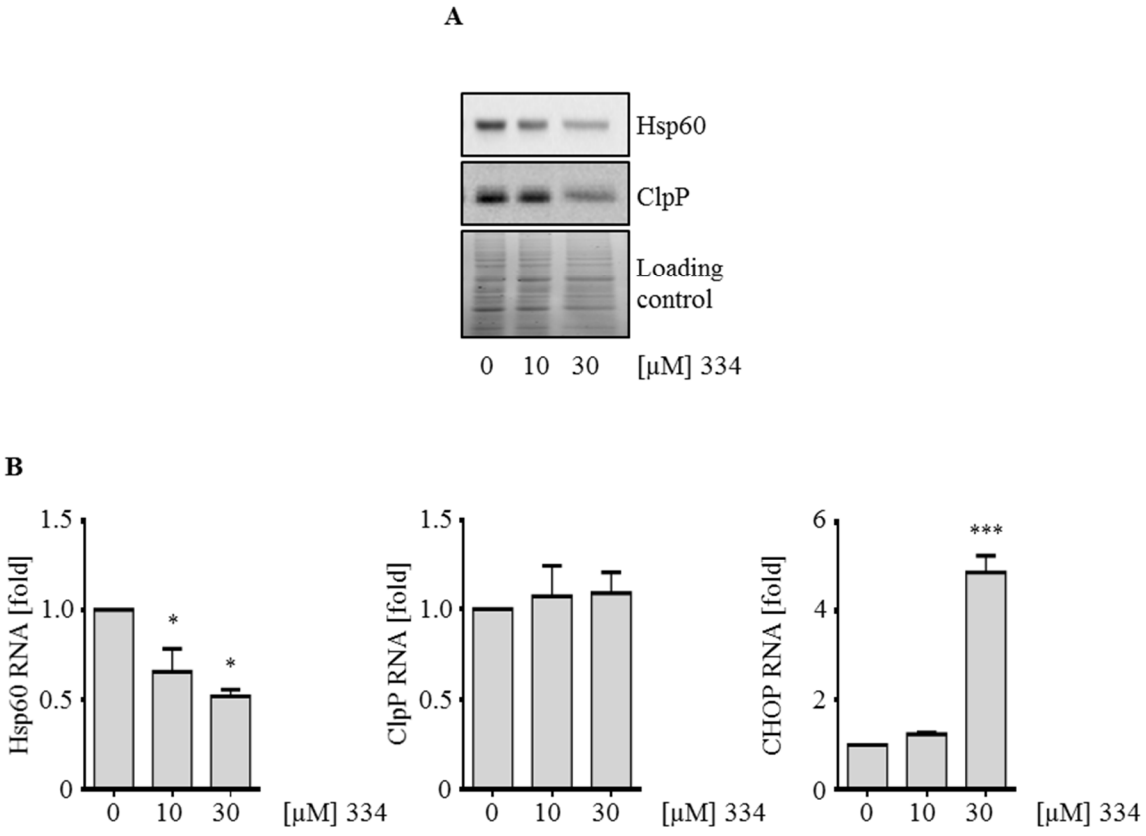

Figure 3.11: ClpX inhibition impairs Hsp60 protein and RNA and induces CHOP. (A) Western blot shows Hsp60 and ClpP protein expression in Jurkat cells after indicated 334 treatment (24 h) (n=3). (B) Bar diagrams represent RNA levels of Hsp60, ClpP, and CHOP for the indicated treatments (24 h). GAPDH and actin were used as housekeeping genes (* $p < 0.05$, *** $p < 0.001$, One-way ANOVA, Tukey's Multiple Comparison Test, n=3).

3.2.5 ClpX inhibition affects proteins implicated in mitochondrial function, stress, and DNA integrity

Besides the above mentioned functional effects of the ClpX inhibitor and mechanistic studies, we aimed to identify involved signaling proteins and potential ClpXP substrates by quantitative mass spectrometry using stable isotope labeling with amino acids in cell culture (SILAC). K562 cells labeled with different amino acids (light, medium or heavy arginine and lysine) were treated with ClpX inhibitor 334 for 24 and 48 h. Quantitative proteomics using mass spectrometry was performed by Anja Fux and Matthias Stahl (Department of Chemistry, Technical University of Munich, Garching).

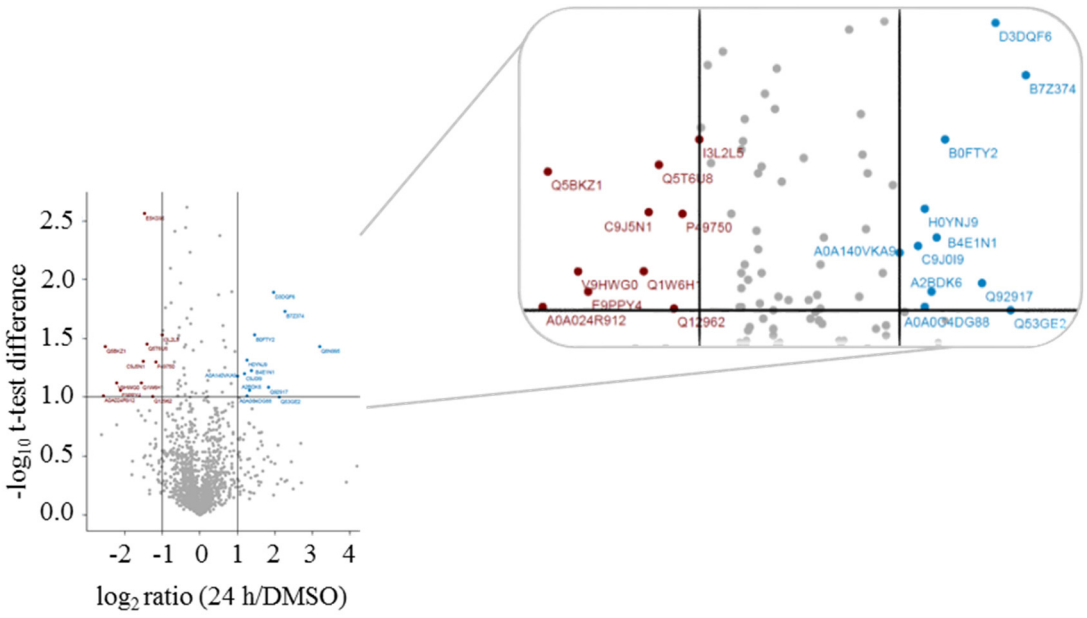

Figure 3.12: ClpX inhibition alters proteins involved in cellular stress, DNA integrity, transcription and translation processes, and metabolism. Representative scatter plot of quantitative proteomics mass spectrometry is shown. Light, medium, and heavy labeled K562 cells were treated with ClpX inhibitor (10 µM) for 24 and 48 h or with DMSO. Significantly enriched (blue) or depleted (red) proteins out of three independent experiments are shown (–log10 t-test difference cut-off = 1, log2 ratio 24 h/DMSO = –1/1, n=3).

Among the significantly changed proteins, mitochondrial as well as stress response related proteins were identified. Of note, proteins implicated in mitochondrial and nuclear translation and transcription were affected, such as mitochondrial elongation factor Ts or transcription initiation factor TFIID subunit 10. Furthermore, DNA-3-methyladenine glycosylase and DNA polymerase delta catalytic subunit implicated in DNA repair were found to be depleted. Notably, mitochondrial carnitine O-palmitoyltransferase 2 taking part in β-oxidation and cytoplasmic hydroxymethylglutaryl-CoA synthase were enriched which point to changes in cellular metabolism. Proteins significantly altered are summarized in Table 3.1 and 3.2. A complete list of further altered proteins identified by this approach is attached (Appendix A.3, Table A.1/A.2).

Table 3.1: Significantly enriched proteins identified by quantitative mass spectrometry

Protein ID	Enriched	Relevance
H0YNJ9	Deoxyuridine 5′-triphosphate nucleotidohydrolase, mitochondrial	Nucleotide metabolism
D3DQF6	RNA-binding protein 27	
B7Z374	Gephyrin	Molybdenum cofactor synthesis
B0FTY2	NudC domain-containing protein 3	Stability of dynein
Q8N995	Hydroxymethylglutaryl-CoA synthase, cytoplasmic	Cholesterol synthesis
B4E1N1	Armadillo repeat-containing protein 6	
C9J0I9	Nuclear-interacting partner of ALK	Zinc-ion binding
A0A140VKA9	Dihydropteridine reductase	Phe-decomposition, amino acid metabolic process
A2BDK6	Microtubule-associated protein 1B	Microtubule cytoskeleton organization
Q92917	G patch domain and KOW motifs-containing protein	Nuclear RNA-binding protein, pre-mRNA splicing
A0A0C4DG88	POU domain protein	Transcription factor activity
Q53GE2	F-actin-capping protein subunit alpha-2	Actin-filament capping
B2RDU4	Pentatricopeptide repeat domain-containing protein 3, mitochondrial	RNA-binding and mitochondrial translation regulation
B2RAH5	Protein phosphatase 1 regulatory subunit	Phosphatase regulator activity, signal transduction
B4DEI4	Golgi reassembly-stacking protein 2	
Q7L0Y3	Mitochondrial ribonuclease P protein 1	Mitochondrial tRNA processing and methylation
A0A140VK13	Carnitine O-palmitoyltransferase 2, mitochondrial	Fatty acid import in mitochondria, β-oxidation

Table 3.2: Significantly depleted proteins identified by quantitative mass spectrometry

Protein ID	Depleted	Relevance
E9PPY4	G patch domain-containing protein 4	Nucleic acid binding
I3L2L5	Protein FAM195B	MAPK-regulated corepressor-interacting protein 1
Q5T6U8	High mobility group AT-hook 1	DNA binding, transcription regulation
Q5BKZ1	DBIRD complex subunit ZNF326	Transcription-, alternative splicing-regulation
C9J5N1	Alanyl-tRNA editing protein Aarsd1	Alanyl-tRNA amino acylation
P49750	YLP motif-containing protein 1	Transcription repressor, reduction of telomerase activity during embryonic stem cell differentiation
V9HWG0	Chromobox protein homolog 5	Heterochromatin-formation
Q1W6H1	DNA-3-methyladenine glycosylase	Base excision repair
Q12962	Transcription initiation factor TFIID subunit 10	Transcription coactivator
A0A024R912	Uridine-cytidine kinase 2	CTP salvage pathway
E5KS95	Elongation factor Ts, mitochondrial	Translation elongation
H3BRL3	Ubiquitin domain-containing protein UBFD1	
B2RDW9	GTP-binding protein 1	
A0A024R4F4	DNA polymerase delta catalytic subunit	Base excision repair, gap-filling, DNA replication proofreading

3.2.6 ClpX inhibition affects mitochondrial morphology

Furthermore, we focused on mitochondrial morphology because the dynamic organelles underlie, e.g., fusion and fission dynamics in order to adapt to cellular stress conditions. Therefore, we performed live-cell imaging using MitoTracker® Red CMXRos to stain mitochondria and electron microscopy (Figure 3.13). Mitochondria of control cells showed to be near the nucleus, whereas the staining of ClpX inhibitor treated cells appeared to be more diffuse (Figure 3.13 A). Likewise, electron micrographs revealed similar observations

concerning localization of the mitochondria (Figure 3.13 B) with slight effects on mitochondrial size and shape. However, no prominent effects were observed in terms of fusion or fission dynamics upon ClpX inhibition.

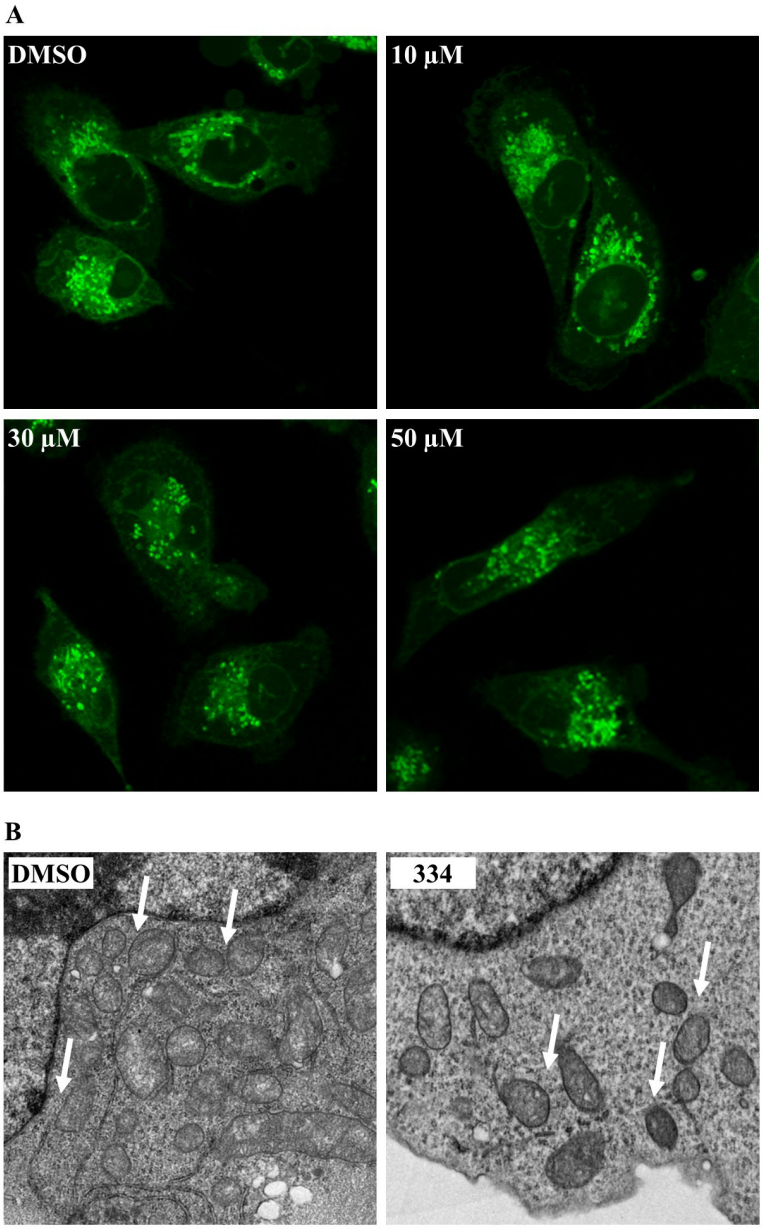

Figure 3.13: ClpX inhibition slightly affects mitochondrial morphology. (A) Confocal stainings show mitochondria of MDA-MB-231 cells treated with 334 or DMSO as indicated for 24 h. Mitochondria were visualized using MitoTracker® Red CMXRos (n=3). (B) Electron micrographs display Jurkat cells treated with 334 (20 µM) or DMSO for 24 h. White arrows indicate mitochondria (n=1).

3.3 ClpX inhibition enhances chemosensitivity of leukemia cells

Previous results revealed cell death induction by the compound 334 in several leukemic cancer cell lines as well as in PDX cells. Notably, the cell line with the lowest ClpXP protein expression, HL-60, exhibited low sensitivity towards the ClpX inhibitor emphasizing the selective effect of the compound on cells expressing the target protein. In contrast, analysis of cell death of PDX cells revealed no obvious correlation between ClpXP protein expression and sensitivity towards 334. Furthermore, PBMCs were also sensitive towards the inhibitor and expressed ClpX to a comparable extent. As a consequence, treatment with the inhibitor in cell death inducing concentrations may be problematic if the expression of ClpXP and sensitivity towards the inhibitor of non-cancer cells is similar to tumor cells.

Moreover, ClpX inhibitor treatment revealed to induce protein carbonylation, mitochondrial dysfunction, and overall cellular stress conditions, which is underlined by the previously shown mechanistic effects and the proteome data. Hence, we aimed to interfere with mitochondrial metabolism and proteostasis to sensitize tumor cells towards common cytostatic drugs. Low inhibitor concentrations (10 μM) were used to trigger mitochondrial stress in order to enhance the cancer cells' susceptibility to cell death. As shown in Figure 3.14, sensitivity of K562 cells towards the tyrosine kinase inhibitor imatinib increased the most in combination with the ClpX inhibitor. Mitochondrial stress induced by ClpX inhibition in combination with other chemotherapeutics such as etoposide or vincristine led to an increased cell death induction in Jurkat, CEM, and even vincristine-resistant CEM cells (VCR-CEM).

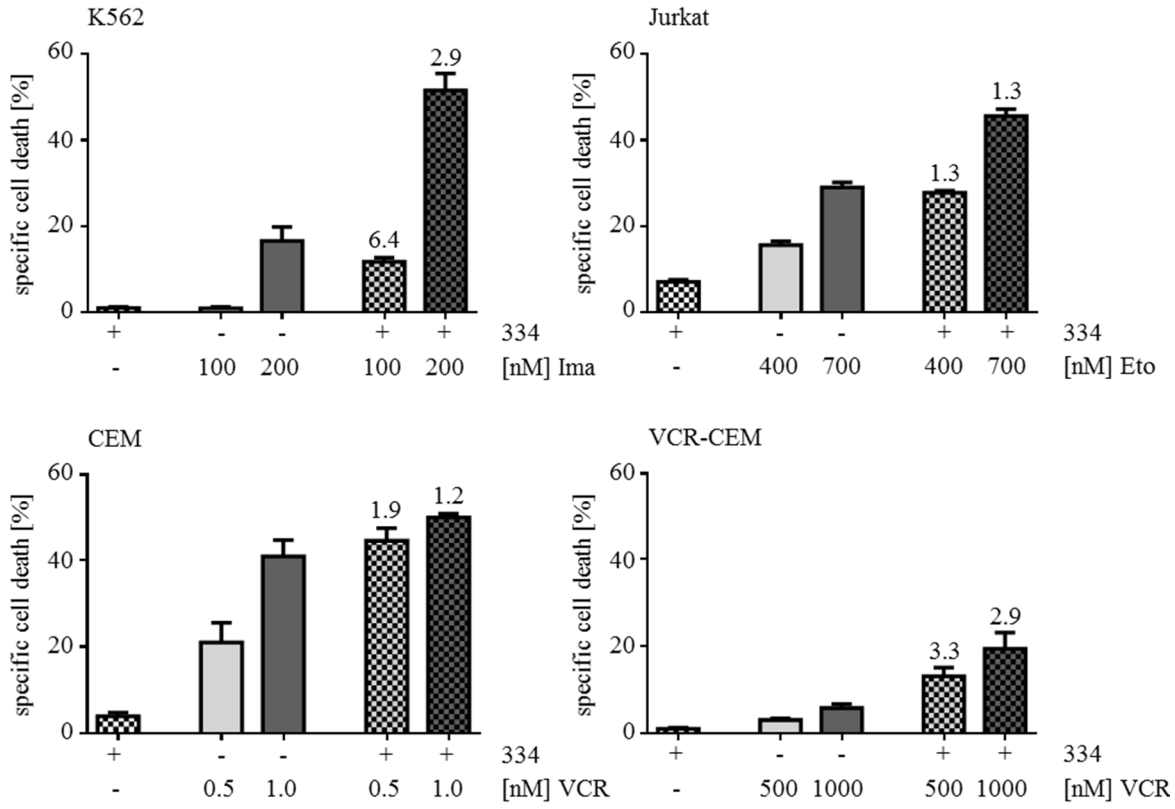

Figure 3.14: ClpX inhibitor sensitizes leukemia cells towards chemotherapy. Bars represent specific cell death induced in K562, Jurkat, CEM, and vincristine-resistant CEM cells (VCR-CEM). Cells were treated as indicated with 334 (10 µM), imatinib (Ima; K562), etoposide (Eto; Jurkat), and vincristine (VCR; CEM and VCR-CEM) alone or in combination for 48 h. Cell death was measured by flow cytometry using Nicoletti assay. Bliss values calculated for the combined chemotherapy display the extent of synergism. Values above 1.05 indicate synergistic effects (n=3).

Furthermore, we analyzed if chemosensitivity of HL-60 cells, which poorly responded to the ClpX inhibitor in viability and cell death assays, was enhanced by 334 treatment. Likewise, the inhibitor in low (10 µM) and high (50 µM) concentrations did not enhance sensitivity of the cells towards etoposide or cytarabine (Figure 3.15).

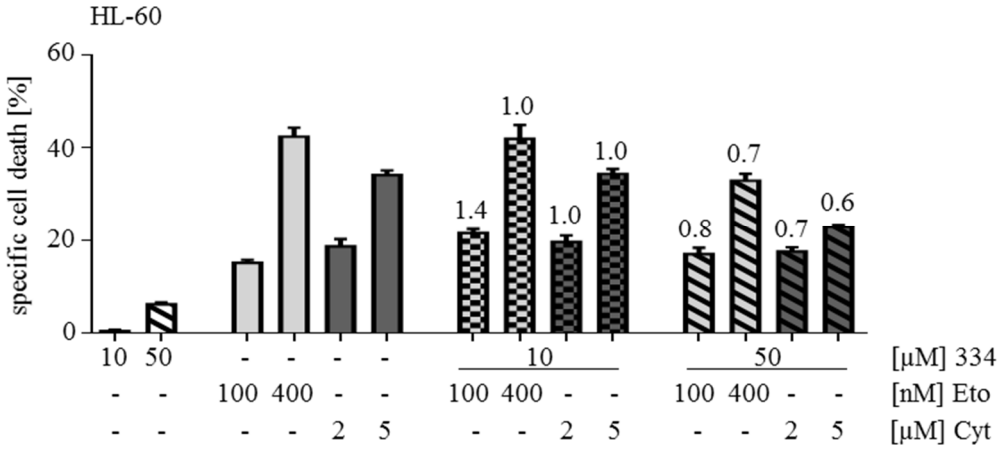

Figure 3.15: ClpX inhibitor does not enhance chemosensitivity of HL-60 cells. Bars represent specific cell death induced in HL-60 cells treated as indicated with 334 (10 µM and 50µM), etoposide (Eto), and cytarabine (Cyt) alone or in combination for 48 h. Cell death was measured by flow cytometry using Nicoletti assay. Bliss values calculated for the combined chemotherapy display the extent of synergism. Values above 1.05 indicate synergistic effects (n=3).

4 Discussion

4.1 Targeting mitochondria as anti-cancer strategy

This thesis outlines the inhibition of the mitochondrial ClpXP protease as a novel and promising anti-cancer strategy. Aside from conventional cytostatic therapy, the mitochondrion has gained attention as a new target for cancer treatment. Therefore, the organelle harbors various structures to interfere with. One possibility is to address the intrinsic apoptosis signaling. BH3 mimetics such as ABT-263 which bind anti-apoptotic Bcl-2 family proteins, e.g., Bcl-2 or Bcl-xL and thereby trigger apoptosis, are currently in clinical trials. They are evaluated in various cancer types ranging from hematological malignancies to solid tumors such as colon or pancreatic cancer and have shown promising results so far.[83] Besides mitochondrial apoptosis signaling, the mitochondrial energy production provides possible targets for anti-cancer drugs. As an example, the antidiabetic drug metformin revealed anti-tumor effects and showed to be an inhibitor of complex I of the electron transport chain (ETC).[84] Other ETC inhibitors such as VLX600 also aim to affect metabolic flexibility of cancer cells and have been reported to eradicate quiescent tumor cells.[84]

Alternatively, the interference with mitochondrial proteostasis is a novel option aside from targeting the mitochondrial cell death machinery or energy metabolism. Proper mitochondrial function relies on an efficient folding, quality control, and degradation of proteins imported and synthesized in the mitochondrion, which is regulated by chaperones and proteases.[49-52] For example, the small molecule gamitrinib specifically acts as an inhibitor of Hsp90/TRAP-1 (heat shock protein 90, TNF receptor associated protein 1). The mitochondrial chaperone is responsible for ETC complex II stability and regulates opening of the mitochondrial permeability transition pore that mediates mitochondrial swelling and also induction of cell death.[85,86] Similarly, the mitochondrial heat shock protein 60 (Hsp60), another mitochondrial chaperone, presents an attractive target with regard to mitochondrial proteostasis. Hsp60, together with other chaperones, permits proper folding and assembly of newly synthesized or imported preproteins in the mitochondrial matrix. Further, the chaperone is transcribed in the course of the mitochondrial unfolded protein response (UPR^{mt}) to restore proteostasis.[71,87] Overexpressed in a large number of tumors, Hsp60 crosstalks with the mitochondrial apoptosis machinery by stabilization of anti-apoptotic survivin and interacts with the tumor suppressor p53 to suppress its pro-apoptotic activity.[88] Hence, the mitochondrion provides various promising target structures to counteract the development and progression of oncological diseases.

4.2 Targeting mitochondrial proteostasis by ClpXP inhibition

Herein, we introduce another crucial part of the mitochondrial proteostasis maintaining network, the protease ClpXP, as a drugable target for cancer therapy. Recent reports stunningly demonstrated ClpXP's role in cancer, for example, in acute myeloid leukemia, prostate, and breast cancer cells.[54,56] Most of the recent studies were performed by ClpP or ClpX subunit silencing or overexpression. As targeting ClpXP in human cancer displays a very novel approach, appropriate compounds to inhibit ClpXP are missing so far.

Initial characterization of various ClpXP inhibitor compounds and their derivatives identified in high-throughput screenings by the group of Prof. Dr. Stephan A. Sieber demonstrated their effectivity in various leukemia cell lines regarding cell viability. This is in line with other studies proposing decreased cell viability and growth upon ClpP knockdown or inhibition. Accordingly, Seo *et al.* described lower levels of cell cycle regulating cyclins and aberrant reactive oxygen species (ROS) production explaining for the proliferation inhibition.[54,56,89] In terms of cell viability, ClpP subunit inhibitors exhibited weaker effects than ClpX or ClpXP inhibitors which may be due to the lower stability of the phenyl ester compounds. Consequently, a statement whether targeting of the chaperone subunit ClpX, the peptidase ClpP subunit or the whole ClpXP complex is the most effective strategy, is difficult. As previously shown by others, silencing of ClpP or ClpX exhibited similar effects on tumor cell proliferation and clonogenicity and may additionally depend on cell type.[56] Thus, targeting of either the subunits or the whole complex may present an efficient way to inhibit ClpXP which offers more possibilities for the development of novel inhibitor compounds.

Further characterization of the ClpX inhibitor 334 revealed its anti-leukemic effects in terms of colony formation, an indicator for tumorigenicity, and the induction of caspase-dependent apoptosis. Of note, sensitivity towards the inhibitor correlated with ClpXP expression that is reflected in a less pronounced apoptosis induction of the HL-60 cell line compared to K562 and Jurkat cell lines. Accordingly, the inhibitor induced cell death in various patient-derived xenograft AML and ALL cells but also in control PBMCs which expressed the target ClpX to a comparable extent. Hence, applicability of ClpXP inhibitors in higher doses may be critical if protein expression in tumor cells does not differ greatly from healthy tissue counterparts. Thus, toxicity, tumor-targeted or local application of the inhibitors, and possible combinations with other drugs to lower the inhibitor dose need to be evaluated.

Consistent with other reports, ClpXP targeting impaired mitochondrial integrity and function. Accordingly, we showed an early decrease of cellular ATP levels upon short-term ClpX and ClpP inhibition displaying a decreased mitochondrial respiration. As previously

described, ClpX and ClpP silencing disturbed ETC complex II activity and folding of its succinate-dehydrogenase subunit B concomitant with lowered oxygen consumption rates of cancer cells.[54,56] According to the effect on energy metabolism, ClpX inhibition led to the aberrant production of mitochondrial reactive oxygen species (ROS^{mt}) and a loss of mitochondrial membrane potential. As a consequence of elevated ROS^{mt}, we revealed an increase of carbonyl proteins upon ClpX inhibition. The accumulation of oxidized proteins may be another cause for the observed functional effects such as apoptosis induction. Protein carbonylation leads to protein aggregation, disturbed proteostasis, and is linked to cell ageing.[90] Further, the implication of accumulating carbonyl proteins was described to be involved in neurodegenerative diseases and cell death.[91-93] These data confirm the inhibitors' effect on mitochondrial function and simultaneously reinforce ClpXP as a drugable target.

4.3 Mitochondrial unfolded protein response and chemosensitization

ClpXP was described to be implicated in the UPR^{mt}, a mitochondrion-to-nucleus signaling triggered by unfolded proteins exceeding the capacity of the mitochondrial chaperones and proteases network.[73,74] The retrograde signaling includes nuclear transcription of chaperones and proteases, e.g., Hsp60 and ClpP, preventing excessive protein stress and organelle damage and therefore promoting cell survival.[71] Only recently, ClpP knockdown was shown to suppress the induction of Hsp60 upon doxycycline induced UPR^{mt} in mouse myoblasts.[89]

As crucial part of the mitochondrial protein quality control network, ClpXP maintains proteostasis. Consequently, our data suggest that ClpXP inhibition triggers protein stress which is displayed by the increase of carbonyl proteins. Further, ClpXP inhibition enhanced chemosensitivity towards diverse cytostatic drugs, such as imatinib, a tyrosine kinase inhibitor, etoposide, a topoisomerase II inhibitor, and vincristine, a microtubule polymerization blocker. In line, ClpP was proposed to mediate cisplatin resistance in a cervical and hepatoma cell line lately. The authors postulated an enhanced expression of copper efflux pumps upon ClpP overexpression driving cisplatin export. Consistently, copper transport systems were reported to be involved in multidrug resistances including also etoposide and vincristine.[94]

Our proteomics data suggest that ClpXP inhibition modulates mitochondrial proteins, transcription and translation processes, stress related proteins, as well as proteins implicated in DNA repair and integrity. Of note, accumulating stress, for example, aggregated proteins or missing flexibility of energy metabolism caused by ClpXP inhibition may sensitize cancer cells to the cytostatic drugs. Accordingly, Seo *et al.* showed an increased sensitivity of tumor cells to oxidative stress, glucose or amino acid deprivation upon ClpXP silencing.[56] Further,

the decrease of the UPR^{mt}-specific chaperone Hsp60 and the missing induction of ClpP reinforce the hypothesis of a suppressed pro-survival UPR^{mt} signaling upon ClpXP inhibition. Concluding, we propose rather a general induction of cellular stress concomitant with an attenuated UPR^{mt} which enhance susceptibility to cell death and chemosensitivity of cancer cells.

4.4 Challenges, efforts, and future perspectives

This thesis investigates the mitochondrial ClpXP complex as a drugable target in cancer therapy and introduces a set of novel structures with activity against human ClpXP. Despite previously shown effects of the inhibitors in various leukemia cells, there are several challenges yet to overcome. Diverse questions arise regarding the selective effect of the compounds on cancer cells, their toxicity, and potential side-effects of ClpXP targeting. Further issues of interest include the investigation of tumor cells that specifically respond to ClpXP targeting and the identification of the optimal drug partners for ClpXP inhibitors to enhance their anti-tumor effects.

4.4.1 On-going studies

In order to address these issues and to establish ClpXP targeting and appropriate inhibitor compounds as anti-cancer agents, there are still on-going studies on the presented inhibitors in our laboratory. We are currently verifying the ClpP inhibitors' specifity towards the target protein ClpP by means of confocal microscopy. Therefore, the inhibitor probes are visualized by a copper-catalyzed cycloaddition with rhodamine-azide (click chemistry) and co-localization with mitochondria is analyzed. Additionally, the role of ClpXP complex in mtDNA integrity is still elusive. Lon protease, for example, is known to bind and stabilize mitochondrial DNA.[95] We plan to address this issue by means of immunoprecipitation with mtDNA and ClpX/ClpP. Investigations on mtDNA damage, e.g., caused by ROS, using a qPCR approach to measure lesions represents another issue of interest.[96]

Due to limited knowledge of the protease's involvement in the retrograde UPR^{mt} signaling, the identification of ClpXP substrates or peptides released from mitochondria represents a further currently studied and unanswered matter. Peptides released from isolated and ClpP inhibitor treated mitochondria are analyzed by mass spectrometry by the group of Prof. Dr. Stephan A. Sieber at the moment.[97] Furthermore, due to the high selectivity of the ClpP subunit inhibitors, their use as a diagnostic tool is conceivable.

The question whether cancer cells with a strong dependence on oxidative phosphorylation exhibit higher sensitivity towards ClpXP inhibitors is another field of interest. If so, ClpXP

targeting could be attractive in terms of eradication of quiescent cancer cells which often account for tumor recurrence and therapy resistance. To address this issue, comparison of sensitivity of different cancer cell lines towards ClpXP inhibitors could give further information. Cell viability and cell death assays in Huh7 cells, a hepato carcinoma cell line, revealed a stronger sensitivity towards ClpP inhibitors compared to leukemia cells. Along this line, the ClpX inhibitor exhibited a proliferation inhibiting effect in sorafenib resistant Huh7 cells (done by Martina Meßner, data not shown) that poorly responded to any other cytostatic drug, such as doxorubicin, SN38 or cisplatin. The identification of cancer types which predominantly respond to ClpXP inhibition or a correlation of the response to ClpXP inhibitors with a specific metabolic profile could open up new possibilities for personalized cancer therapy.

4.4.2 Challenges and future perspectives

ClpXP targeting may represent an attractive new strategy to address metabolic flexibility of tumor cells. A switch from aerobe glycolysis to oxidative phosphorylation in case of glucose starvation characterizes distinct tumor subpopulations with high drug resistance and tumorigenicity.[40-45] Seo *et al.* reported a compensatory switch to glycolysis upon ClpP silencing. Simultaneously, replacement of glucose by galactose, which forces oxidative phosphorylation, enhanced anti-proliferative effects of ClpXP silencing.[56] This underlines the potential application of ClpXP targeting compounds in combination with inhibitors of other energy pathways. Based on our chemosensitivity and proteome data the combination of ClpXP inhibitors with other cytostatic drugs is conceivable. Regarding the decreased DNA repair and integrity due to ClpXP inhibition, the combination with DNA-damaging agents may be beneficial. Exploiting other effects of the compounds such as the increased ROS^{mt} production, e.g., by combination with inhibitors of mitochondrial anti-oxidant pathways, presents another attractive possibility.

Finally, toxicity of the compounds and side effects of ClpXP inhibition need to be evaluated in the future. It is still elusive if a therapeutic window for ClpXP targeting drugs can be established. Notably, non-cancerous PBMCs as well as endothelial cells (data not shown) responded to the ClpX inhibitor making its applicability as single agent in high doses or systemic treatment questionable. So far, there is not much knowledge of possible side effects of ClpXP inhibition. As Cole *et al.* reported, mice treated with their β-lactone inhibitor showed no liver, muscle or renal toxicity.[54] With respect to the differences of their chemical structure and thus stability of the various inhibitor compounds, a comparison with our inhibitors or general conclusions should be drawn with caution.

Moreover, homozygous deletion of another mitochondrial matrix protease, Lon, is lethal in early embryonic phase.[59] In comparison, mice with ClpP knockout only showed shortened

pre-/post-natal survival and growth retardation. Furthermore, movement and respiratory activities were slightly impaired. ClpP knockout mice exhibited normal hematopoiesis but were infertile and displayed auditory defects.[54,98] *In vivo* studies on ClpX deletion are completely missing.

Besides mitochondrial dysfunction, increased oxidative stress, loss of ClpP in mouse myoblasts inhibited protein translation, cell proliferation, and differentiation *in vitro*.[89] It stays elusive if healthy tissues with high mitochondrial mass, such as liver, heart, and muscles, are predominantly affected by the inhibitors in contrast to others. Due to the lack of compounds for pharmacological ClpXP inhibition, studies regarding side-effects and toxicity are missing so far and will be of particular interest for establishment of ClpXP inhibitor based cancer treatment.

In summary, this thesis presents the protease ClpXP as a drugable anti-cancer target by introduction and characterization of novel ClpXP inhibitors. As crucial part of the mitochondrial proteostasis network, ClpXP contributes to cancer cell viability, tumorigenicity, and cellular survival by maintenance of mitochondrial function and driving the pro-survival UPR^{mt} signaling. Therefore, we elucidated various intriguing effects of ClpXP inhibition, for example, an enhanced chemosensitivity of cancer cells. There is now great interest in the development and improvement of ClpXP inhibitors in order to exploit ClpXP's key role in mitochondrial function and integrity. Concluding, this thesis provides evidence that ClpXP inhibition may serve as an attractive and potential anti-cancer strategy in the future.

References

1 Stewart, B. W. & Wild, C. P. *World Cancer Report 2014*. Vol. 3 482-494 (Lyon: International Agency for Research on Cancer, 2014).

2 Leukemia & Lymphoma Society. *Signs and symptoms*, <https://www.lls.org/leukemia/acute-myeloid-leukemia/signs-and-symptoms> (n. d.).

3 Mateos, M. K., Barbaric, D., Byatt, S. A., Sutton, R. & Marshall, G. M. Down syndrome and leukemia: insights into leukemogenesis and translational targets. *Translational pediatrics* **4**, 76-92, doi:10.3978/j.issn.2224-4336.2015.03.03 (2015).

4 American Cancer Society. *Cancer Facts & Figures 2016*. 13-18 (Atlanta: American Cancer Society, 2016).

5 Howlader, N. *et al. SEER Cancer Statistics Review, 1975-2012*, <http://seer.cancer.gov/csr/1975_2012/> (2015).

6 Larson, R. A. *et al.* A five-drug remission induction regimen with intensive consolidation for adults with acute lymphoblastic leukemia: cancer and leukemia group B study 8811. *Blood* **85**, 2025-2037 (1995).

7 Rowe, J. M. *et al.* Induction therapy for adults with acute lymphoblastic leukemia: results of more than 1500 patients from the international ALL trial: MRC UKALL XII/ECOG E2993. *Blood* **106**, 3760-3767, doi:10.1182/blood-2005-04-1623 (2005).

8 Thomas, X. *et al.* Outcome of treatment in adults with acute lymphoblastic leukemia: analysis of the LALA-94 trial. *Journal of clinical oncology : official journal of the American Society of Clinical Oncology* **22**, 4075-4086, doi:10.1200/JCO.2004.10.050 (2004).

9 Kantarjian, H. *et al.* Long-term follow-up results of hyperfractionated cyclophosphamide, vincristine, doxorubicin, and dexamethasone (Hyper-CVAD), a dose-intensive regimen, in adult acute lymphocytic leukemia. *Cancer* **101**, 2788-2801, doi:10.1002/cncr.20668 (2004).

10 Lowenthal, R. M. *et al.* A phase I/II study of intensive dose escalation of cytarabine in combination with idarubicin and etoposide in induction and consolidation treatment of adult acute myeloid leukemia. Australian Leukaemia Study Group (ALSG). *Leukemia & lymphoma* **34**, 501-510, doi:10.3109/10428199909058477 (1999).

11 Lee, K. H. *et al.* Clinical effect of imatinib added to intensive combination chemotherapy for newly diagnosed Philadelphia chromosome-positive acute lymphoblastic leukemia. *Leukemia* **19**, 1509-1516, doi:10.1038/sj.leu.2403886 (2005).

12 de Labarthe, A. *et al.* Imatinib combined with induction or consolidation chemotherapy in patients with de novo Philadelphia chromosome-positive acute lymphoblastic leukemia: results of the GRAAPH-2003 study. *Blood* **109**, 1408-1413, doi:10.1182/blood-2006-03-011908 (2007).

13 Hunault, M. *et al.* Better outcome of adult acute lymphoblastic leukemia after early genoidentical allogeneic bone marrow transplantation (BMT) than after late high-dose therapy and autologous BMT: a GOELAMS trial. *Blood* **104**, 3028-3037, doi:10.1182/blood-2003-10-3560 (2004).

14 Ribera, J. M. *et al.* Comparison of intensive chemotherapy, allogeneic or autologous stem cell transplantation as post-remission treatment for adult patients with high-risk acute lymphoblastic leukemia. Results of the PETHEMA ALL-93 trial. *Haematologica* **90**, 1346-1356 (2005).

15 Goldstone, A. H. *et al.* In adults with standard-risk acute lymphoblastic leukemia, the greatest benefit is achieved from a matched sibling allogeneic transplantation in first complete remission, and an autologous transplantation is less effective than conventional consolidation/maintenance chemotherapy in all patients: final results of the International ALL Trial (MRC UKALL XII/ECOG E2993). *Blood* **111**, 1827-1833, doi:10.1182/blood-2007-10-116582 (2008).

16 Chan, D. C. Mitochondria: dynamic organelles in disease, aging, and development. *Cell* **125**, 1241-1252, doi:10.1016/j.cell.2006.06.010 (2006).
17 Wallace, D. C. A mitochondrial paradigm of metabolic and degenerative diseases, aging, and cancer: a dawn for evolutionary medicine. *Annual review of genetics* **39**, 359-407, doi:10.1146/annurev.genet.39.110304.095751 (2005).
18 Lin, M. T. & Beal, M. F. Mitochondrial dysfunction and oxidative stress in neurodegenerative diseases. *Nature* **443**, 787-795, doi:10.1038/nature05292 (2006).
19 Weinberg, S. E. & Chandel, N. S. Targeting mitochondria metabolism for cancer therapy. *Nature chemical biology* **11**, 9-15, doi:10.1038/nchembio.1712 (2015).
20 Kang, M. H. & Reynolds, C. P. Bcl-2 inhibitors: targeting mitochondrial apoptotic pathways in cancer therapy. *Clinical cancer research : an official journal of the American Association for Cancer Research* **15**, 1126-1132, doi:10.1158/1078-0432.CCR-08-0144 (2009).
21 Camara, A. K., Lesnefsky, E. J. & Stowe, D. F. Potential therapeutic benefits of strategies directed to mitochondria. *Antioxidants & redox signaling* **13**, 279-347, doi:10.1089/ars.2009.2788 (2010).
22 Green, D. R. & Evan, G. I. A matter of life and death. *Cancer cell* **1**, 19-30 (2002).
23 Chipuk, J. E., Moldoveanu, T., Llambi, F., Parsons, M. J. & Green, D. R. The BCL-2 family reunion. *Molecular cell* **37**, 299-310, doi:10.1016/j.molcel.2010.01.025 (2010).
24 Williams, M. *et al.* Key Survival Factor, Mcl-1, Correlates with Sensitivity to Combined Bcl-2/Bcl-xL Blockade. *Molecular cancer research : MCR*, doi:10.1158/1541-7786.MCR-16-0280-T (2016).
25 Keitel, U. *et al.* Bcl-xL mediates therapeutic resistance of a mesenchymal breast cancer cell subpopulation. *Oncotarget* **5**, 11778-11791, doi:10.18632/oncotarget.2634 (2014).
26 Certo, M. *et al.* Mitochondria primed by death signals determine cellular addiction to antiapoptotic BCL-2 family members. *Cancer cell* **9**, 351-365, doi:10.1016/j.ccr.2006.03.027 (2006).
27 Letai, A. *et al.* Distinct BH3 domains either sensitize or activate mitochondrial apoptosis, serving as prototype cancer therapeutics. *Cancer cell* **2**, 183-192 (2002).
28 Deng, J. *et al.* BH3 profiling identifies three distinct classes of apoptotic blocks to predict response to ABT-737 and conventional chemotherapeutic agents. *Cancer cell* **12**, 171-185, doi:10.1016/j.ccr.2007.07.001 (2007).
29 Cairns, R. A., Harris, I. S. & Mak, T. W. Regulation of cancer cell metabolism. *Nat Rev Cancer* **11**, 85-95, doi:10.1038/nrc2981 (2011).
30 Sena, L. A. & Chandel, N. S. Physiological roles of mitochondrial reactive oxygen species. *Molecular cell* **48**, 158-167, doi:10.1016/j.molcel.2012.09.025 (2012).
31 Wiseman, H. & Halliwell, B. Damage to DNA by reactive oxygen and nitrogen species: role in inflammatory disease and progression to cancer. *The Biochemical journal* **313 (Pt 1)**, 17-29 (1996).
32 Trachootham, D., Alexandre, J. & Huang, P. Targeting cancer cells by ROS-mediated mechanisms: a radical therapeutic approach? *Nature reviews. Drug discovery* **8**, 579-591, doi:10.1038/nrd2803 (2009).
33 Trachootham, D. *et al.* Selective killing of oncogenically transformed cells through a ROS-mediated mechanism by beta-phenylethyl isothiocyanate. *Cancer cell* **10**, 241-252, doi:10.1016/j.ccr.2006.08.009 (2006).
34 Weinberg, F. *et al.* Mitochondrial metabolism and ROS generation are essential for Kras-mediated tumorigenicity. *Proceedings of the National Academy of Sciences of the United States of America* **107**, 8788-8793, doi:10.1073/pnas.1003428107 (2010).
35 Harris, I. S. *et al.* Glutathione and thioredoxin antioxidant pathways synergize to drive cancer initiation and progression. *Cancer cell* **27**, 211-222, doi:10.1016/j.ccell.2014.11.019 (2015).
36 Warburg, O. On the origin of cancer cells. *Science* **123**, 309-314 (1956).
37 Warburg, O. On respiratory impairment in cancer cells. *Science* **124**, 269-270 (1956).
38 Frezza, C. & Gottlieb, E. Mitochondria in cancer: not just innocent bystanders. *Seminars in cancer biology* **19**, 4-11, doi:10.1016/j.semcancer.2008.11.008 (2009).

39 Weinhouse, S. The Warburg hypothesis fifty years later. *Zeitschrift fur Krebsforschung und klinische Onkologie. Cancer research and clinical oncology* **87**, 115-126 (1976).

40 Gao, C., Shen, Y., Jin, F., Miao, Y. & Qiu, X. Cancer Stem Cells in Small Cell Lung Cancer Cell Line H446: Higher Dependency on Oxidative Phosphorylation and Mitochondrial Substrate-Level Phosphorylation than Non-Stem Cancer Cells. *PloS one* **11**, e0154576, doi:10.1371/journal.pone.0154576 (2016).

41 Ippolito, L. *et al.* Metabolic shift toward oxidative phosphorylation in docetaxel resistant prostate cancer cells. *Oncotarget* **7**, 61890-61904, doi:10.18632/oncotarget.11301 (2016).

42 Denise, C. *et al.* 5-fluorouracil resistant colon cancer cells are addicted to OXPHOS to survive and enhance stem-like traits. *Oncotarget* **6**, 41706-41721, doi:10.18632/oncotarget.5991 (2015).

43 Viale, A. *et al.* Oncogene ablation-resistant pancreatic cancer cells depend on mitochondrial function. *Nature* **514**, 628-632, doi:10.1038/nature13611 (2014).

44 Ye, X. Q. *et al.* Mitochondrial and energy metabolism-related properties as novel indicators of lung cancer stem cells. *International journal of cancer* **129**, 820-831, doi:10.1002/ijc.25944 (2011).

45 Lagadinou, E. D. *et al.* BCL-2 inhibition targets oxidative phosphorylation and selectively eradicates quiescent human leukemia stem cells. *Cell stem cell* **12**, 329-341, doi:10.1016/j.stem.2012.12.013 (2013).

46 Anderson, S. *et al.* Sequence and organization of the human mitochondrial genome. *Nature* **290**, 457-465 (1981).

47 Lopez, M. F. *et al.* High-throughput profiling of the mitochondrial proteome using affinity fractionation and automation. *Electrophoresis* **21**, 3427-3440, doi:10.1002/1522-2683(20001001)21:16<3427::AID-ELPS3427>3.0.CO;2-L (2000).

48 Chen, Q., Vazquez, E. J., Moghaddas, S., Hoppel, C. L. & Lesnefsky, E. J. Production of reactive oxygen species by mitochondria: central role of complex III. *The Journal of biological chemistry* **278**, 36027-36031, doi:10.1074/jbc.M304854200 (2003).

49 Richter, U., Lahtinen, T., Marttinen, P., Suomi, F. & Battersby, B. J. Quality control of mitochondrial protein synthesis is required for membrane integrity and cell fitness. *The Journal of cell biology* **211**, 373-389, doi:10.1083/jcb.201504062 (2015).

50 Quiros, P. M., Langer, T. & Lopez-Otin, C. New roles for mitochondrial proteases in health, ageing and disease. *Nature reviews. Molecular cell biology* **16**, 345-359, doi:10.1038/nrm3984 (2015).

51 Harbauer, A. B., Zahedi, R. P., Sickmann, A., Pfanner, N. & Meisinger, C. The protein import machinery of mitochondria-a regulatory hub in metabolism, stress, and disease. *Cell metabolism* **19**, 357-372, doi:10.1016/j.cmet.2014.01.010 (2014).

52 Baker, M. J., Palmer, C. S. & Stojanovski, D. Mitochondrial protein quality control in health and disease. *British journal of pharmacology* **171**, 1870-1889, doi:10.1111/bph.12430 (2014).

53 Di, K., Lomeli, N., Wood, S. D., Vanderwal, C. D. & Bota, D. A. Mitochondrial Lon is over-expressed in high-grade gliomas, and mediates hypoxic adaptation: potential role of Lon as a therapeutic target in glioma. *Oncotarget* **7**, 77457-77467, doi:10.18632/oncotarget.12681 (2016).

54 Cole, A. *et al.* Inhibition of the Mitochondrial Protease ClpP as a Therapeutic Strategy for Human Acute Myeloid Leukemia. *Cancer cell* **27**, 864-876, doi:10.1016/j.ccell.2015.05.004 (2015).

55 Liu, Y. *et al.* Inhibition of Lon blocks cell proliferation, enhances chemosensitivity by promoting apoptosis and decreases cellular bioenergetics of bladder cancer: potential roles of Lon as a prognostic marker and therapeutic target in baldder cancer. *Oncotarget* **5**, 11209-11224, doi:10.18632/oncotarget.2026 (2014).

56 Seo, J. H. *et al.* The Mitochondrial Unfoldase-Peptidase Complex ClpXP Controls Bioenergetics Stress and Metastasis. *PLoS biology* **14**, e1002507, doi:10.1371/journal.pbio.1002507 (2016).

57 Zhang, Y. & Maurizi, M. R. Mitochondrial ClpP activity is required for cisplatin resistance in human cells. *Biochimica et biophysica acta* **1862**, 252-264, doi:10.1016/j.bbadis.2015.12.005 (2016).

58 Quiros, P. M., Barcena, C. & Lopez-Otin, C. Lon protease: A key enzyme controlling mitochondrial bioenergetics in cancer. *Molecular & cellular oncology* **1**, e968505, doi:10.4161/23723548.2014.968505 (2014).

59 Quiros, P. M. *et al.* ATP-dependent Lon protease controls tumor bioenergetics by reprogramming mitochondrial activity. *Cell reports* **8**, 542-556, doi:10.1016/j.celrep.2014.06.018 (2014).

60 Goard, C. A. & Schimmer, A. D. Mitochondrial matrix proteases as novel therapeutic targets in malignancy. *Oncogene* **33**, 2690-2699, doi:10.1038/onc.2013.228 (2014).

61 Gaillot, O., Pellegrini, E., Bregenholt, S., Nair, S. & Berche, P. The ClpP serine protease is essential for the intracellular parasitism and virulence of Listeria monocytogenes. *Molecular microbiology* **35**, 1286-1294 (2000).

62 Robertson, G. T., Ng, W. L., Foley, J., Gilmour, R. & Winkler, M. E. Global transcriptional analysis of clpP mutations of type 2 Streptococcus pneumoniae and their effects on physiology and virulence. *Journal of bacteriology* **184**, 3508-3520 (2002).

63 Raju, R. M. *et al.* Mycobacterium tuberculosis ClpP1 and ClpP2 function together in protein degradation and are required for viability in vitro and during infection. *PLoS pathogens* **8**, e1002511, doi:10.1371/journal.ppat.1002511 (2012).

64 Frees, D. *et al.* Clp ATPases are required for stress tolerance, intracellular replication and biofilm formation in Staphylococcus aureus. *Molecular microbiology* **54**, 1445-1462, doi:10.1111/j.1365-2958.2004.04368.x (2004).

65 Brotz-Oesterhelt, H. *et al.* Dysregulation of bacterial proteolytic machinery by a new class of antibiotics. *Nature medicine* **11**, 1082-1087, doi:10.1038/nm1306 (2005).

66 Kirstein, J. *et al.* The antibiotic ADEP reprogrammes ClpP, switching it from a regulated to an uncontrolled protease. *EMBO molecular medicine* **1**, 37-49, doi:10.1002/emmm.200900002 (2009).

67 Zeiler, E., Korotkov, V. S., Lorenz-Baath, K., Bottcher, T. & Sieber, S. A. Development and characterization of improved beta-lactone-based anti-virulence drugs targeting ClpP. *Bioorganic & medicinal chemistry* **20**, 583-591, doi:10.1016/j.bmc.2011.07.047 (2012).

68 Theunissen, T. E. *et al.* Specific MRI Abnormalities Reveal Severe Perrault Syndrome due to CLPP Defects. *Frontiers in neurology* **7**, 203, doi:10.3389/fneur.2016.00203 (2016).

69 Jenkinson, E. M. *et al.* Perrault syndrome is caused by recessive mutations in CLPP, encoding a mitochondrial ATP-dependent chambered protease. *American journal of human genetics* **92**, 605-613, doi:10.1016/j.ajhg.2013.02.013 (2013).

70 Baker, T. A. & Sauer, R. T. ClpXP, an ATP-powered unfolding and protein-degradation machine. *Biochimica et biophysica acta* **1823**, 15-28, doi:10.1016/j.bbamcr.2011.06.007 (2012).

71 Zhao, Q. *et al.* A mitochondrial specific stress response in mammalian cells. *The EMBO journal* **21**, 4411-4419 (2002).

72 Arnould, T., Michel, S. & Renard, P. Mitochondria Retrograde Signaling and the UPR mt: Where Are We in Mammals? *International journal of molecular sciences* **16**, 18224-18251, doi:10.3390/ijms160818224 (2015).

73 Al-Furoukh, N. *et al.* ClpX stimulates the mitochondrial unfolded protein response (UPRmt) in mammalian cells. *Biochimica et biophysica acta* **1853**, 2580-2591, doi:10.1016/j.bbamcr.2015.06.016 (2015).

74 Haynes, C. M., Petrova, K., Benedetti, C., Yang, Y. & Ron, D. ClpP mediates activation of a mitochondrial unfolded protein response in C. elegans. *Developmental cell* **13**, 467-480, doi:10.1016/j.devcel.2007.07.016 (2007).

75 Horibe, T. & Hoogenraad, N. J. The chop gene contains an element for the positive regulation of the mitochondrial unfolded protein response. *PloS one* **2**, e835, doi:10.1371/journal.pone.0000835 (2007).

76 Pellegrino, M. W., Nargund, A. M. & Haynes, C. M. Signaling the mitochondrial unfolded protein response. *Biochimica et biophysica acta* **1833**, 410-416, doi:10.1016/j.bbamcr.2012.02.019 (2013).

77 Hackl, M. W. *et al.* Phenyl Esters Are Potent Inhibitors of Caseinolytic Protease P and Reveal a Stereogenic Switch for Deoligomerization. *Journal of the American Chemical Society* **137**, 8475-8483, doi:10.1021/jacs.5b03084 (2015).
78 Terziyska, N. *et al.* In vivo imaging enables high resolution preclinical trials on patients' leukemia cells growing in mice. *PloS one* **7**, e52798, doi:10.1371/journal.pone.0052798 (2012).
79 Vick, B. *et al.* An advanced preclinical mouse model for acute myeloid leukemia using patients' cells of various genetic subgroups and in vivo bioluminescence imaging. *PloS one* **10**, e0120925, doi:10.1371/journal.pone.0120925 (2015).
80 Nicoletti, I., Migliorati, G., Pagliacci, M. C., Grignani, F. & Riccardi, C. A rapid and simple method for measuring thymocyte apoptosis by propidium iodide staining and flow cytometry. *Journal of immunological methods* **139**, 271-279 (1991).
81 Fulda, S. *et al.* Sensitization for death receptor- or drug-induced apoptosis by re-expression of caspase-8 through demethylation or gene transfer. *Oncogene* **20**, 5865-5877, doi:10.1038/sj.onc.1204750 (2001).
82 Webb, J. L. Effect of more than one inhibitor, antagonism, summation, and synergism. *Enzyme and Metabolic Inhibitors, New York: Academic Press*, 488-512 (1963).
83 Delbridge, A. R., Grabow, S., Strasser, A. & Vaux, D. L. Thirty years of BCL-2: translating cell death discoveries into novel cancer therapies. *Nat Rev Cancer* **16**, 99-109, doi:10.1038/nrc.2015.17 (2016).
84 Zhang, X. *et al.* Induction of mitochondrial dysfunction as a strategy for targeting tumour cells in metabolically compromised microenvironments. *Nature communications* **5**, 3295, doi:10.1038/ncomms4295 (2014).
85 Leav, I. *et al.* Cytoprotective mitochondrial chaperone TRAP-1 as a novel molecular target in localized and metastatic prostate cancer. *The American journal of pathology* **176**, 393-401, doi:10.2353/ajpath.2010.090521 (2010).
86 Chae, Y. C. *et al.* Landscape of the mitochondrial Hsp90 metabolome in tumours. *Nature communications* **4**, 2139, doi:10.1038/ncomms3139 (2013).
87 Cheng, M. Y., Hartl, F. U. & Horwich, A. L. The mitochondrial chaperonin hsp60 is required for its own assembly. *Nature* **348**, 455-458, doi:10.1038/348455a0 (1990).
88 Ghosh, J. C., Dohi, T., Kang, B. H. & Altieri, D. C. Hsp60 regulation of tumor cell apoptosis. *The Journal of biological chemistry* **283**, 5188-5194, doi:10.1074/jbc.M705904200 (2008).
89 Deepa, S. S. *et al.* Down-regulation of the mitochondrial matrix peptidase ClpP in muscle cells causes mitochondrial dysfunction and decreases cell proliferation. *Free radical biology & medicine* **91**, 281-292, doi:10.1016/j.freeradbiomed.2015.12.021 (2016).
90 Tanase, M. *et al.* Role of Carbonyl Modifications on Aging-Associated Protein Aggregation. *Scientific reports* **6**, 19311, doi:10.1038/srep19311 (2016).
91 Dasgupta, A., Zheng, J. & Bizzozero, O. A. Protein carbonylation and aggregation precede neuronal apoptosis induced by partial glutathione depletion. *ASN neuro* **4**, doi:10.1042/AN20110064 (2012).
92 Aksenov, M. Y., Aksenova, M. V., Butterfield, D. A., Geddes, J. W. & Markesbery, W. R. Protein oxidation in the brain in Alzheimer's disease. *Neuroscience* **103**, 373-383 (2001).
93 Bizzozero, O. A., DeJesus, G., Callahan, K. & Pastuszyn, A. Elevated protein carbonylation in the brain white matter and gray matter of patients with multiple sclerosis. *Journal of neuroscience research* **81**, 687-695, doi:10.1002/jnr.20587 (2005).
94 Furukawa, T., Komatsu, M., Ikeda, R., Tsujikawa, K. & Akiyama, S. Copper transport systems are involved in multidrug resistance and drug transport. *Current medicinal chemistry* **15**, 3268-3278 (2008).
95 Lu, B. *et al.* Roles for the human ATP-dependent Lon protease in mitochondrial DNA maintenance. *The Journal of biological chemistry* **282**, 17363-17374, doi:10.1074/jbc.M611540200 (2007).
96 Furda, A., Santos, J. H., Meyer, J. N. & Van Houten, B. Quantitative PCR-based measurement of nuclear and mitochondrial DNA damage and repair in mammalian

cells. *Methods in molecular biology* **1105**, 419-437, doi:10.1007/978-1-62703-739-6_31 (2014).

97 Augustin, S. *et al.* Characterization of peptides released from mitochondria: evidence for constant proteolysis and peptide efflux. *The Journal of biological chemistry* **280**, 2691-2699, doi:10.1074/jbc.M410609200 (2005).

98 Gispert, S. *et al.* Loss of mitochondrial peptidase Clpp leads to infertility, hearing loss plus growth retardation via accumulation of CLPX, mtDNA and inflammatory factors. *Human molecular genetics* **22**, 4871-4887, doi:10.1093/hmg/ddt338 (2013).

A Appendix

A.1 Abbreviations

α-TG	α-Thioglycerol
AAA	ATPase associated with diverse cellular activities
ALL	Acute lymphoid leukemia
AML	Acute myeloid leukemia
ANOVA	Analysis of variance
AntiA	Antimycin A
APS	Ammonium persulfate
ATP	Adenosine triphosphate
Bcl-2	B-cell lymphoma 2
BH3	Bcl-2 homology domain 3
Bcr-Abl	Breakpoint cluster region-Abelson
BSA	Bovine serum albumin
Caspase	Cysteinyl-aspartate specific protease
CCCP	Carbonyl cyanide 3-chlorophenylhydrazone
Cdk5	Cyclin-dependent kinase 5
CHOP	CCAAT7-enhancer-binding protein (C/EBP) homologous protein
ClpP	Caseinolytic peptidase proteolytic subunit
ClpX	Caseinolytic peptidase X homolog
CLL	Chronic lymphoid leukemia
CML	Chronic myeloid leukemia
CTB	CellTiter-Blue™
CTG	CellTiter-Glo™
DMSO	Dimethyl sulfoxide
DNA, mt	Deoxyribonucleic acid, mitochondrial
DNP	2,4-dinitrophenyl
DNPH	2,4-dinitrophenylhydrazine
DTT	Dithiothreitol

ECL	Enhanced chemiluminescence
EDTA	Ethylenediaminetetraacetic acid
EMT	Epithelial-mesenchymal transition
ETC	Electron transport chain
FACS	Fluorescence activated cell sorting
FCS	Fetal calf serum
FLT3-L	FMS-like tyrosine kinase 3 ligand
Foxo1	Forkhead-box-protein O-1
FSC	Forward scatter
GAPDH	Glyceraldehyde 3-phosphate dehydrogenase
h	hour(s)
HBSS	Hanks' Balanced Salt Solution
HCl	Hydrogen chloride
HFS	Hypotonic fluorochrome solution
HRP	Horseradish peroxidase
Hsp60	Heat shock protein 60
HTS	High-throughput screening
IC50	Half maximal inhibitory concentration
IgG	Immunoglobulin G
IL-3	Interleukin-3
IMDM	Iscove's Modified Dulbecco's Medium
ITS	Insulin-transferrin-selenium
JC-1	5,5′,6,6′-tetrachloro-1,1′,3,3′-tetraethylbenzimidazolylcarbocyanine iodide
L-Arg HCl	L-Arginine monohydrochloride
L-Lys HCl, L-Lys 2HCl	L-Lysine monohydrochloride, -dihydrochloride
min	minute(s)
MMP	Mitochondrial membrane potential
MTT	3-(4,5-dimethylthiazol-2-yl)-2,5-diphenyltetrazolium bromide
PARP	Poly (ADP-ribose) polymerase
PBMC	Peripheral blood mononuclear cell

PBS	Phosphate buffered saline
PCR, q, rt	Polymerase chain reaction, quantitative, real-time
PDX	Patient-derived xenograft
PE	Phycoerythrin
Pen/Strep	Penicillin/streptomycin
PI	Propidium iodide
PMSF	Phenylmethanesulfonyl fluoride
Q-VD-OPh	(3S)-5-(2,6-Difluorophenoxy)-3-[[(2S)-3-methyl-1-oxo-2-[(2-quinolinylcarbonyl)amino]butyl]amino]-4-oxo-pentanoic acid hydrate
RIPA	Radioimmunoprecipitation assay buffer
RNA	Ribonucleic acid
ROS^{mt}	Reactive oxygen species, mitochondrial
RPMI	Roswell Park Memorial Institute
RT	Room temperature
Sa	Staphylococcus aureus
SCF	Stem cell factor, c-Kit ligand
SDS-PAGE	Sodium dodecyl sulfate polyacrylamide gel electrophoresis
SEM	Standard error of the mean
SILAC	Stable isotope labeling with amino acids in cell culture
SSC	Side scatter
TCE	2,2,2-Trichlorethanol
TEMED	Tetramethylethylenediamine
TIC	Tumor-initiating cell
TIM	Translocase inner membrane
TOM	Translocase outer membrane
TPO	Thrombopoietin
TRAP-1	TNF-receptor associated protein 1
Tris	Tris-(hydroxymethyl)-aminomethane
UPR^{mt}	Unfolded protein response, mitochondrial
w/o	without

A.2 IC50 values of ClpXP inhibitor compounds

Inhibitor	IC50 [µM] K562	IC50 [µM] Jurkat
319	n.c.	31.03
334	21.83	12.93
335	n.c.	n.c.
339	43.34	23.73
AV167	n.c.	n.c.
TG42	n.c.	n.c.
TG53	75.53	32.49
TG54	n.c.	46.26

Figure A.1: IC50 values of ClpXP inhibitors in K562 and Jurkat cells. Cell viability of K562 and Jurkat cells upon inhibitor treatment (72 h) served for IC50 value calculation using nonlinear regression. CellTiter-Blue™ reagent was used. Viability was normalized to DMSO treated control (n=3). n.c. not calculated.

A.3 Proteome data (SILAC)

Tables A.1 and A.2 summarize proteome results for ClpX inhibitor treated K562 cells for 24 and 48 h (–log10 t-test difference cut-off = 0, log2 ratio (24h or 48 h/DMSO) = –1.5/+1.5).

Table A.1: Enriched proteins after 24 and 48h of ClpX inhibitor treatment versus DMSO treated control

Protein ID	Enriched	Relevance
D3DQF6*	RNA-binding protein 27	
B7Z374	Gephyrin	Molybdenum cofactor synthesis
Q8N995	Hydroxymethylglutaryl-CoA synthase, cytoplasmic	Cholesterol synthesis
B4E1N1	Armadillo repeat-containing protein 6	
Q92917	G patch domain and KOW motifs-containing protein	Nuclear RNA-binding protein, pre-mRNA splicing
Q53GE2	F-actin-capping protein subunit alpha-2	Actin-filament capping
F5H7R9	Parathymosin	
Q8TCJ8	Glutamate-rich WD repeat-containing protein 1	

Q9H9T3	Elongator complex protein 3	Histone acetylation
C9JTT8	BET1 homolog	Vesicular transport from ER to Golgi
Q0P685*	Eyes absent homolog 3	Tyrosine-phosphatase activity
A0A140VK13*	Carnitine O-palmitoyltransferase 2, mitochondrial	Fatty acid import in mitochondria, β-oxidation
B1Q3B3	Ferritin light chain	Iron storage in a soluble, readily available form
B4DGV1	Inositol hexakisphosphate / diphosphoinositol-pentakisphosphate	Apoptosis, vesicle trafficking and cytoskeletal dynamics
Q8WTW2	N-Myc-interactor	
H0Y9G6	39S ribosomal protein L3, mitochondrial	
A0A0C4DGZ0	DNA-directed RNA polymerase II subunit RPB1	
A0A0A6YYC7	E3 ubiquitin-protein ligase ZFP91	
B7Z5N7	Sec1 family domain-containing protein 1	Vesicle docking involved in exocytosis
C9JKQ2	NADH dehydrogenase [ubiquinone] 1 β subcomplex subunit 3	Respiration complex
Q9H1A4	Anaphase-promoting complex subunit 1	Cell cycle progress
Q71UI9*	Histone H2A	
Q0D2M2	Histone H2B	
E7END7*	Ras-related protein Rab-1A	Oncogene
B4E380	Histone H3	
B2R4R0	Histone H4	
B4DRA5	Protein transport protein Sec23B	ER to Golgi vesicle-mediated transport
B0YJ76	Dihydrofolate reductase, mitochondrial	
K7EK35	Signal transducer and activator of transcription 5A	
B7ZKR8*	Ubiquitin carboxyl-terminal hydrolase 48	Deubiquitinylation

Q9Y5J9*	Mitochondrial import inner membrane translocase subunit Tim8 B	
Q53FC7*	Heat shock 70 kDa protein 6	
H3BTL1	Microtubule-associated proteins 1A/1B light chain 3B	
A0A087X2D8	C-Jun-amino-terminal kinase-interacting protein 4	
P80217	Interferon-induced 35 kDa protein	
F5GX99	Caseinolytic peptidase B protein homolog	
A0A090N7U2	Cytosolic 5-nucleotidase 3A	
V9HW45	Pyridoxine-5-phosphate oxidase	
P56381	ATP synthase subunit epsilon, mitochondrial	
B7Z4U6	Gelsolin	Actin-binding protein, depolymerization
A0A0S2Z4X1	RNA-binding protein 10	
Q9BRF8	Serine/threonine-protein phosphatase CPPED1	
Q96C86	m7GpppX diphosphatase	
H0Y9P1	BMP-2-inducible protein kinase	
A0A024R3V4	Peptidyl-prolyl cis-trans isomerase	
P05204	Non-histone chromosomal protein HMG-17	

* Identified in 24 and 48 h treatment

Table A.2: Depleted proteins after 24 and 48h ClpX inhibitor treatment versus DMSO treated control

Protein ID	Depleted	Relevance
Q5BKZ1*	DBIRD complex subunit ZNF326	Transcription / alternative splicing-regulation
C9J5N1	Alanyl-tRNA editing protein Aarsd1	Alanyl-tRNA amino acylation
V9HWG0*	Chromobox protein homolog 5	Heterochromatin-formation
Q1W6H1	DNA-3-methyladenine glycosylase	Base excision repair
E9PPY4*	G patch domain-containing protein 4	
A0A024R912	Uridine-cytidine kinase 2	CTP salvage pathway
E9PS41	WD repeat-containing protein 74	
Q9BSH4	Translational activator of cytochrome c oxidase 1	
Q96ST3*	Paired amphipathic helix protein Sin3a	Corepressor; antagonizes Myc oncogenic activities
P60468*	Protein transport protein Sec61 subunit β	Protein translocation in the ER
A0A024RBD0	Diphosphoinositol polyphosphate phosphohydrolase 2	Signal transduction
A0A0S2Z3V0	Apolipoprotein E	Fatty acids and cholesterol transport
A0A024R4F4	DNA polymerase delta catalytic subunit	DNA repair, damage response
B4DUE1	DNA ligase	
Q5VTR2	E3 ubiquitin-protein ligase BRE1A	
Q9BU61	NADH dehydrogenase [ubiquinone] 1 alpha subcomplex assembly factor 3	Mitochondrial ETC complex 1 assembly
Q6FG43	Flotillin-2	Located in lipid-rafts, tumor progression, metastasis
Q16643	Drebrin	Actin-binding protein, polymerizing

* Identified in 24 and 48 h treatment

B Cyclin-dependent kinase 5 in tumor-initiating cells

I am thankful for the opportunity I had to work on another project during the last years. Before I started with the investigations on ClpXP inhibitors, I continued my studies on the role of Cyclin-dependent kinase 5 (Cdk5) in tumor-initiating cells (TICs), a project started by Siwei Zhang during his Ph.D. in Prof. Dr. Vollmar's group. In addition to several functional effects of Cdk5 silencing and inhibition, I further focused on the impact of Cdk5 on tumorsphere formation and on the underlying signaling. I elucidated a novel mechanism, the Cdk5-Foxo1-Bim axis, which mediates cell death of TICs. Please find the original article attached which was successfully published in the *British Journal of Cancer* in February 2017.

Mandl, M. M. *et al*. Inhibition of Cdk5 induces cell death of tumor-initiating cells. *British journal of cancer*, doi:10.1038/bjc.2017.39 (2017).

FULL PAPER

BJC

British Journal of Cancer (2017), 1–11 | doi: 10.1038/bjc.2017.39

Keywords: Cdk5; cancer; tumour-initiating cells

Inhibition of Cdk5 induces cell death of tumor-initiating cells

Melanie M Mandl[1], Siwei Zhang[1], Melanie Ulrich[1], Elisa Schmoeckel[2], Doris Mayr[2], Angelika M Vollmar[1] and Johanna Liebl*[,1]

[1]Department of Pharmacy, Pharmaceutical Biology, Ludwig-Maximilians-University of Munich (LMU), Butenandtstr 5-13, Munich 81377, Germany and [2]LMU Hospital, Institute of Pathology, Ludwig-Maximilians-University of Munich (LMU), Thalkirchnerstraße 36, Munich 80337, Germany

Background: Tumour-initiating cells (TICs) account for chemoresistance, tumour recurrence and metastasis, and therefore represent a major problem in tumour therapy. However, strategies to address TICs are limited. Recent studies indicate Cdk5 as a promising target for anti-cancer therapy and Cdk5 has recently been associated with epithelial–mesenchymal transition (EMT). However, a role of Cdk5 in TICs has not been described yet.

Methods: Expression of Cdk5 in human cancer tissue was analysed by staining of a human tissue microarray (TMA). Functional effects of Cdk5 overexpression, genetic knockdown by siRNA and shRNA, and pharmacologic inhibition by the small molecule roscovitine were tested in migration, invasion, cell death, and tumorsphere assays and in tumour establishment *in vivo*. For mechanistic studies, molecular biology methods were applied.

Results: In fact, here we pin down a novel function of Cdk5 in TICs: knockdown and pharmacological inhibition of Cdk5 impaired tumorsphere formation and reduced tumour establishment *in vivo*. Conversely, Cdk5 overexpression promoted tumorsphere formation which was in line with increased expression of Cdk5 in human breast cancer tissues as shown by staining of a human TMA. In order to understand how Cdk5 inhibition affects tumorsphere formation, we identify a role of Cdk5 in detachment-induced cell death: Cdk5 inhibition induced apoptosis in tumorspheres by stabilizing the transcription factor Foxo1 which results in increased levels of the pro-apoptotic protein Bim.

Conclusions: In summary, our study elucidates a Cdk5-Foxo1-Bim pathway in cell death in tumorspheres and suggests Cdk5 as a potential target to address TICs.

Tumour-initiating cells (TICs) limit therapeutic success of anti-cancer chemotherapy as they show high tumour-initiating potential, cause the establishment of metastases and are resistant to standard therapy (Mani *et al*, 2008; Scheel and Weinberg, 2012; Pinto *et al*, 2013; Pattabiraman and Weinberg, 2014). Consequently, therapeutic strategies that address TICs may substantially improve anti-cancer treatment and patient prognosis.

In order to find new approaches for targeting TICs, research on TICs has been strongly intensified during recent years. Various mechanisms that contribute to TIC generation and survival have been elucidated (Scheel and Weinberg, 2012); TIC generation has been associated with epithelial–mesenchymal transition (EMT), a process of cellular plasticity that confers mesenchymal properties to epithelial cells. During EMT, epithelial cells change their morphology, acquire highly migratory and invasive mesenchymal traits and gain stem-like properties (Mani *et al*, 2008; Scheel *et al*, 2011; Schmidt *et al*, 2015). Mechanisms responsible for the increased survival of TICs include increased DNA damage repair, altered cell cycle checkpoint control, overexpression of drug efflux proteins like multidrug resistance transporters as well as impaired

*Correspondence: Dr J Liebl; E-mail: johanna.liebl@cup.uni-muenchen.de

Received 12 January 2017; revised 23 January 2017; accepted 26 January 2017

apoptosis (Signore *et al*, 2013). Nevertheless, our understanding of the mechanisms and the regulation of signalling components contributing to TIC survival is still limited.

Cdk5 is a serine/threonine kinase pivotal for neuronal development, synaptic plasticity and neurotransmission and implicated in neurodegenerative diseases like Alzheimer's and Parkinson's disease (Dhavan and Tsai, 2001). During the last years, important non-neuronal functions of Cdk5 have been elucidated (Liebl *et al*, 2011a). Amongst others, our own studies demonstrated indispensable functions of endothelial Cdk5 in lymphatic vessel development (Liebl *et al*, 2015) and in tumour angiogenesis (Merk *et al*, 2016). Moreover, recent studies elucidated functions of Cdk5 in cancer, for example, we elucidated a role of Cdk5 in DNA damage response in hepatocellular carcinoma (HCC; Ehrlich *et al*, 2015). Importantly, Cdk5 was associated with tumour initiation: aberrant Cdk5 activity induced neuroendocrine medullary thyroid carcinoma (Pozo *et al*, 2013) and ASCL1-driven upregulation of Cdk5 contributed to the establishment of neuroendocrine and small-cell cancers (Meder *et al*, 2016). Notably, Cdk5 has recently been linked with EMT (Liang *et al*, 2013; Ren *et al*, 2015; Sun *et al*, 2015). However, a function of Cdk5 in TICs has not been described yet.

Along this line, we hypothesised that Cdk5 might contribute to tumour initiation. According, the aim of the present study was to evaluate a potential role and the molecular signalling of Cdk5 in TICs in order to judge Cdk5 as a potential target to address TICs.

MATERIALS AND METHODS

Cells. Cells were cultured under constant humidity at 37 °C and 5% CO_2. MCF10A cells were from ATCC (Manassas, VA, USA) and cultured with DMEM/Ham's F12 containing Horse serum 5%, EGF 20 ng ml^{-1}, Insulin 5 μg ml^{-1}, Hydrocortisone 0.5 μg ml^{-1}, Choleratoxin 0.1 μg ml^{-1} and penicillin/streptomycin (P/S). MCF7 cells were from DSMZ (Braunschweig, Germany) and cultured with RPMI 1640 containing FCS 10%, Insulin 5 μg ml^{-1}, Pyruvate 1 mM, NEAA 1% and P/S. The human urinary carcinoma cell line T24 was kindly provided by Dr B Mayer (Surgical Clinic, LMU, Munich, Germany). T24 were cultured with McCoy's medium containing FCS 10%, glutamine (1.5 mM) and for lentiviral-transduced T24 cells, puromycin (1 μg ml^{-1}) was used. Immortalised human mammary epithelial (HMLE) cells stably transfected with Twist-ER were described previously (Scheel *et al*, 2011). In brief, HMLE cells were cultivated in mammary epithelial cell growth medium (PromoCell GmbH, Heidelberg, Germany) supplemented with P/S (PAA Laboratories, Pasching, Austria) and 10 μg ml^{-1} blasticidin (Gibco, Germering, Germany). To induce EMT, HMLE Twist-ER cells were treated with 20 nM 4-Hydroxytamoxifen (4-OH-TX; Sigma-Aldrich, Taufkirchen, Germany) for 10 days, whereby cells were split and supplied with fresh medium and stimulation reagents every 3 days.

Transfection of cells. Overexpression experiments were performed using FuGENE HD reagent (Promega, Madison, WI, USA) according to the manufacturers protocol with a reagent:DNA ratio of 3 : 1. The following plasmids were used: Cdk5 (addgene 1871), p35 (addgene 1347).

Silencing experiments were performed with DharmaFECT 1 Transfection Reagent (Thermo Scientific, Waltham, MA, USA) corresponding to the manufacturers recommendation. The following siRNAs were used: non-targeting (nt) siRNA: D-001810-01; Cdk5 siRNA: J-003239-09 and J-003239-10 (Thermo Scientific/Dharmacon, Lafayette, CO, USA).

For stable downregulation of Cdk5, lentiviral transduction with non-targeting (nt) and Cdk5 shRNA was performed using MISSION shRNA Lentiviral Transduction Particles (Sigma-Aldrich) according to the manufacturer's protocol.

Cell viability assay. Cells were seeded in 96-well plates and incubated for 24 h. Cells were treated as indicated for further 24 h. Cell viability was measured using CellTiter-Blue reagent (Promega) according to the manufacturers protocol.

Proliferation assay. Cells were seeded in 96-well plates and incubated for 24 h. The initial cell number was determined. Cells were treated as indicated for further 72 h. Cell viability was measured using CellTiter-Blue reagent (Promega) according to the manufacturers protocol. For proliferation assay cells were stained with crystal violet (0.5% in methanol 20%), lysed with sodium citrate (0.05 M in ethanol 50%) and absorbance (550 nm) was measured in a plate-reading photometer (SpectraFluor PlusTM, Tecan, Crailsheim, Germany).

Apoptosis analysis. Apoptosis was performed according to Nicoletti *et al* (1991). Briefly, tumorspheres were collected, washed and stained with HFS-solution containing PI (50 μg ml^{-1}, overnight, 4 °C) followed by flow cytometry (FACSCantoII, BD Biosciences, Franklin Lakes, NJ, USA) the next day. SubG1 cells were analysed using the FlowJo 7.6 analysis software (Tree Star Inc., Ashland, OR, USA). Percentage of specific apoptosis was calculated using the formula $100 \times ((\text{experimental apoptosis (\%)} - \text{spontaneous apoptosis (\%)})/(100\% - \text{spontaneous apoptosis (\%)})$; Fulda *et al*, 2001).

Clonogenic growth. Cells were treated as indicated for 24 h. Afterwards, cells were trypsinized and freshly seeded (5000 cells per 6-well) and incubated for 7 days. Colonies were stained with crystal violet (0.5% in methanol 20%), lysed with sodium citrate (0.05 M in ethanol 50%) and the absorbance was measured in a plate-reading photometer (SpectraFluor PlusTM, Tecan, Crailsheim, Germany).

Migration and invasion. After indicated treatments (24 h), cells were labelled with CellTrackerGreen CMFDA (Life Technologies, Carlsbad, CA, USA), resuspended in medium without serum and added to the upper compartment of the transwell chamber (6.5 mm, polycarbonate membrane, 8.0 μm pore size, Corning Incorporated, Tewksbury, MA, USA). For invasion assays, the transwell inserts were coated with Matrigel. Culture medium containing 10% serum was added to the lower chamber, medium without serum served as negative control. After migration, cells were fixed in 4% PFA (10 min) and cells in the upper chamber were removed using cotton buds. Four pictures per well were taken by means of an inverted microscope (Axiovert 25/200, Zeiss, Jena, Germany) at 10-fold magnification. Cells were counted using ImageJ software.

Sphere formation assay. Sphere formation assays were performed as described (Dontu *et al*, 2003). Cells were treated with Roscovitine (24 h) or transfected as indicated (48 h). Cells were resuspended in sphere-formation medium containing 1% methyl cellulose (Sigma-Aldrich) and seeded into poly-(2-hydroxyethyl methacrylate; pHEMA, Sigma-Aldrich)-coated 12-well plates at 4×10^4 cells per well. After incubation for 10 days, 12 pictures per well were taken by using a LSM 510 Meta (Zeiss, Jena, Germany) microscope. Number of spheres bigger than 50 μm was evaluated using ImageJ.

Immunoblotting. Immunoblotting was performed as described (Ehrlich *et al*, 2015). The following primary antibodies were used: AKT (9272, Cell Signaling), AKT phospho (Ser 473; 4051, Cell Signaling), β-actin (MAB1501, Millipore), β-tubulin (2146, Cell Signaling), Bim (2819, Cell Signaling), Cdk5 (AHZ0492, Life Technologies), COX IV (4844, Cell Signaling), CREB (9104, Cell Signaling), ERK (9102, Cell Signaling), ERK phospho (9106, Cell Signaling), Foxo1 (2880, Cell Signaling), GAPDH (sc-69778, Santa Cruz), HIF1α (610958, BD Biosciences), phospho-histone H2aX (γH2aX, 2577, Cell Signaling), matrix metalloproteinase-9

(MMP-9; 3852 Cell Signaling), MMP-2 (4022 Cell Signaling), NICD-1 (4147, Cell Signaling), NICD-4 (sc-5594, Santa Cruz), Notch 1 (3608, Cell Signaling), Retinoblastoma protein phospho (Ser807/811; 8516, Cell Signaling), Retinoblastoma protein (554136, BD Biosciences), Stat3 phospho (Ser 727; 9134, Cell Signaling), Stat3 (9132, Cell Signaling). Anti-vimentin, -snail, -β-catenin, -claudin-1, N-cadherin were from Cell Signaling (EMT Sampler Kit, 9782), c-Myc (sc-788, Santa Cruz). Loading control by stain-free gels was performed by adding 0.5% TCE (2,2,2-Trichloroethanol, Sigma-Aldrich) to the PAGE gels according to the TGX Stain-Free Gels system (BioRad, Hercules, CA, USA).

Kinase activity assay. Cdk5 was immunoprecipitated using anti-Cdk5 antibody (sc-173, Santa Cruz Biotechnology) and Protein G Agarose beads (Sigma-Aldrich). Beads were resuspended in 50 μl kinase buffer (50 mM HEPES pH 7.0, 10 mM MgCl2, 1 mM DTT, 1 mM NaF, 1 mM Na3VO4, 1 mM PMSF, 3 mM β-glycerophosphate, 4 mM Complete EDTAfree). An aliquot of 2 μM ATP, 10 μCi 32P-γ-ATP (Hartmann Analytic, Braunschweig, Germany) and 0.05 μg μl^{-1} histone H1 (Type III from calf thymus, Sigma-Aldrich) were added and samples were incubated at 30 °C for 20 min before termination by boiling with 5 × SDS sample buffer (5 min, 95 °C). Electrophoresis and autoradiography was performed.

Immunostaining. Cells were seeded in 8-well slides (ibidi GmbH, μ-Slide 8-Well ibiTreat, 80826), washed, fixed with 4% PFA and permeabilized using 0.1% TritonX-100. After blocking, cells were incubated with anti-Foxo1 antibody and a secondary antibody (Alexa Fluor 488, A-11008, Invitrogen (Carlsbad, CA, USA); 1 h each). Nuclei were visualised using 5 μg ml^{-1} Hoechst33342. Microscopy was conducted using LSM 510 Meta (Zeiss, Jena, Germany) microscope.

Mitochondrial fractionation. Cells were collected, incubated with permeabilization buffer for 20 min on ice (210 mM mannitol, 200 mM sucrose, 10 mM HEPES, pH 7.2, 0.2 mM Na_2EGTA, 5 mM succinate, bovine serum albumin 0.15%, 80 µg ml^{-1} digitonin) and centrifuged (1300 r.p.m., 4 °C, 10 min). The supernatant was collected (cytosolic fraction) and the pellet permeabilized with 0.1% TritonX-100 (15 min, on ice; mitochondrial fraction).

Cytosol-nuclei fractionation. Cells were collected, washed and pelleted (1500 r.p.m., 4 °C, 5 min). The pellet was incubated with BufferA (10 mM HEPES, pH 7.9, 10 mM KCl, 0.1 mM EDTA, 0.1 mM EGTA, 1 mM DTT, 0,5 mM PMSF, Complete 1 : 100) for 15 min. After addition of Nonidet P-40 10% cells were again pelleted (12 000 r.p.m., 4 °C, 1 min). The supernatant (cytosolic fraction) was removed and the pellet was resuspended in hypertonic BufferB (20 mM HEPES, pH 7.9, 0,4 mM NaCl, 1 mM EDTA, 1 mM EGTA, 25% Glycerol, 1 mM DTT, 1 mM PMSF, Complete 1 : 100; 15 min, 4 °C shaker). After centrifugation (12 000 r.p.m., 4 °C, 5 min) the supernatant was taken as nuclei fraction.

Quantitative real-time PCR. Cells were collected and RNA was isolated using RNeasy Mini Kit (74106, Qiagen, Hilden, Germany) according to the manufacturers protocol. Reverse transcription was conducted using High Capacity cDNA Reverse Transcription Kit (4368814, Life technologies). Bim primers were purchased from Life technologies (4453320). E-cadherin, N-cadherin and vimentin primers were purchased from Metabion international AG. (E-Cadherin fw 5′ CAG CAC GTA CAC AGC CCT AA 3′, rv 5′ AAG ATA CCG GGG GAC ACT CA 3′; N-Cadherin fw 5′ ACA GTG GCC ACC TAC AAA GG 3′, rv 5′ CCG AGA TGG GGT TGA TAA TG 3′; Vimentin fw 5′ CGG CGG GAC AGC AGG 3′, rv 5′ TCG TTG GTT AGC TGG TCC AC 3′). GAPDH was used as control.

CD44 staining and FACS analysis. For CD44 surface protein quantification, a FITC labelled CD44 antibody was used (560977, BD Pharmingen). CD44 staining was carried out according to the manufacturers protocol. FITC Mouse IgG2b κ antibody was used as isotype control (555742, BD Pharmingen). Surface expression was measured by a flow cytometer (FACS Canto, BD Pharmingen). For gating and population analysis FlowJo 7.6 software (Tree Star Unc.) was used.

Tumour xenograft model. Mouse experiments were performed with approval by the District Government of Upper Bavaria in accordance with the German animal welfare and institutional guidelines. T24 cells stably transfected with non-targeting shRNA and Cdk5 shRNA (1×10^5 cells in 100 μl PBS) were subcutaneously injected into the flanks of 6-week-old female Balb/c nude mice (Harlan Envigo). Five mice per group were used. The time of tumour establishment and the number of established tumours was determined.

Immunohistochemistry. For staining of tumour sections, tumours were removed, fixed with PFA 4% for 24 h, left in PFA 1%, embedded into paraffin and 10 μm sections were prepared. The slides were deparaffinized in xylene (15 min) and rehydrated through descending concentrations of ethanol (20 min in 100% and 20 min in 95%). For antigen retrieval sections were boiled in sodium citrate buffer (10 mM sodium citrate, 0.05% Tween 20, pH 6.0) for 20 min. Endogenous peroxidase was blocked by incubation in 7.5% hydrogen peroxide for 10 min. For staining of the human tissue microarray (TMA), anti-Cdk5 antibody (Thermo Fisher Scientific, AHZ0492), diluted 1 : 100 in PBS, was applied as primary antibodies for 1 h at room temperature. For antibody detection Vectastain Universal Elite ABC Kit (Vector Laboratories, Burlingame, CA, USA) was taken according to the manual and AEC (Vector Laboratories) was used as a chromogen. Slides were counterstained with hematoxylin for 1 min and mounted using FluorSave Reagent mounting medium (Merck, Darmstadt, Germany). Images were obtained with an Olympus BX41 microscope and an Olympus DP25 camera (Olympus, Tokyo, Japan). Cdk5 staining of the TMA section was assessed using the (Remmele and Stegner, 1987) immunoreactive score as described 0 absent; 1–4 weak; 5–8 moderate; 9–12 strong expression.

Statistical analysis. All experiments were performed at least three times unless otherwise indicated in the figure legend. Data are expressed as mean ± s.e.m. Statistical analysis was performed with GraphPad Prism (version 5.04, GraphPad Software, Inc., La Jolla, CA, USA). Statistical significance was assumed if $P \leqslant 0.05$.

RESULTS

Expression of Cdk5 in human cancer tissue. Analysis of Cdk5 expression revealed increased levels of Cdk5 in the cancer cell lines MCF7 and T24, and MDA-MB-231 in comparison to the non-cancerous epithelial cell line MCF10A (Figure 1A). This was in line with the expression of Cdk5 in human cancer tissue: staining of a human TMA from 198 female breast cancer patients revealed that Cdk5 expression seemed to be stronger in cancer tissue compared to healthy breast tissue. The staining was evaluated according to the IRS score showing that human tumour tissues expressed Cdk5 in 22.5% at low IRS score, in 46.1% at medium IRS score and in 31.4% at high-IRS score, whereas healthy tissues expressed Cdk5 only at low (28.6%) or median (71.4%) intensity (Figure 1B). A strong staining-intensity was not detected in healthy breast tissue. Moreover, Cdk5 expression and kinase activity (Histone H1 phosphorylation) were increased in cells with an EMT-induced mesenchymal phenotype in comparison to epithelial cells (Figure 1C and D). This set of data points to a role of Cdk5 in mesenchymal tumour cells.

Cdk5 regulates growth and motility of cancer cells. Next, the impact of genetic knockdown of Cdk5 with transient silencing by

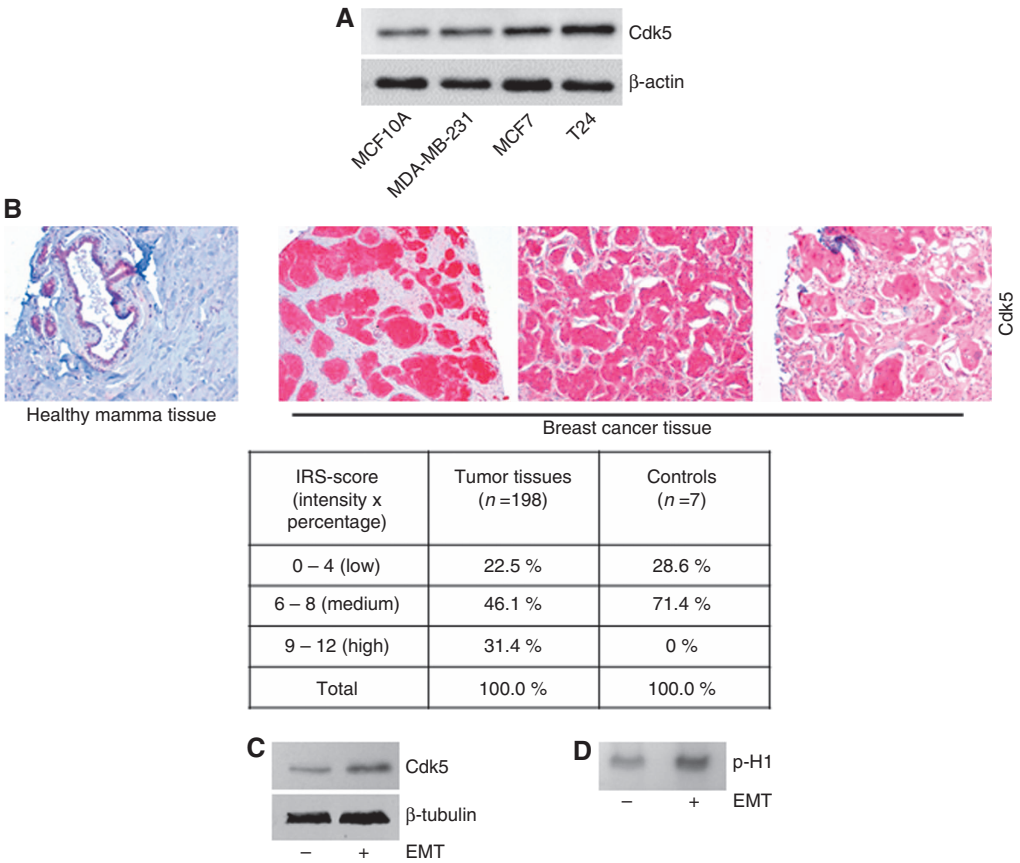

IRS-score (intensity x percentage)	Tumor tissues (n =198)	Controls (n =7)
0 – 4 (low)	22.5 %	28.6 %
6 – 8 (medium)	46.1 %	71.4 %
9 – 12 (high)	31.4 %	0 %
Total	100.0 %	100.0 %

Figure 1. Expression of Cdk5 in human cell lines and cancer tissue. (**A**) The immunoblots show levels of Cdk5 in breast epithelial cells MCF10A, and cancer cell lines MDA-MB-231, MCF7 and T24. Actin indicates equal loading ($n=3$). (**B**) Representative immunostainings from a human breast cancer TMA show Cdk5 expression in healthy mamma tissue and breast cancer tissues. The table displays the evaluation of Cdk5 expression in tumour tissues ($n=198$) and healthy tissues (controls, $n=7$) according to the IRS score (intensity × positivity). (**C**) Immunoblots show Cdk5 expression in HMLE cells that have (+) or have not (−) undergone EMT. Tubulin indicates equal loading ($n=3$). (**D**) Cdk5 activity in HMLE cells that have (+) or have not (−) undergone EMT is shown by phosphorylated histone H1 (p-H1; $n=3$).

siRNA and stable lentiviral shRNA transduction as well as pharmacological inhibition of Cdk5 with the small molecule roscovitine on cancer cell functions was analysed. Cdk5 inhibition impaired cancer cell growth as the proliferation of Cdk5 shRNA cells was reduced (Figure 2A). In line, pharmacological inhibition of Cdk5 with roscovitine concentration dependently reduced proliferation and cell viability of various breast and bladder cancer cell lines (Figure 2B and C). Although Cdk5 expression and kinase activity was increased in cells with a mesenchymal phenotype, EC50 of roscovitine was similar in epithelial (MCF10A, MCF7, T24), as well as in mesenchymal (MDA-MB-231, EMT-induced HMLE) cell lines. This might be due to the expression of different Cdks by the cell lines which are inhibited by roscovitine and therefore contribute to its anti-proliferative effect. Moreover, both Cdk5 downregulation and inhibition reduced long-term colony formation (Figure 2D and E).

Besides abrogating cancer cell growth, Cdk5 knockdown reduced cancer cell migration and invasion (Figure 3A and B Supplementary Figure 1). A concentration-dependent decrease of migration by Cdk5 inhibition with roscovitine again demonstrates pharmacologic accessibility of Cdk5 (Figure 3C).

Cdk5 regulates sphere formation. To analyse a potential function of Cdk5 in cancer stem cell (TIC) formation, we performed tumorsphere assays with cultivation of cells under specific conditions in suspension and with serum starvation which exclusively allows clonal expansion of TICs. In fact, Cdk5 knockdown with shRNA (Figure 4A) as well as inhibition with roscovitine (Figure 4B and C and Supplementary Figure 2) reduced tumorsphere formation. Conversely, Cdk5 overexpression in non-cancerous epithelial cells led to increased sphere formation (Figure 4D). Furthermore, time of establishment and number of established tumours was reduced by Cdk5 knockdown *in vivo* (Figure 4E). In sum, this set of data suggests a potential contribution of Cdk5 to tumour initiation.

Cdk5 does not regulate tumorsphere formation by modulating EMT and cell survival. To understand how Cdk5 contributes to tumorsphere formation, we first focused on EMT as Cdk5 was recently described to contribute to TGFβ-induced EMT (Liang *et al*, 2013) and as our data showed that Cdk5 was activated in cells that have undergone EMT (Figure 1C and D). However, common EMT markers like the epithelial marker E-cadherin and the mesenchymal markers N-cadherin and vimentin were not changed by Cdk5 knockdown (Figure 5A and B). The generation of TICs as well as the EMT process itself are described to be influenced by Notch signalling pathways (Harrison *et al*, 2010a) and we recently elucidated that Cdk5 interferes with Notch signalling in tumour angiogenesis (Merk *et al*, 2016). Nevertheless, Cdk5 neither influenced the generation of active Notch1 and Notch4 intracellular domains N1-ICD and N4-ICD nor the Notch downstream target c-Myc that have been associated with TICs (Cho *et al*, 2010; Harrison *et al*, 2010b; Lombardo *et al*, 2012; Figure 5C). Moreover, the expression of CD44, a transmembrane adhesion receptor that directs the migration of mesenchymal stem cells and represents a characteristic surface molecule of TICs (Zoller, 2011) was not changed in Cdk5 knockdown cells (Figure 5D). Finally, keeping in mind that Cdk5 affects cell migration and invasion we

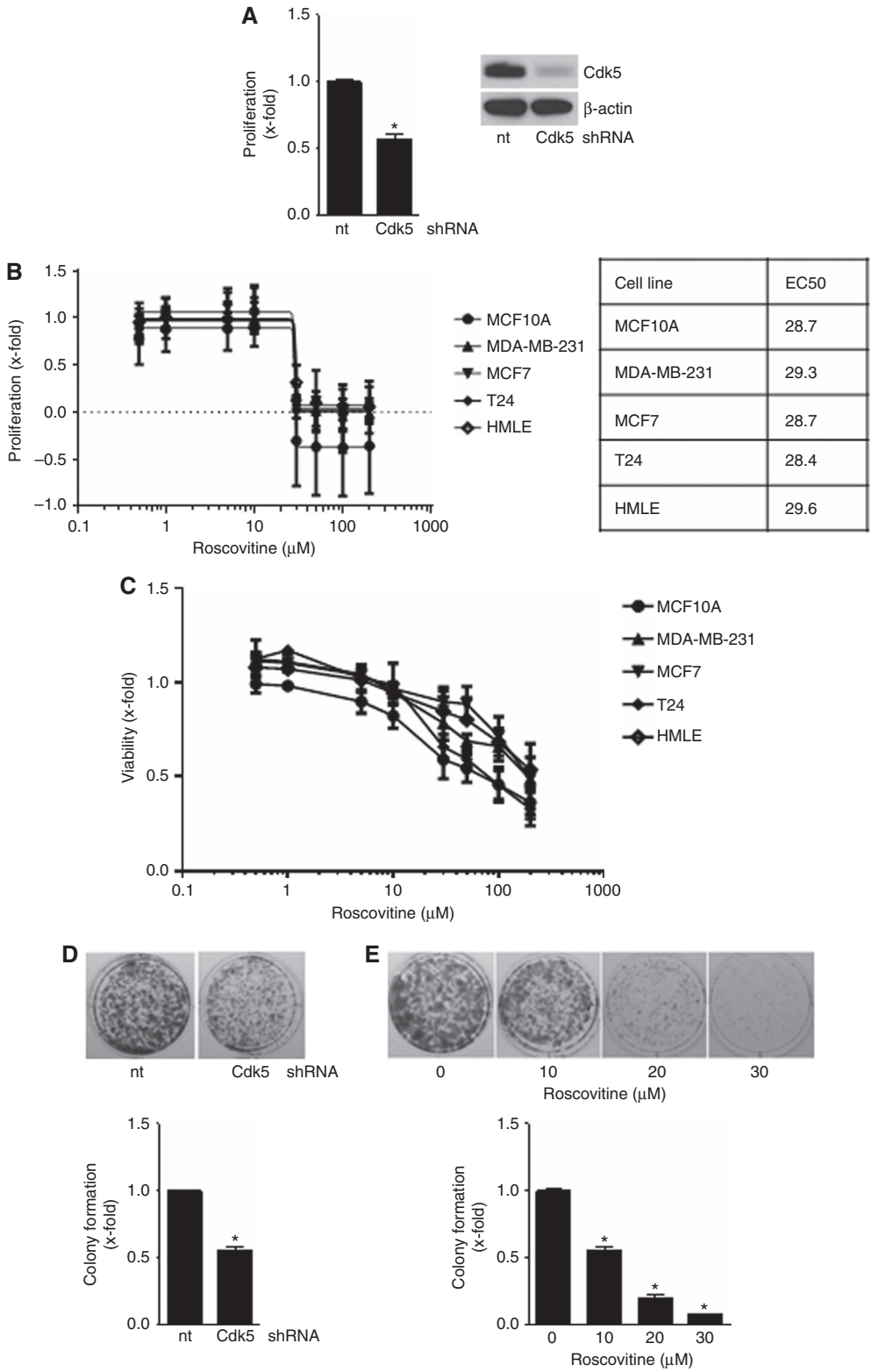

Cell line	EC50
MCF10A	28.7
MDA-MB-231	29.3
MCF7	28.7
T24	28.4
HMLE	29.6

Figure 2. Cdk5 inhibition impairs cancer cell growth. (**A**) Proliferation of non-targeting (nt) or Cdk5 shRNA-transduced cells is shown (mean ± s.e.m., *$P<0.001$, $n=3$). Immunoblots of non-targeting (nt) or Cdk5 shRNA-transduced T24 cells for Cdk5 and β-actin (loading control) proof Cdk5 knockdown. (**B**) Proliferation of MCF10A, MCF7, T24, MDA-MB-231, epithelial and mesenchymal HMLE cells treated with roscovitine for 72 h at indicated concentrations is shown. EC50 values for the various cell lines are indicated. (**C**) Viability of MCF10A, MCF7, T24, MDA-MB-231, epithelial and mesenchymal HMLE cells treated with roscovitine for 24 h at indicated concentrations is shown. (**D**) Colony formation of non-targeting (nt) and Cdk5 shRNA T24 cells after 7 days is shown. Bar graph shows quantification (mean ± s.e.m., *$P<0.001$, $n=3$). (**E**) Colony formation of T24 cells treated with roscovitine for 24 h before freshly seeding at low density and cultivation for further 7 days is shown. Bar graph shows quantification (mean ± s.e.m., *$P<0.001$, $n=3$).

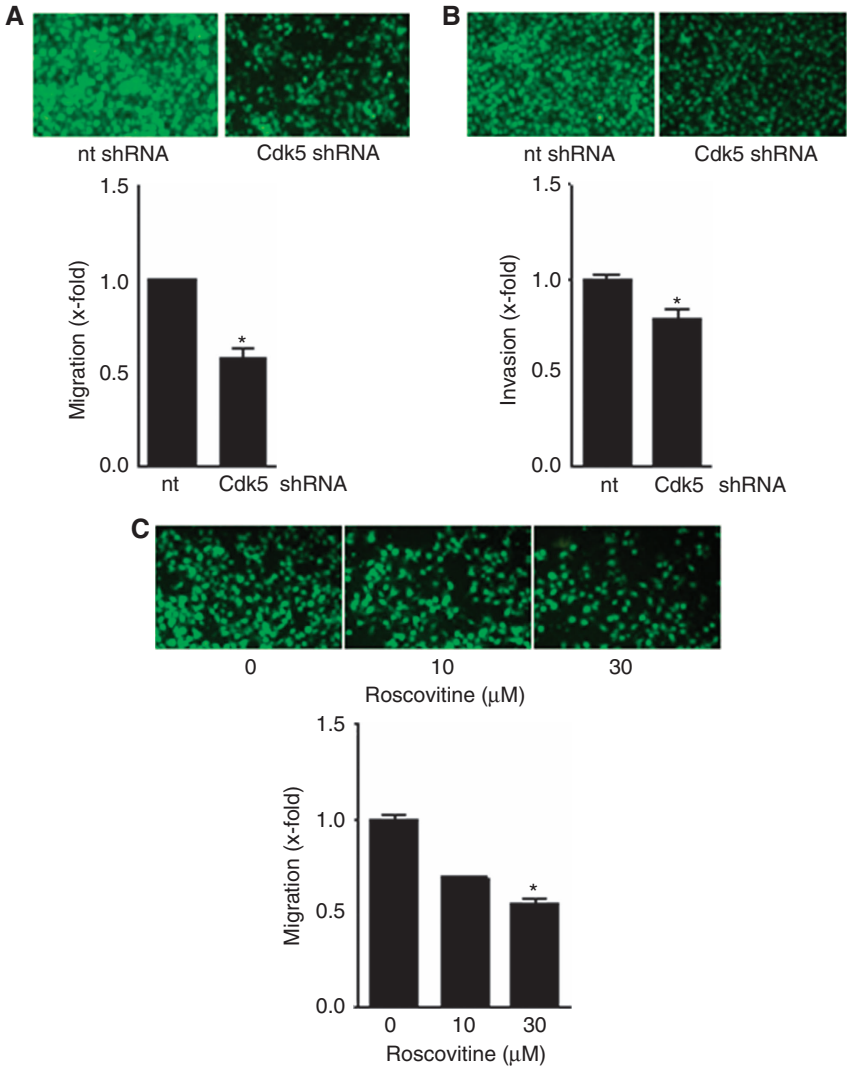

Figure 3. Cdk5 inhibition reduces cancer cell motility. (**A**) FCS-induced migration of non-targeting (nt) or Cdk5 shRNA-transduced T24 cells is shown (mean ± s.e.m., *$P<0.001$, $n=3$). (**B**) FCS-induced invasion of T24 cells transduced with non-targeting (nt) or Cdk5 shRNA is shown (mean ± s.e.m., *$P<0.001$, $n=3$). (**C**) FCS-induced migration of T24 cells with/without treatment with roscovitine is shown (mean ± s.e.m., *$P<0.001$, $n=3$).

further focused on MMPs which were also described to drive cancer progression via the EMT process (Radisky and Radisky, 2010). However, MMP2 and MMP9 were not influenced by Cdk5 (Figure 5E). This set of data suggests that the observed impact of Cdk5 on sphere formation is not due to a regulation of the EMT process. Next, we investigated whether pathways that have been associated with cancer cell survival are influenced by Cdk5. AKT, ERK, Hypoxia-inducible factor HIF1α or Stat3 can contribute to detachment-induced survival (Lin *et al*, 2007; Courapied *et al*, 2010; Hsu *et al*, 2013; Buchheit *et al*, 2014; Hu *et al*, 2015b), but were not modulated by Cdk5 knockdown in tumorspheres (Figure 5F). Additionally, the phosphorylation of Retinoblastoma protein (Rb), a cell cycle regulator and target of Cdk5 in neuroendocrine thyroid cancer (Pozo *et al*, 2013) was not affected by Cdk5 knockdown (Figure 5F). We previously elucidated that Cdk5 regulates DNA damage response in HCC (Ehrlich *et al*, 2015). However, phosphorylation of histone H2aX which is caused by DNA damage was not modulated by Cdk5 knockdown in T24 cells (Figure 5G).

Cdk5 inhibition mediates cell death in tumorspheres by increasing the pro-apoptotic protein Bim. TICs are often resistant to apoptotic cell death by altering proteins of the apoptosis machinery (Keitel *et al*, 2014). In fact, cell death was increased in tumorspheres from Cdk5 knockdown cells (Figure 6A) or in cells with pharmacologic Cdk5 inhibition (Figure 6B, Supplementary Figure 3). In addition, the pro-apoptotic BH3-only protein Bim that is a known mediator of detachment-induced cell death (Maamer-Azzabi *et al*, 2013; Buchheit *et al*, 2015) was increased in Cdk5 knockdown cells (Figure 6C). As the intrinsic apoptosis machinery is activated by Bim translocation to mitochondria (Buchheit *et al*, 2015), we performed mitochondria fractionation at different time points of cell detachment which revealed that Bim protein was increased in mitochondria from Cdk5 knockdown cells (Figure 6D). By investigating how Cdk5 knockdown affects Bim, we observed an increase in Bim mRNA in Cdk5 knockdown cells (Figure 6E). The transcription of Bim is regulated by forkhead transcription factor type O (Foxo) proteins and Cdk5 has previously been linked with Foxo1 in neurons (Zhou *et al*, 2015). In fact, we observed that Cdk5 knockdown and inhibition increased Foxo1 (Figure 6F and G) both in the cytoplasm as well as in the nucleus (Figure 6H and I), whereas mRNA transcription was not affected (Supplementary Figure 4). In sum, this set of data suggests that Cdk5 regulates cell death in tumorspheres by mediating Bim transcription via Foxo1.

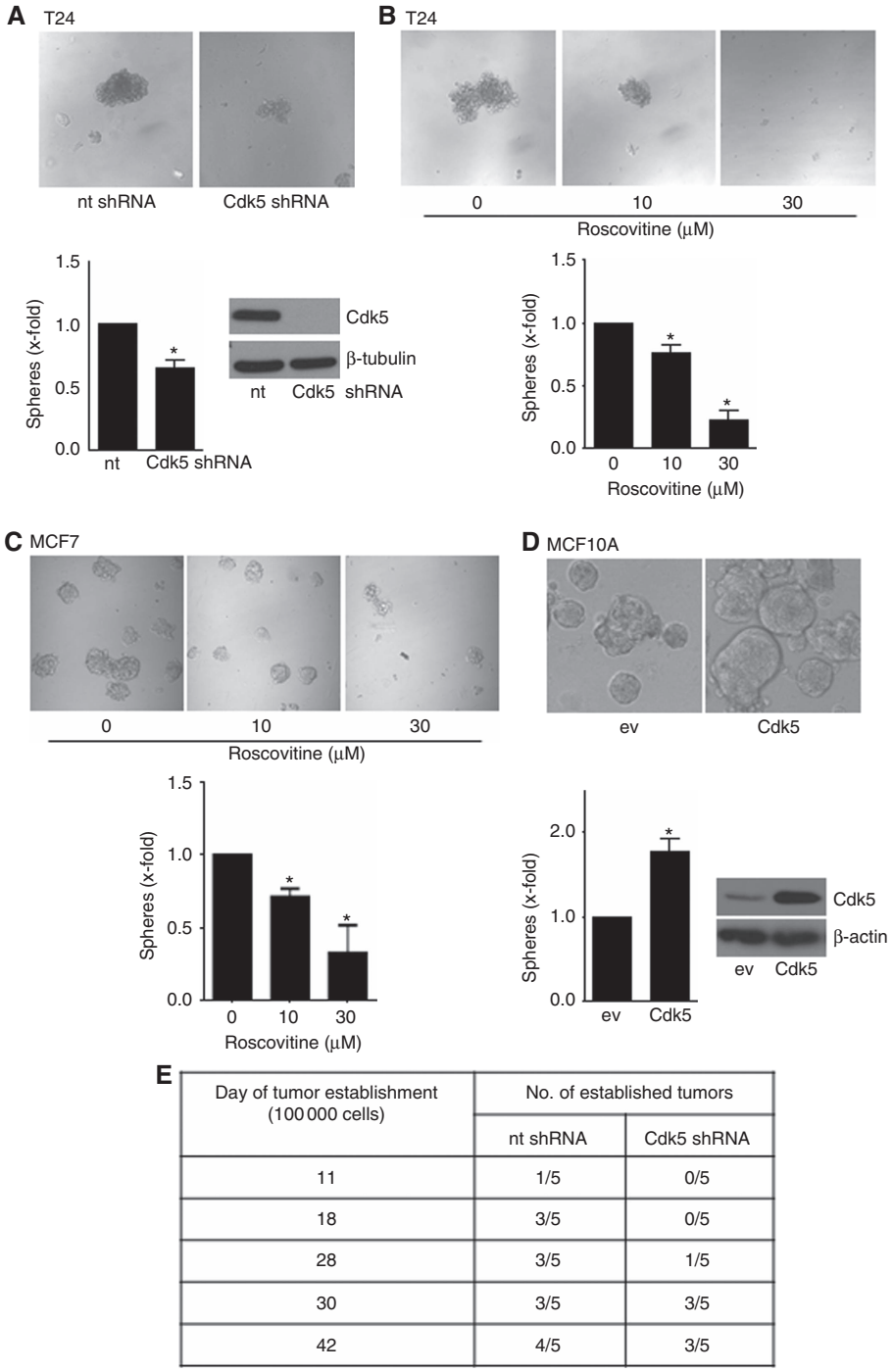

E

Day of tumor establishment (100 000 cells)	No. of established tumors	
	nt shRNA	Cdk5 shRNA
11	1/5	0/5
18	3/5	0/5
28	3/5	1/5
30	3/5	3/5
42	4/5	3/5

Figure 4. Cdk5 regulates sphere formation and tumour establishment. (**A**) Tumorsphere formation of non-targeting (nt) and Cdk5 shRNA T24 cells is shown (mean ± s.e.m., $*P<0.05$, $n=3$). Immunoblots of non-targeting (nt) or Cdk5 shRNA-transduced T24 cells for Cdk5 and β-tubulin (loading control) proof Cdk5 knockdown. (**B**) Tumorsphere formation after pretreatment of T24 cells with roscovitine for 24 h before resuspension in fresh sphere-formation medium and cultivation for further 10 days in presence of roscovitine is shown (mean ± s.e.m., $*P<0.001$, $n=3$). (**C**) Tumorsphere formation after pretreatment of MCF7 cells with roscovitine for 24 h before resuspension in fresh sphere-formation medium and cultivation for further 10 days in presence of roscovitine is shown (mean ± s.e.m., $*P<0.05$, $n=3$). (**D**) Sphere formation of non-tumorous MCF10A cells overexpressing empty vector (ev) or Cdk5/p35 (Cdk5) is shown (mean ± s.e.m., $*P<0.05$, $n=3$). The immunoblot of MCF10A cells overexpressing either empty vector (ev) or Cdk5/p35 (Cdk5) for Cdk5 and β-actin (loading control) proofs Cdk5 overexpression. (**E**) Cdk5 inhibition impairs tumor establishment *in vivo*. The tables indicate the time of tumour establishment and the number of established tumours of mice injected with non-targeting (nt) shRNA and Cdk5 shRNA tumour cells (1×10^5 cells).

DISCUSSION

Tumor-initiating cells represent a major problem in cancer therapy as they account for tumour recurrence, establishment of metastasis and resistance towards therapeutics. Thus, recent research strongly focused on investigating TIC properties and mechanisms that are involved in TIC formation and maintenance in order to drive the development of anti-TIC therapies (Pattabiraman and Weinberg, 2014): Signalling pathways which contribute to the self-renewing

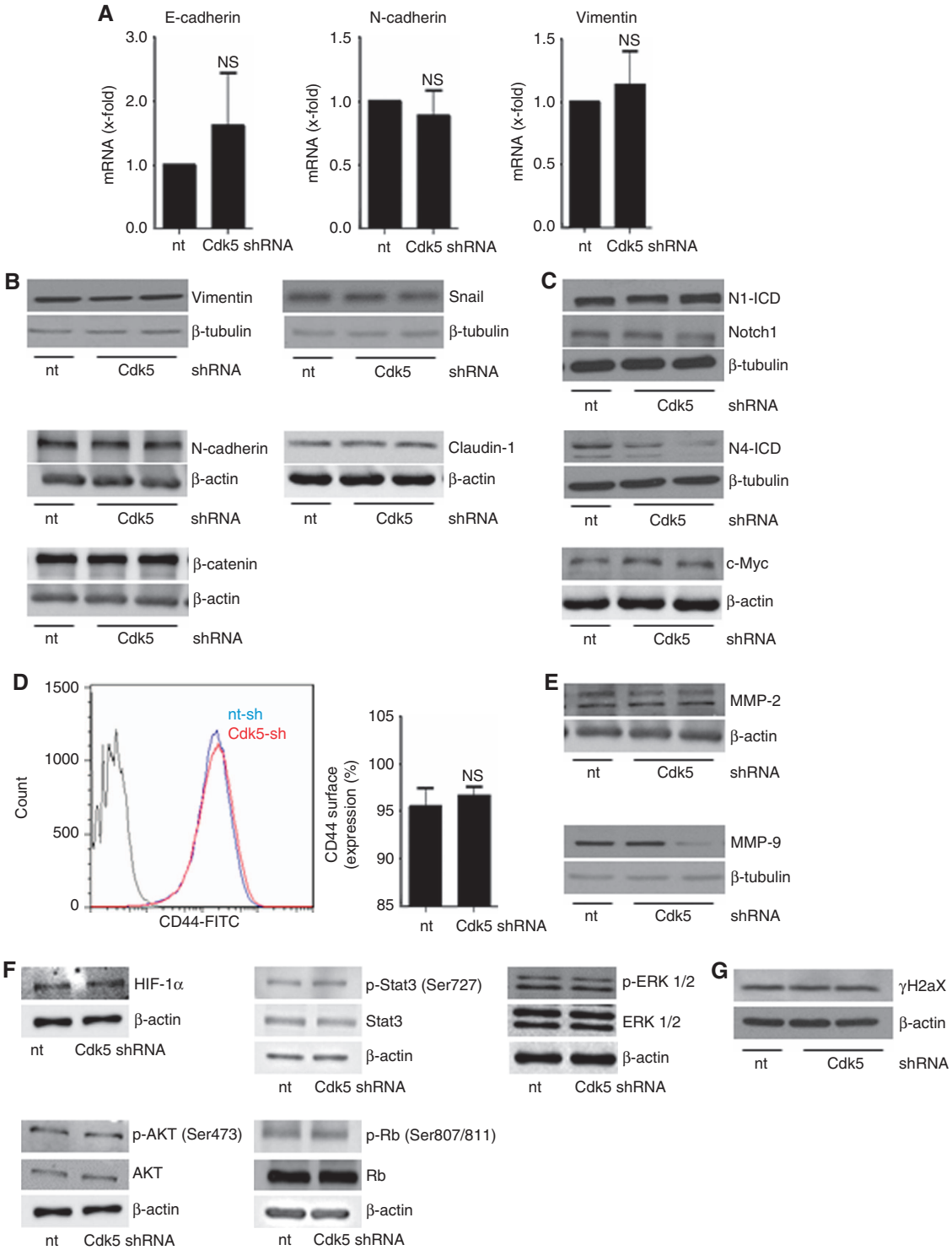

Figure 5. Cdk5 knockdown does neither affect EMT related signalling nor common cell survival pathways or DNA damage. (**A**) Bar graphs show mRNA levels of the EMT markers E-cadherin, N-cadherin and vimentin in non-targeting (nt) and Cdk5 shRNA-transduced cells ($n = 3$). (**B**) Immunoblots show protein levels of the EMT markers vimentin, snail, β-catenin, N-cadherin and claudin-1 from non-targeting (nt) and Cdk5 shRNA cells. β-actin and β-tubulin indicate equal loading. ($n = 3$). (**C**) Immunoblots for Notch1 and Notch4 intracellular domain (N1-ICD, N4-ICD) and the Notch downstream target c-Myc in non-targeting (nt) and Cdk5 knockdown cells are shown. β-actin and β-tubulin indicate equal loading. ($n = 3$). (**D**) Histogram plot from FACS analysis from CD44 surface expression is shown. Bars represent quantification of CD44-positive cells in non-targeting (nt) and Cdk5 shRNA cells (mean ± s.e.m., NS = not significant, $n = 3$). (**E**) MMP-2 and MMP-9 immunoblots are shown. β-actin and β-tubulin indicate equal loading. ($n = 3$). (**F**) Immunoblots show different proteins related to cell survival in non-targeting (nt) and Cdk5 shRNA cells. HIF1α, total and phosphorylated Stat3 (S727), ERK1/2, AKT (S473) and Retinoblastoma protein (807/811) are shown. β-actin indicates equal loading ($n = 3$). (**G**) The immunoblots show phospho-histone H2aX (γH2aX) in non-targeting (nt) and Cdk5 shRNA cells. β-actin indicates equal loading ($n = 3$).

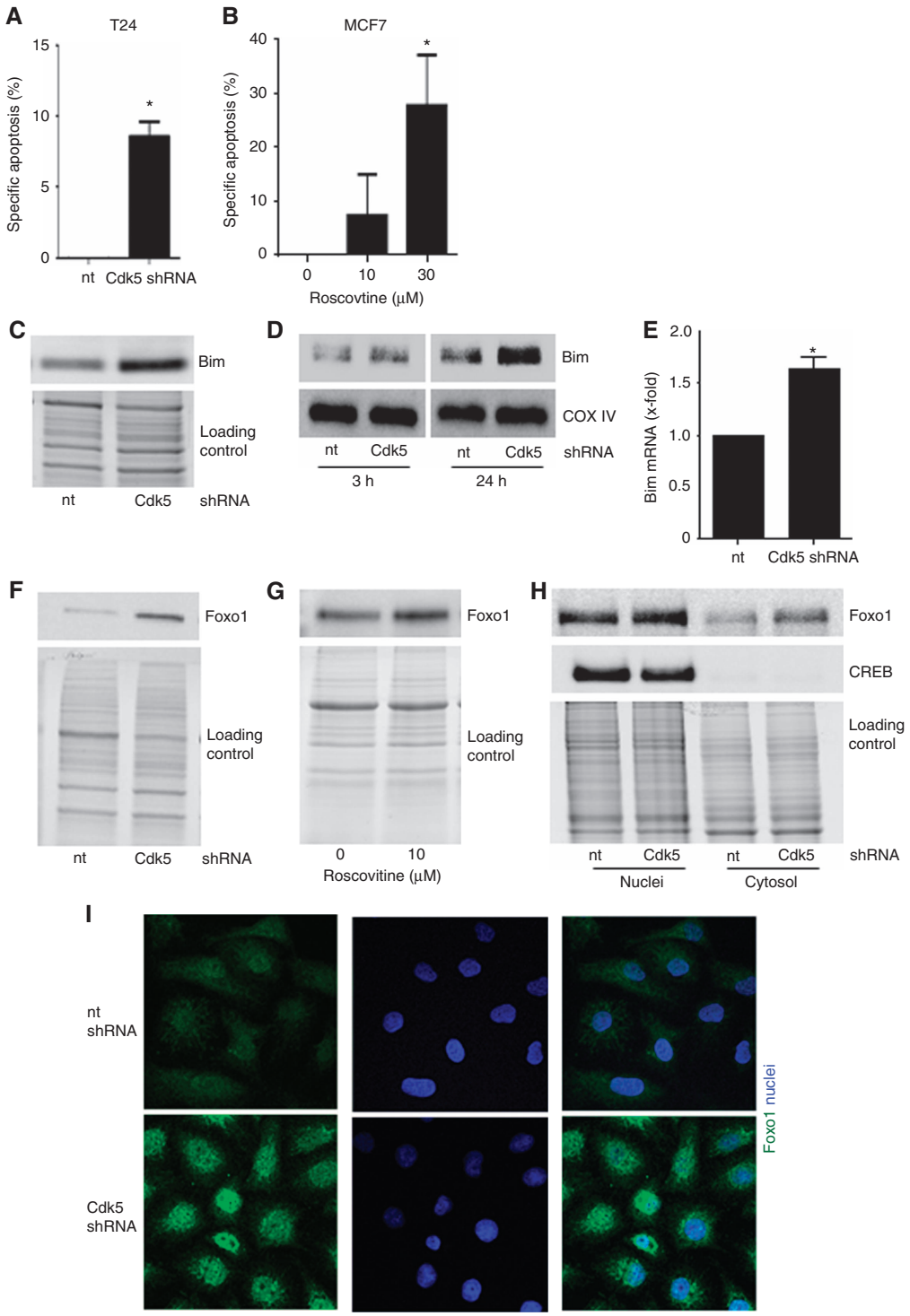

Figure 6. Cdk5 knockdown induces apoptosis in tumorspheres by increasing the pro-apoptotic protein Bim. (**A**) Cdk5 knockdown induces apoptosis in tumorspheres. Specific apoptosis in sphere-forming T24 cells is shown (mean ± s.e.m., $*P<0.01$, $n=3$). (**B**) Cdk5 inhibition induces apoptosis in tumorspheres. Specific apoptosis of MCF7 tumorspheres after pretreatment of cells with roscovitine for 24 h before resuspension in fresh sphere-formation medium and cultivation for further 10 days in presence of roscovitine is shown (mean ± s.e.m., $*P<0.05$, $n=3$). (**C**) The immunoblot shows levels of the pro-apoptotic protein Bim in non-targeting (nt) and Cdk5 shRNA cells. Equal loading is indicated ($n=3$). (**D**) Immunoblots show Bim protein in mitochondrial fractions of non-targeting (nt) and Cdk5 shRNA T24 cells at detachment of 3 h and 24 h. The mitochondrial marker COX IV indicates equal loading ($n=3$). (**E**) The bar graph displays Bim mRNA levels of non-targeting shRNA (nt) and Cdk5 shRNA cells (mean ± s.e.m., $*P<0.05$, $n=3$). (**F**) Immunoblots indicate increased Foxo1 protein levels in Cdk5 knockdown T24 cells. Whole-protein bands indicate equal loading ($n=3$). (**G**) Immunoblots indicate increased Foxo1 protein levels in mesenchymal HMLE cells treated with roscovitine (24 h). Whole-protein bands indicate equal loading ($n=3$). (**H**) Cdk5 knockdown leads to an increase of Foxo1. Immunoblots show Foxo1 protein of cytosolic and nuclear fractionation of T24 cells. cAMP response element-binding protein (CREB) serves as marker for the nuclei fraction. Whole-protein bands indicate equal loading ($n=3$). (**I**) Immunostainings show Foxo1 protein (green) and nucleus (Hoechst33342, blue) of non-targeting (nt) and Cdk5 shRNA T24 cells ($n=3$).

properties of stem cells like TGFβ, WNT, Notch and Hedgehog are supposed as potential attractive targets to address TICs. In fact, various compounds addressing components of these pathways have shown anti-TIC effects and are currently investigated in clinical trials. In order to identify targeted therapies that address TICs, compound library screens have been carried out and, amongst others, identified the compound salinomycine as anti-TIC drug. Moreover, anti-TIC approaches include targeting of the tumour microenvironment which often triggers EMT induction and tumour initiation. Differentiation therapy by all-trans retinoic acid promotes the differentiation of promyelocytic leukaemic cells into mature granulocytes and is successfully used in therapy of promyelocytic leukaemia. Likewise, also other forms of cancers associated with TICs might be effectively treated by differentiation inducing therapeutics. In addition, immunotherapy and the targeting of TIC metabolism were supposed as promising potential anti-TIC strategies. All in all, there are some promising drugs and strategies, but there is still a craving need for more candidates to address TICs.

In fact, here, we elucidate Cdk5 as a novel player in TICs which might point to Cdk5 as a potential target to address TICs. Cdk5 can be addressed pharmacologically and Cdk-inhibiting small molecules are currently investigated as potential anti-cancer drugs (Liebl *et al*, 2011b; Weitensteiner *et al*, 2013; Ehrlich *et al*, 2015). Two Cdk inhibitors are currently evaluated in clinical trials: Roscovitine represents a well-established inhibitor of Cdks that has been developed in the late 1990 (Meijer *et al*, 1997). It has shown modest anti-cancer activity in xenograft tumour models *in vivo* and has been tested in a number of Phase I and II clinical trials where it has shown some anti-cancer activity in around half of the patients (Khalil *et al*, 2015). Dinaciclib, a newer Cdk inhibitor, has demonstrated significant clinical activity in patients with lymphocytic leukaemia and multiple myeloma (Flynn *et al*, 2015; Kumar *et al*, 2015). Moreover, dinaciclib in combination with an AKT-inhibitor showed therapeutic efficiency in patient-derived human pancreatic cancer xenograft models and will be followed by clinical trial evaluation (Hu *et al*, 2015a). These results are very promising, however, in contrast, a phase I trial with patients suffering from triple-negative breast cancer has demonstrated severe toxic effects and failure of treatment response of a combination treatment of dinaciclib and epirubicin (Mitri *et al*, 2015). Thus, further trials are required to evaluate the potential of dinaciclib as anti-cancer agents.

In order to investigate the underlying mechanism of Cdk5 in TICs, we first focused on EMT as recent studies demonstrated an involvement of Cdk5 in EMT (Liang *et al*, 2013; Ren *et al*, 2015; Sun *et al*, 2015). Moreover, the forkhead transcription factor Foxc2 was identified as a critical regulator of EMT and TICs in breast cancer (Hollier *et al*, 2013) and we recently elucidated a relationship between Cdk5 and Foxc2 in the lymphatic endothelium (Liebl *et al*, 2015). In line, our results revealed that Cdk5 expression was increased in cells that have undergone EMT and in human cancer tissues. Nevertheless, Cdk5 did not regulate tumorsphere formation by EMT, suggesting a specific function of Cdk5 in TICs. Recently, Cdk5 was shown to contribute to the initiation of small-cell lung cancer: overexpression of the NOTCH target ASCL1-induced activation of Cdk5 that phosphorylated and inactivated Rb1 (Meder *et al*, 2016). In line, aberrant Cdk5 activity was shown to promote tumorigenesis of medullary thyroid cancer by phosphorylation of the retinoblastoma protein (Rb1; Pozo *et al*, 2013). Nevertheless, Cdk5 did not modulate Notch or Rb1 in Cdk5 knockdown cells. In fact, our work proposed a role of Cdk5 in cell death of tumorspheres by regulating the pro-apoptotic protein Bim. This is in line with previous studies showing that pro-apoptotic proteins like Bim were diminished in cells that have undergone EMT which contributed to apoptosis resistance of TICs (Keitel *et al*, 2014). As Bim suppressed the survival of disseminated tumour cells (Merino *et al*, 2015) and induced apoptosis in leukaemia stem/progenitor cells (Pan *et al*, 2015), induction of Bim might represent a potential anti-TIC strategy. As mechanism of Cdk5 to control Bim, we found that Cdk5 knockdown increased Bim at the transcriptional level by increasing the Forkhead box Type O transcription factor 1 (Foxo1). This is in line with findings in neurons, as neuronal Cdk5 regulates Foxo1 by phosphorylation at its S249 site, favoring its nuclear export and inhibiting its transcriptional activity (Zhou *et al*, 2015). Foxos play a pivotal role in tumour suppression and are regulated by PI3K/AKT; nuclear Foxos induce the expression of pro-apoptotic genes such as Bim, leading to cell death, whereas AKT-mediated phosphorylation induces cytoplasmic translocation and inhibits Foxo target gene transcription (Calnan and Brunet, 2008). In line with our study, the Akt/Foxo3/Bim pathway has been previously shown to be associated with cancer stem cell survival (Gargini *et al*, 2015).

In summary, our results demonstrate a Cdk5-Foxo1-Bim pathway in cell death in tumorspheres. As Cdk5 is pharmacologically accessible, it is suggested as a potential target to address TICs.

ACKNOWLEDGEMENTS

We thank Dr Christina Scheel (Helmholtz Zentrum München, Institute of Stem Cell Research, Neuherberg, Germany) for providing HMLE cells. We thank Kerstin Loske, Rita Socher, Silvia Schnegg and Julia Blenninger for their help with the experiments. The animal facility of the Department of Pharmacy, Ludwig-Maximilians-University Munich is gratefully acknowledged.

CONFLICT OF INTEREST

The authors declare no conflict of interest.

REFERENCES

Buchheit CL, Angarola BL, Steiner A, Weigel KJ, Schafer ZT (2015) Anoikis evasion in inflammatory breast cancer cells is mediated by Bim-EL sequestration. *Cell Death Differ* **22**(8): 1275–1286.

Buchheit CL, Weigel KJ, Schafer ZT (2014) Cancer cell survival during detachment from the ECM: multiple barriers to tumour progression. *Nat Rev Cancer* **14**(9): 632–641.

Calnan DR, Brunet A (2008) The FoxO code. *Oncogene* **27**(16): 2276–2288.

Cho KB, Cho MK, Lee WY, Kang KW (2010) Overexpression of c-myc induces epithelial mesenchymal transition in mammary epithelial cells. *Cancer Lett* **293**(2): 230–239.

Courapied S, Sellier H, de Carne Trecesson S, Vigneron A, Bernard AC, Gamelin E, Barre B, Coqueret O (2010) The cdk5 kinase regulates the STAT3 transcription factor to prevent DNA damage upon topoisomerase I inhibition. *J Biol Chem* **285**(35): 26765–26778.

Dhavan R, Tsai LH (2001) A decade of CDK5. *Nat Rev Mol Cell Biol* **2**(10): 749–759.

Dontu G, Abdallah WM, Foley JM, Jackson KW, Clarke MF, Kawamura MJ, Wicha MS (2003) *In vitro* propagation and transcriptional profiling of human mammary stem/progenitor cells. *Genes Dev* **17**(10): 1253–1270.

Ehrlich SM, Liebl J, Ardelt MA, Lehr T, De Toni EN, Mayr D, Brandl L, Kirchner T, Zahler S, Gerbes AL, Vollmar AM (2015) Targeting cyclin dependent kinase 5 in hepatocellular carcinoma–a novel therapeutic approach. *J Hepatol* **63**(1): 102–113.

Flynn J, Jones J, Johnson AJ, Andritsos L, Maddocks K, Jaglowski S, Hessler J, Grever MR, Im E, Zhou H, Zhu Y, Zhang D, Small K, Bannerji R, Byrd JC (2015) Dinaciclib is a novel cyclin-dependent kinase inhibitor with significant clinical activity in relapsed and refractory chronic lymphocytic leukemia. *Leukemia* **29**(7): 1524–1529.

Fulda S, Kufer MU, Meyer E, van Valen F, Dockhorn-Dworniczak B, Debatin KM (2001) Sensitization for death receptor- or drug-induced apoptosis by re-expression of caspase-8 through demethylation or gene transfer. *Oncogene* **20**(41): 5865–5877.

Gargini R, Cerliani JP, Escoll M, Anton IM, Wandosell F (2015) Cancer stem cell-like phenotype and survival are coordinately regulated by Akt/FoxO/Bim pathway. *Stem Cells* **33**(3): 646–660.

Harrison H, Farnie G, Brennan KR, Clarke RB (2010a) Breast cancer stem cells: something out of notching? *Cancer Res* **70**(22): 8973–8976.

Harrison H, Farnie G, Howell SJ, Rock RE, Stylianou S, Brennan KR, Bundred NJ, Clarke RB (2010b) Regulation of breast cancer stem cell activity by signaling through the Notch4 receptor. *Cancer Res* **70**(2): 709–718.

Hollier BG, Tinnirello AA, Werden SJ, Evans KW, Taube JH, Sarkar TR, Sphyris N, Shariati M, Kumar SV, Battula VL, Herschkowitz JI, Guerra R, Chang JT, Miura N, Rosen JM, Mani SA (2013) FOXC2 expression links epithelial-mesenchymal transition and stem cell properties in breast cancer. *Cancer Res* **73**(6): 1981–1992.

Hsu FN, Chen MC, Lin KC, Peng YT, Li PC, Lin E, Chiang MC, Hsieh JT, Lin H (2013) Cyclin-dependent kinase 5 modulates STAT3 and androgen receptor activation through phosphorylation of Ser727 on STAT3 in prostate cancer cells. *Am J Physiol Endocrinol Metab* **305**(8): E975–E986.

Hu C, Dadon T, Chenna V, Yabuuchi S, Bannerji R, Booher R, Strack P, Azad N, Nelkin BD, Maitra A (2015a) Combined inhibition of cyclin-dependent kinases (dinaciclib) and AKT (MK-2206) blocks pancreatic tumor growth and metastases in patient-derived xenograft models. *Mol Cancer Ther* **14**(7): 1532–1539.

Hu M, Peng S, He Y, Qin M, Cong X, Xing Y, Liu M, Yi Z (2015b) Lycorine is a novel inhibitor of the growth and metastasis of hormone-refractory prostate cancer. *Oncotarget* **6**(17): 15348–15361.

Keitel U, Scheel A, Thomale J, Halpape R, Kaulfuss S, Scheel C, Dobbelstein M (2014) Bcl-xL mediates therapeutic resistance of a mesenchymal breast cancer cell subpopulation. *Oncotarget* **5**(23): 11778–11791.

Khalil HS, Mitev V, Vlaykova T, Cavicchi L, Zhelev N (2015) Discovery and development of Seliciclib. How systems biology approaches can lead to better drug performance. *J Biotechnol* **202**: 40–49.

Kumar SK, LaPlant B, Chng WJ, Zonder J, Callander N, Fonseca R, Fruth B, Roy V, Erlichman C, Stewart AK, Mayo Phase C (2015) Dinaciclib, a novel CDK inhibitor, demonstrates encouraging single-agent activity in patients with relapsed multiple myeloma. *Blood* **125**(3): 443–448.

Liang Q, Li L, Zhang J, Lei Y, Wang L, Liu DX, Feng J, Hou P, Yao R, Zhang Y, Huang B, Lu J (2013) CDK5 is essential for TGF-beta1-induced epithelial-mesenchymal transition and breast cancer progression. *Sci Rep* **3**: 2932.

Liebl J, Furst R, Vollmar AM, Zahler S (2011a) Twice switched at birth: cell cycle-independent roles of the 'neuron-specific' cyclin-dependent kinase 5 (Cdk5) in non-neuronal cells. *Cell Signal* **23**(11): 1698–1707.

Liebl J, Krystof V, Vereb G, Takacs L, Strnad M, Pechan P, Havlicek L, Zatloukal M, Furst R, Vollmar AM, Zahler S (2011b) Anti-angiogenic effects of purine inhibitors of cyclin dependent kinases. *Angiogenesis* **14**(3): 281–291.

Liebl J, Zhang S, Moser M, Agalarov Y, Demir CS, Hager B, Bibb JA, Adams RH, Kiefer F, Miura N, Petrova TV, Vollmar AM, Zahler S (2015) Cdk5 controls lymphatic vessel development and function by phosphorylation of Foxc2. *Nat Commun* **6**: 7274.

Lin H, Chen MC, Chiu CY, Song YM, Lin SY (2007) Cdk5 regulates STAT3 activation and cell proliferation in medullary thyroid carcinoma cells. *J Biol Chem* **282**(5): 2776–2784.

Lombardo Y, Filipovic A, Molyneux G, Periyasamy M, Giamas G, Hu Y, Trivedi PS, Wang J, Yague E, Michel L, Coombes RC (2012) Nicastrin regulates breast cancer stem cell properties and tumor growth in vitro and in vivo. *Proc Natl Acad Sci USA* **109**(41): 16558–16563.

Maamer-Azzabi A, Ndozangue-Touriguine O, Breard J (2013) Metastatic SW620 colon cancer cells are primed for death when detached and can be sensitized to anoikis by the BH3-mimetic ABT-737. *Cell Death Dis* **4**: e801.

Mani SA, Guo W, Liao MJ, Eaton EN, Ayyanan A, Zhou AY, Brooks M, Reinhard F, Zhang CC, Shipitsin M, Campbell LL, Polyak K, Brisken C, Yang J, Weinberg RA (2008) The epithelial-mesenchymal transition generates cells with properties of stem cells. *Cell* **133**(4): 704–715.

Meder L, Konig K, Ozretic L, Schultheis AM, Ueckeroth F, Ade CP, Albus K, Boehm D, Rommerscheidt-Fuss U, Florin A, Buhl T, Hartmann W, Wolf J, Merkelbach-Bruse S, Eilers M, Perner S, Heukamp LC, Buettner R (2016) NOTCH, ASCL1, p53 and RB alterations define an alternative pathway driving neuroendocrine and small cell lung carcinomas. *Int J Cancer* **138**(4): 927–938.

Meijer L, Borgne A, Mulner O, Chong JP, Blow JJ, Inagaki N, Inagaki M, Delcros JG, Moulinoux JP (1997) Biochemical and cellular effects of roscovitine, a potent and selective inhibitor of the cyclin-dependent kinases cdc2, cdk2 and cdk5. *Eur J Biochem* **243**(1-2): 527–536.

Merino D, Best SA, Asselin-Labat ML, Vaillant F, Pal B, Dickins RA, Anderson RL, Strasser A, Bouillet P, Lindeman GJ, Visvader JE (2015) Pro-apoptotic Bim suppresses breast tumor cell metastasis and is a target gene of SNAI2. *Oncogene* **34**(30): 3926–3934.

Merk H, Zhang S, Lehr T, Muller C, Ulrich M, Bibb JA, Adams RH, Bracher F, Zahler S, Vollmar AM, Liebl J (2016a) Inhibition of endothelial Cdk5 reduces tumor growth by promoting non-productive angiogenesis. *Oncotarget* **7**(5): 6088–6104.

Mitri Z, Karakas C, Wei C, Briones B, Simmons H, Ibrahim N, Alvarez R, Murray JL, Keyomarsi K, Moulder S (2015) A phase 1 study with dose expansion of the CDK inhibitor dinaciclib (SCH 727965) in combination with epirubicin in patients with metastatic triple negative breast cancer. *Invest New Drugs* **33**(4): 890–894.

Nicoletti I, Migliorati G, Pagliacci MC, Grignani F, Riccardi C (1991) A rapid and simple method for measuring thymocyte apoptosis by propidium iodide staining and flow cytometry. *J Immunol Methods* **139**(2): 271–279.

Pan R, Ruvolo VR, Wei J, Konopleva M, Reed JC, Pellecchia M, Andreeff M, Ruvolo PP (2015) Inhibition of Mcl-1 with the pan-Bcl-2 family inhibitor (−)BI97D6 overcomes ABT-737 resistance in acute myeloid leukemia. *Blood* **126**(3): 363–372.

Pattabiraman DR, Weinberg RA (2014) Tackling the cancer stem cells—what challenges do they pose? *Nat Rev Drug Discov* **13**(7): 497–512.

Pinto CA, Widodo E, Waltham M, Thompson EW (2013) Breast cancer stem cells and epithelial mesenchymal plasticity—implications for chemoresistance. *Cancer Lett* **341**(1): 56–62.

Pozo K, Castro-Rivera E, Tan C, Plattner F, Schwach G, Siegl V, Meyer D, Guo A, Gundara J, Mettlach G, Richer E, Guevara JA, Ning L, Gupta A, Hao G, Tsai LH, Sun X, Antich P, Sidhu S, Robinson BG, Chen H, Nwariaku FE, Pfragner R, Richardson JA, Bibb JA (2013) The role of Cdk5 in neuroendocrine thyroid cancer. *Cancer Cell* **24**(4): 499–511.

Radisky ES, Radisky DC (2010) Matrix metalloproteinase-induced epithelial-mesenchymal transition in breast cancer. *J Mammary Gland Biol Neoplasia* **15**(2): 201–212.

Remmele W, Stegner HE (1987) Recommendation for uniform definition of an immunoreactive score (IRS) for immunohistochemical estrogen receptor detection (ER-ICA) in breast cancer tissue. *Pathologe* **8**(3): 138–140.

Ren Y, Zhou X, Yang JJ, Liu X, Zhao XH, Wang QX, Han L, Song X, Zhu ZY, Tian WP, Zhang L, Mei M, Kang CS (2015) AC1MMYR2 impairs high dose paclitaxel-induced tumor metastasis by targeting miR-21/CDK5 axis. *Cancer Lett* **362**(2): 174–182.

Scheel C, Eaton EN, Li SH, Chaffer CL, Reinhardt F, Kah KJ, Bell G, Guo W, Rubin J, Richardson AL, Weinberg RA (2011) Paracrine and autocrine signals induce and maintain mesenchymal and stem cell states in the breast. *Cell* **145**(6): 926–940.

Scheel C, Weinberg RA (2012) Cancer stem cells and epithelial-mesenchymal transition: concepts and molecular links. *Semin Cancer Biol* **22**(5-6): 396–403.

Schmidt JM, Panzilius E, Bartsch HS, Irmler M, Beckers J, Kari V, Linnemann JR, Dragoi D, Hirschi B, Kloos UJ, Sass S, Theis F, Kahlert S, Johnsen SA, Sotlar K, Scheel CH (2015) Stem-cell-like properties and epithelial plasticity arise as stable traits after transient Twist1 activation. *Cell Rep* **10**(2): 131–139.

Signore M, Ricci-Vitiani L, De Maria R (2013) Targeting apoptosis pathways in cancer stem cells. *Cancer Lett* **332**(2): 374–382.

Sun SS, Zhou X, Huang YY, Kong LP, Mei M, Guo WY, Zhao MH, Ren Y, Shen Q, Zhang L (2015) Targeting STAT3/miR-21 axis inhibits epithelial-mesenchymal transition via regulating CDK5 in head and neck squamous cell carcinoma. *Mol Cancer* **14**: 213.

Weitensteiner SB, Liebl J, Krystof V, Havlicek L, Gucky T, Strnad M, Furst R, Vollmar AM, Zahler S (2013) Trisubstituted pyrazolopyrimidines as novel angiogenesis inhibitors. *PLoS One* **8**(1): e54607.

Zhou J, Li H, Li X, Zhang G, Niu Y, Yuan Z, Herrup K, Zhang YW, Bu G, Xu H, Zhang J (2015) The roles of Cdk5-mediated subcellular localization of FOXO1 in neuronal death. *J Neurosci* **35**(6): 2624–2635.

Zoller M (2011) CD44: can a cancer-initiating cell profit from an abundantly expressed molecule? *Nat Rev Cancer* **11**(4): 254–267.

Supplementary Information accompanies this paper on British Journal of Cancer website (http://www.nature.com/bjc)

Supplementary Figure 1

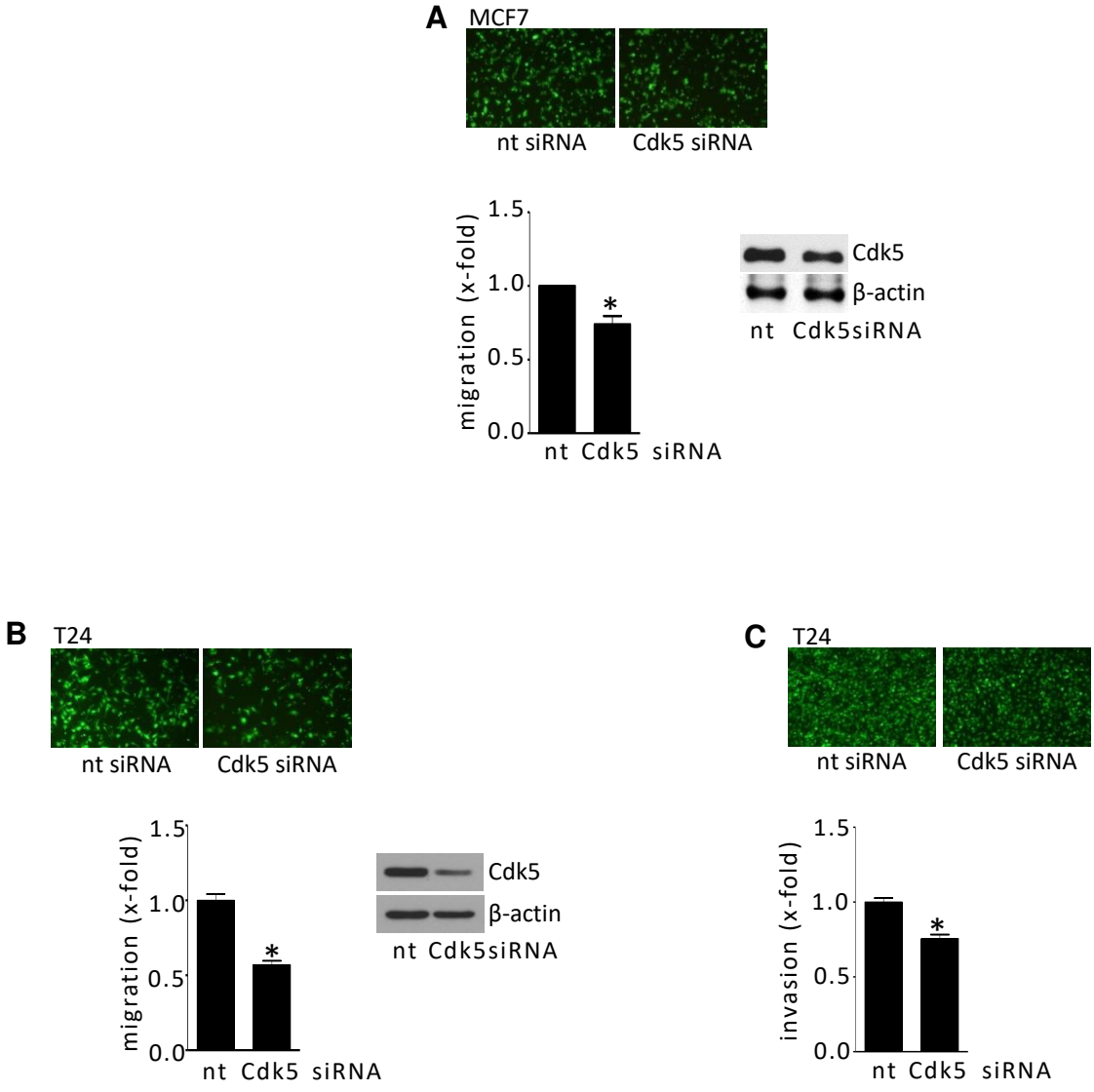

Supplementary Figure 1. Cdk5 inhibition reduces cancer cell motility. (A) FCS-induced migration of non-targeting (nt) or Cdk5 siRNA treated MCF7 cells is shown (mean ± SEM, *p<0.001, n=3). Immunoblots of non-targeting (nt) or Cdk5 siRNA treated MCF7 cells for Cdk5 and β-actin (loading control) proof Cdk5 knockdown. (B) FCS-induced migration of non-targeting (nt) or Cdk5 siRNA treated T24 cells is shown (mean ± SEM, *p<0.001, n=3). Immunoblots of non-targeting (nt) or Cdk5 siRNA treated T24 cells for Cdk5 and β-actin (loading control) proof Cdk5 knockdown. (C) FCS-induced invasion of T24 cells treated with non-targeting (nt) or Cdk5 siRNA is shown (mean ± SEM, *p<0.001, n=3).

Supplementary Figure 2

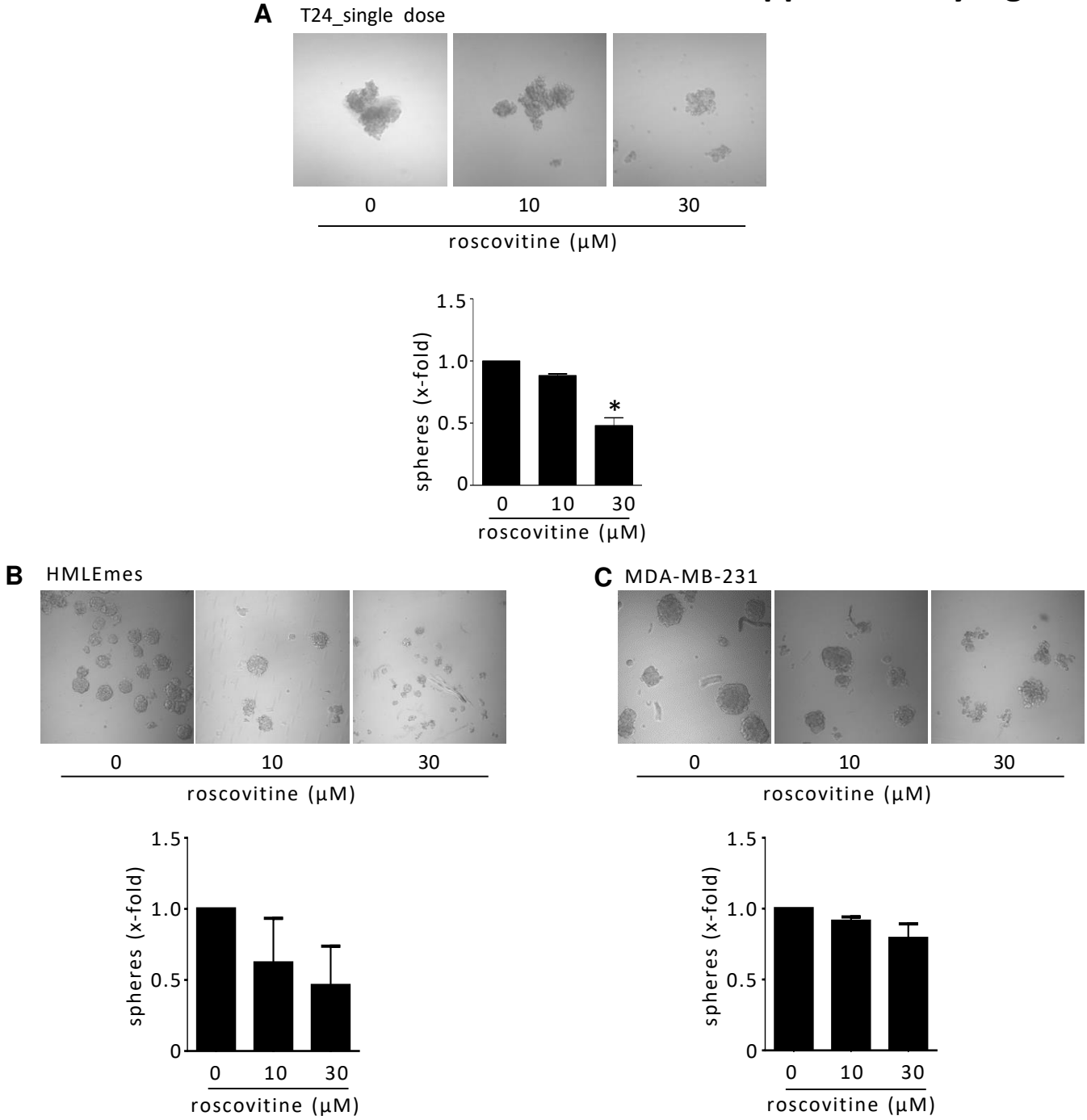

Supplementary Figure 2. Cdk5 regulates tumorsphere formation. (A) Tumorsphere formation after pretreatment of cells with roscovitine for 24 h before resuspension in fresh sphere-formation medium and cultivation for further 10 days is shown (mean ± SEM, *p<0.001, n=3). (B) Tumorsphere formation after pretreatment of mesenchymal HMLE cells with roscovitine for 24 h before resuspension in fresh sphere-formation medium and cultivation for further 10 days in presence of roscovitine is shown (mean ± SEM, n=3). (C) Tumorsphere formation after pretreatment of MDA-MB-231 cells with roscovitine for 24 h before resuspension in fresh sphere-formation medium and cultivation for further 10 days in presence of roscovitine is shown (mean ± SEM, n=3).

Supplementary Figure 3

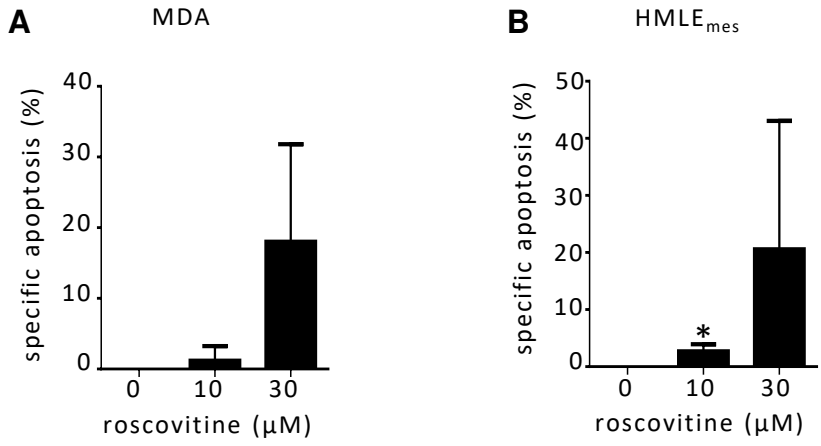

Supplementary Figure 3. Cdk5 induces apoptosis of tumorspheres. (A) Specific apoptosis of MDA-MB-231 tumorspheres after pretreatment of cells with roscovitine for 24 h before resuspension in fresh sphere-formation medium and cultivation for further 10 days in presence of roscovitine is shown (mean ± SEM, n=3). (B) Specific apoptosis of tumorspheres from mesenchymal HMLE cells (HMLE$_{mes}$) after pretreatment of cells with roscovitine for 24 h before resuspension in fresh sphere-formation medium and cultivation for further 10 days in presence of roscovitine is shown (mean ± SEM, *$p<0.05$, n=3).

Supplementary Figure 4

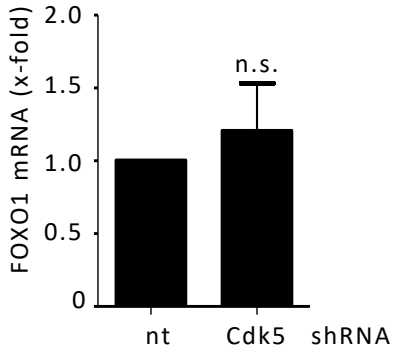

Supplementary Figure 4. Cdk5 does not regulate Foxo1 at mRNA level. Foxo1 mRNA of non-targeting (nt) and Cdk5 shRNA cells is shown (mean ± SEM, n.s. = not significant, n=3).

Acknowledgments

First and foremost, I wish to express my sincere thanks to PD Dr. Johanna Liebl not only for supervising my Ph.D. but also for her constant best possible support, trust, advice, and friendship. The last years have truly strengthened, enriched, and formed me personally.

I am also grateful to Prof. Dr. Angelika M. Vollmar for giving me the opportunity to do my Ph.D. in her lab. I really appreciated her constant support, critical discussion, and always positive energy pushing my projects forward during the last three years.

I would like to thank the additional members of the dissertation committee, Prof. Dr. Christian Wahl-Schott, Prof. Dr. Franz Paintner, PD Dr. Stylianos Michalakis and Prof. Dr. Ernst Wagner for taking their time and their friendly support.

I'm especially thankful for the great cooperation with Prof. Dr. Stephan A. Sieber and his group. I'd like to thank Anja Fux, Christian Fetzer, Matthias Stahl and Thomas Gronauer for compound supply, support, and the great collaboration in the still on-going projects.

I would like to express appreciation to the whole Vollmar's lab for scientific discussion, communications, and support. I really enjoyed the last years and surpassed myself not least because of the motivating and at the same time very family atmosphere in the group.

I'd like to mention Julia Blenninger who constantly worked on the ClpXP as well as the Cdk5 project. Apart from that, I'd like to thank Jana Peliskova for her helping hand, listening ear, and every single encouraging word.

Further, I feel grateful for the close friendship with Christina Moser and the scientific and mental support. In addition, Fabian Koczian and Karin Bartel who simultaneously started their Ph.D. greatly enriched my past three years in the lab, in the PB3 practical course, and the time beyond.

Also, many thanks to the former members of the Vollmar's lab, Katja Stoiber and Henriette Merk, and also to a new member, Carolin Pyka, for their close friendship.

This thesis would not have been possible without my beloved family. Above all, my dearest sister and brother, Manuela and Maximilian. You are my family, my closest friends, my best motivation, and the strongest support I could ever imagine.